

Field Observations during the Tenth Microwave Water and Energy Balance Experiment (MicroWEX-10): from March 1, 2011, through January 5, 2012¹

Tara Bongiovanni, Pang-Wei Liu, Karthik Nagarajan, Daniel Preston, Patrick Rush, Xueyang Duan, Guanbo Chen, Robert Terwilleger, Alejandro Monsivais-Huertero, Jasmeet Judge, Roger De Roo, Ruzbeh Akbar, Mary Morris, Olivia Williams, Lindsey Marks, Courtney Cardozo, Mahta Moghaddam, and Anthony England²

-
1. This document is AE512, one of a series of the Agricultural and Biological Engineering Department, UF/IFAS Extension. First published April 2015. Reviewed February 2018. Visit the EDIS website at <http://edis.ifas.ufl.edu>.
 2. TTara Bongiovanni, research scientist, University of Texas-Austin, Pang-Wei Liu, senior research scientist, NASA Goddard Space Flight Center; Karthik Nagarajan, researcher, Qualcomm; Daniel Preston, engineering technician, Mechanical and Aerospace Engineering; Patrick Rush, engineer, Agricultural and Biological Engineering Department; Xueyang Duan, NASA Jet Propulsion Laboratory, Guanbo Chen, Roger De Roo and Anthony England, Electrical Engineering and Computer Sciences Department, University of Michigan, Ruzbeh Akbar, Mahta Moghaddam, University of Southern California; Robert Terwilleger, Lindsey Marks, and Courtney Cardozo, undergraduate research assistants, CRS, Agricultural and Biological Engineering Department; Alejandro Monsivais-Huertero, professor, ESIME Unidad Ticomán, Instituto Politécnico Nacional, Mexico; Jasmeet Judge (jasmeet@ufl.edu), professor and director, CRS, Agricultural and Biological Engineering Department; Mary Morris and Olivia Williams, UF Research Experience for Undergraduates; UF/IFAS, Gainesville, FL 32611.

The Institute of Food and Agricultural Sciences (IFAS) is an Equal Opportunity Institution authorized to provide research, educational information and other services only to individuals and institutions that function with non-discrimination with respect to race, creed, color, religion, age, disability, sex, sexual orientation, marital status, national origin, political opinions or affiliations. For more information on obtaining other UF/IFAS Extension publications, contact your county's UF/IFAS Extension office.

TABLE OF CONTENTS

1. INTRODUCTION.....	1
2. OBJECTIVES.....	1
3. FIELD SETUP.....	1
4. SENSORS.....	5
4.1 University of Florida Microwave Radiometer Systems.....	5
4.1.1 University of Florida C-band Microwave Radiometer (UFCMR).....	5
4.1.1.1 Theory of operation.....	7
4.1.2 University of Florida L-band Microwave Radiometer (UFLMR)	9
4.1.2.1 Theory of operation.....	11
4.2 University of Michigan Radiometer System.....	13
4.2.1 Truck Mounted Radiometer System L-band (TMRS-L).....	13
4.2.1.1 Theory of operation.....	14
4.3 University of Florida Radar System.....	14
4.3.1 University of Florida L-band Automated Radar System (UF-LARS)	14
4.4 University of Michigan Radar System.....	16
4.4.1 Microwave Observatory of Subcanopy and Subsurface (MOSS).....	16
4.4.1.1 Theory of operation.....	17
4.5 Net Radiometer.....	19
4.6 Air Temperature and Relative Humidity.....	19
4.7 Thermal Infrared Sensor	20
4.7.1 Thermal Infrared Sensor (elephant grass)	20
4.7.2 Thermal Infrared Sensor (sweet corn)	20
4.8 Soil Temperature Probes	20
4.8.1 Soil Temperature Probes (elephant grass)	20
4.8.2 Soil Temperature Probes (sweet corn)	21
4.9 Soil Moisture Probes	21
4.9.1 Soil Moisture Probes (elephant grass)	21
4.9.2 Soil Moisture Probes (sweet corn)	21
4.10 Precipitation	21
4.10.1 Precipitation (elephant grass)	21
4.10.2 Precipitation (sweet corn)	21
4.11 Drip irrigation	22
5. VEGETATION SAMPLING AT THE ELEPHANT GRASS SITE.....	22
5.1 Clump and Tiller Count	22
5.2 Clump Height and Width.....	22
5.3 Tiller Height and Width.....	23

5.4 Wet and Dry Biomass	23
5.5 LAI	23
5.6 Vertical Distribution of Moisture in the Canopy.....	23
5.7 Geometric Description.....	24
6. VEGETATION SAMPLING AT THE SWEET CORN SITE.....	24
6.1 Height and Width.....	24
6.2 Wet and Dry Biomass	24
6.3 LAI	24
6.4 Vertical Distribution of Moisture in the Canopy	24
6.5 Geometric Description	25
7. WELL SAMPLING.....	26
7.1 Water level measurement.....	26
8. SOIL SAMPLING.....	26
8.1 Soil Analysis	26
8.2 Soil Roughness	27
9. OBSERVATIONS.....	29
10. ELEPHANT GRASS FIELD LOG.....	30
11. SWEET CORN FIELD LOG.....	37
12. REFERENCES.....	41
13. ACKNOWLEDGMENTS.....	42
A. FIELD OBSERVATIONS.....	43
B. JULIAN DAY CALENDAR.....	97

1. INTRODUCTION

For accurate prediction of weather and near-term climate, root-zone soil moisture is one of the most crucial components driving surface hydrological processes. Soil moisture in the top meter governs moisture and energy fluxes at the land–atmosphere interface, and it plays a significant role in partitioning of precipitation into runoff and infiltration.

Energy and moisture fluxes at the land surface during growing seasons can be estimated by coupled Soil-Vegetation-Atmosphere-Transfer and crop growth models. Even though the biophysics of moisture and energy transport and of crop growth and development are well-captured in most current models, the errors in initialization, forcings, and computation accumulate over time and the model estimates of soil moisture in the root zone diverge from reality. Remotely sensed microwave observations can be assimilated in these models to improve root zone soil moisture and crop yield estimates.

The microwave signatures at low frequencies, particularly at 1–4 GHz (L-band) and 4–8 GHz (C-band) are very sensitive to soil moisture in the top few centimeters in most vegetated surfaces. Many studies have been conducted in agricultural areas—such as bare soil, grass, soybean, wheat, pasture, and corn—to understand the relationship between soil moisture and microwave remote sensing. It is important to know how microwave signatures vary with soil moisture, evapotranspiration (ET), and biomass during the growing season for a dynamic agricultural canopy with a significant wet biomass of 4–12 kg/m².

2. OBJECTIVES

The goal of MicroWEX-10 was to conduct a season-long experiment, which incorporated active and passive microwave observations for a growing season of elephant grass and sweet corn. The variety of sensors allowed for further understanding of the land–atmosphere interactions during the growing season, and their effect on observed passive microwave signatures at 6.7 GHz and 1.4 GHz and active microwave signatures at 1.14 GHz and 1.25 GHz. These observations match that of the satellite-based passive microwave radiometers, Advanced Microwave Scanning Radiometer-2 (AMSR-2), and the Soil Moisture and Ocean Salinity (SMOS) mission, respectively, and the upcoming National Aeronautics and Space Administration’s Soil Moisture Active Passive (SMAP) mission. Specific objectives of MicroWEX-10 include the following:

1. To acquire simultaneous active and passive data for both elephant grass and corn.
2. To collect passive and active microwave and other ancillary data to develop preliminary algorithms to estimate microwave signatures for elephant grass and corn.
3. To implement alternate irrigation methods when the height of the elephant grass canopy exceeds 3 m.
4. To evaluate feasibility of soil moisture retrievals using passive microwave data at 6.7 GHz and 1.4 GHz and active microwave data at 1.14 GHz and 1.25 GHz for the growing elephant grass canopy and corn.

This report describes the observations conducted during the MicroWEX-10.

3. FIELD SETUP

MicroWEX-10 was conducted at the UF/IFAS Extension Plant Science Research and Education Unit (PSREU), Citra, FL. Figures 1 and 2 show the location of the PSREU and the study site for the MicroWEX-10, respectively. The study site was located at the west side of the PSREU (29.4°N, 82.17°W). The dimensions of the elephant grass study site were 183 m × 183 m with the corners of the field located at 29.410°N 82.179°W; 29.410°N 82.177°W; 29.409°N 82.177°W; 29.409°N 82.179°W. The elephant grass (*Pennisetum purpureum*) of varieties Merkeron, N-13, N-43, and N-51, was in its second year of growth. The row spacing was 182.9 cm (72 inches). A linear move system was used for irrigation in the beginning of the season with drip irrigation installed on May 31 (Day of Year [DoY] 151) in 2011. (See Table B-1 for corresponding months and dates to the DoY mentioned in this document on page 97.) The instruments consisted of two ground-based microwave radiometer systems, a ground-based microwave radar system, and micrometeorological stations. The ground-based microwave radiometer systems were installed at the location

shown in Figure 3(a), facing south to avoid the radiometer shadow interfering with the field of view. The ground-based microwave radar system was installed adjacent to the radiometer with a portion of the radar footprint overlapping the radiometer footprint, facing in the same direction as the radiometer system. The ground-based microwave radiometer systems installation began on DoY 50 in 2011 with micrometeorological stations on DoY 83 in 2011 and radar measurements starting on DoY 241 in 2011. Three micrometeorological stations with soil moisture and soil temperature sensors were installed at the locations shown in Figure 3(a). Rain gauges were installed in line with the outer edge of the L-band radiometer footprint. A relative humidity (RH) and temperature sensor were installed at the C-band station. A net radiometer and thermal infrared sensor were installed south of the C-band radiometer.

The dimensions of the corn study site were 100 m \times 175 m. A linear move system was used for irrigation. The corn of variety Yellow Supersweet Hybrid (SH₂) Saturn was planted on DoY 186 in 2011, at an orientation 0° from the east. The plant spacing was 15.9 cm (6 ¼ inches) and the row spacing was 91.4 cm (36 inches). Instrument installation began on DoY 188 in 2011. The instruments consisted of a ground-based microwave radiometer system, two ground-based microwave radar systems, and micrometeorological stations. The ground-based microwave radiometer system was installed at the location shown in Figure 3(b), facing south to avoid the radiometer shadow interfering with the field of view. The ground-based microwave radar systems were installed adjacent to the radiometer with a portion of the radar footprint overlapping the radiometer footprint, facing in the same direction as the radiometer system. Rain gauges were installed in line with the outer edge of the radar footprint. Two micrometeorological stations with soil moisture and soil temperature sensors were installed at the locations shown in Figure 3(b). A thermal infrared sensor was installed in the southern end of the field out of the range of the footprints. This report provides detailed information regarding sensors deployed and data collected during the MicroWEX-10.

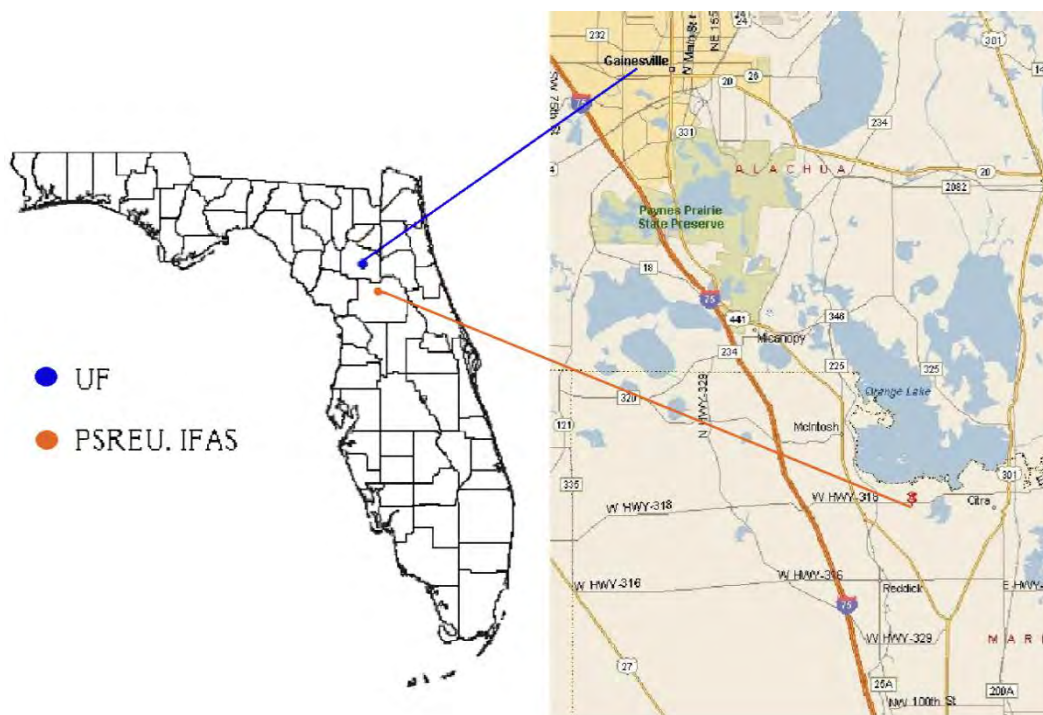


Figure 1. Location of PSREU/IFAS

Credits: <http://plantscienceunit.ifas.ufl.edu/directions.shtml>

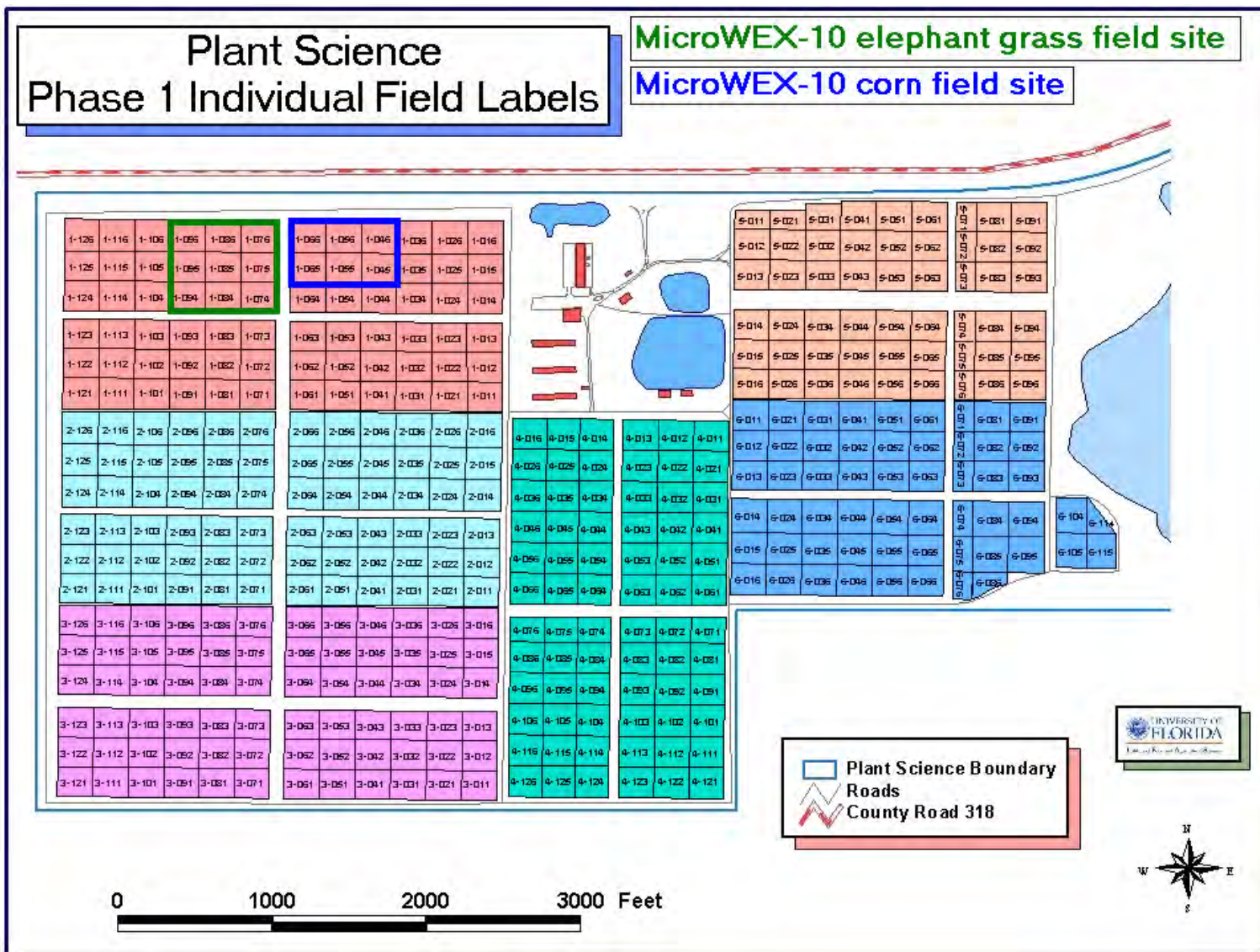


Figure 2. Location of the field site for MicroWEX-10 at the UF/IFAS PSREU

Credits: <http://plantscienceunit.ifas.ufl.edu/images/location/p1.jpg>

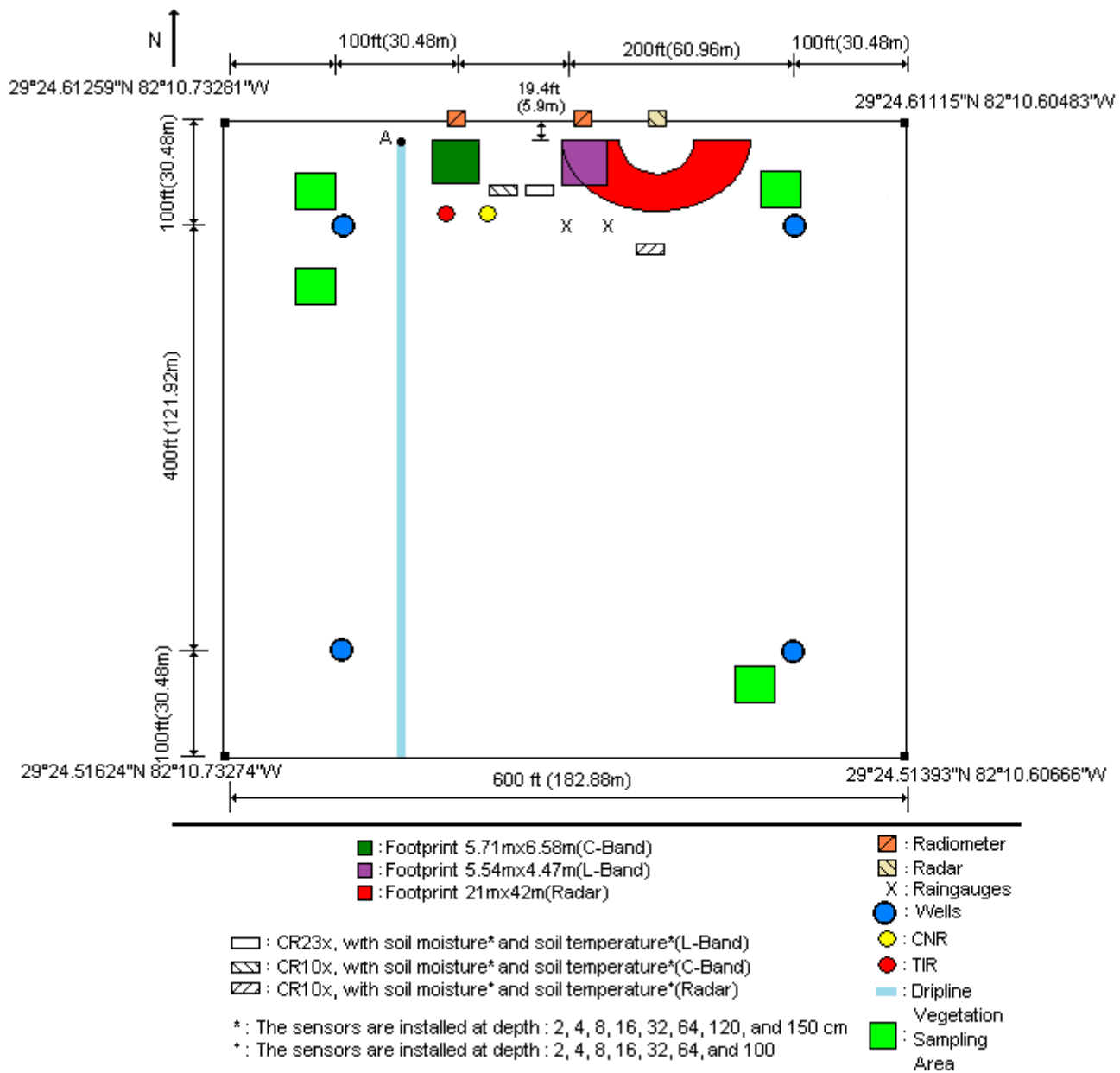


Figure 3(a). Layout of the sensors during MicroWEX-10 elephant grass

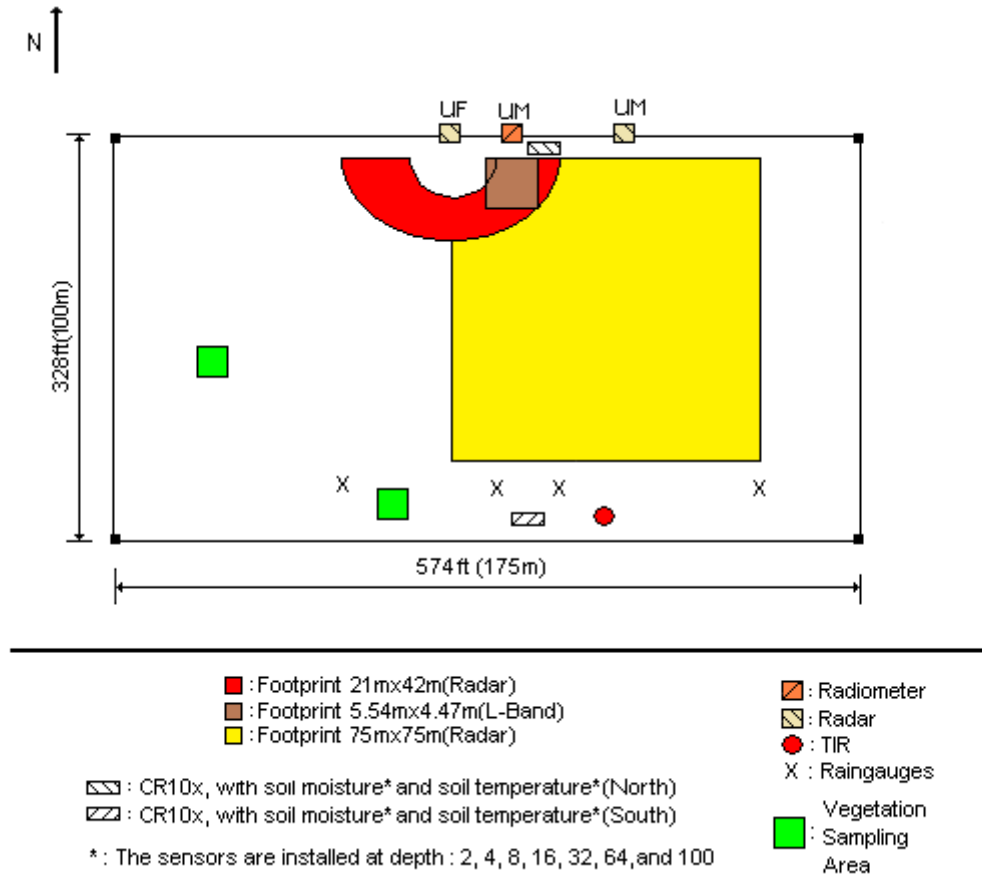


Figure 3(b). Layout of the sensors during MicroWEX-10 corn

4. SENSORS

MicroWEX-10 had six major types of instrument subsystems: (1) the ground-based University of Florida C-band and L-band radiometers, (2) the ground-based University of Michigan L-band radiometer, (3) the ground-based University of Florida L-band radar, (4) the ground-based University of Michigan L-band radar, (5) the micrometeorological, and (6) the soil subsystem.

4.1 University of Florida Microwave Radiometer Systems

4.1.1 University of Florida C-band Microwave Radiometer (UFCMR)

Microwave brightness temperatures at 6.7 GHz ($\lambda = 4.48$ cm) were measured every 15 minutes using the University of Florida's C-band Microwave Radiometer system (UFCMR) (Figure 4[a]). The radiometer system consisted of a dual polarization total power radiometer operating at the center frequency of 6.7 GHz housed atop a 10 m tower installed on a 16' trailer bed. The UFCMR was designed and built by the Microwave Geophysics Group at the University of Michigan. It operates at the center frequency at 6.7 GHz, which is near one of the center frequencies on the space borne AMSR-2 aboard the Japan Aerospace Exploration Agency's Global Change Observation Mission-Water satellite. The UFCMR observed the 6.58 m \times 5.71 m footprint from a height of 7.747 m. A rotary system was used to rotate the look-angle of the UFCMR both for field observations and sky measurements. The brightness temperatures were observed at an incidence angle of 45°. The radiometer was calibrated at least once every week with a microwave absorber as warm load and measurement of sky as cold load. Figure 4(b) shows the close-up of the rotary system and Figure 4(c) shows a close-up of the UFCMR antenna. Table 1 lists the UFCMR specifications. Figure A-1 shows the V- and H-pol brightness temperatures observed at C-band during MicroWEX-10 for the elephant grass field.

Table 1. UFCMR specifications

Parameter	Qualifier	Value
Frequency	Center	6.7 GHz
Bandwidth	3 dB	20 MHz
Beamwidth	3 dB V-pol elevation ^a	23°
	3 dB V-pol azimuth ^b	21°
	3 dB H-pol elevation ^c	21°
	3 dB H-pol azimuth ^d	23°
Isolation		> 27 dB
Polarizations	Sequential	V/H
Receiver temp (T_{rec})		437 K
Noise Figure	From T_{rec}	3.99 dB
RF gain		85 dB
NEDT	1 sec	0.71 K
	8 sec	0.25 K
^a sidelobes < -33 dB ^b sidelobes < -28 dB ^c sidelobes < -27 dB ^d sidelobes < -35 dB		

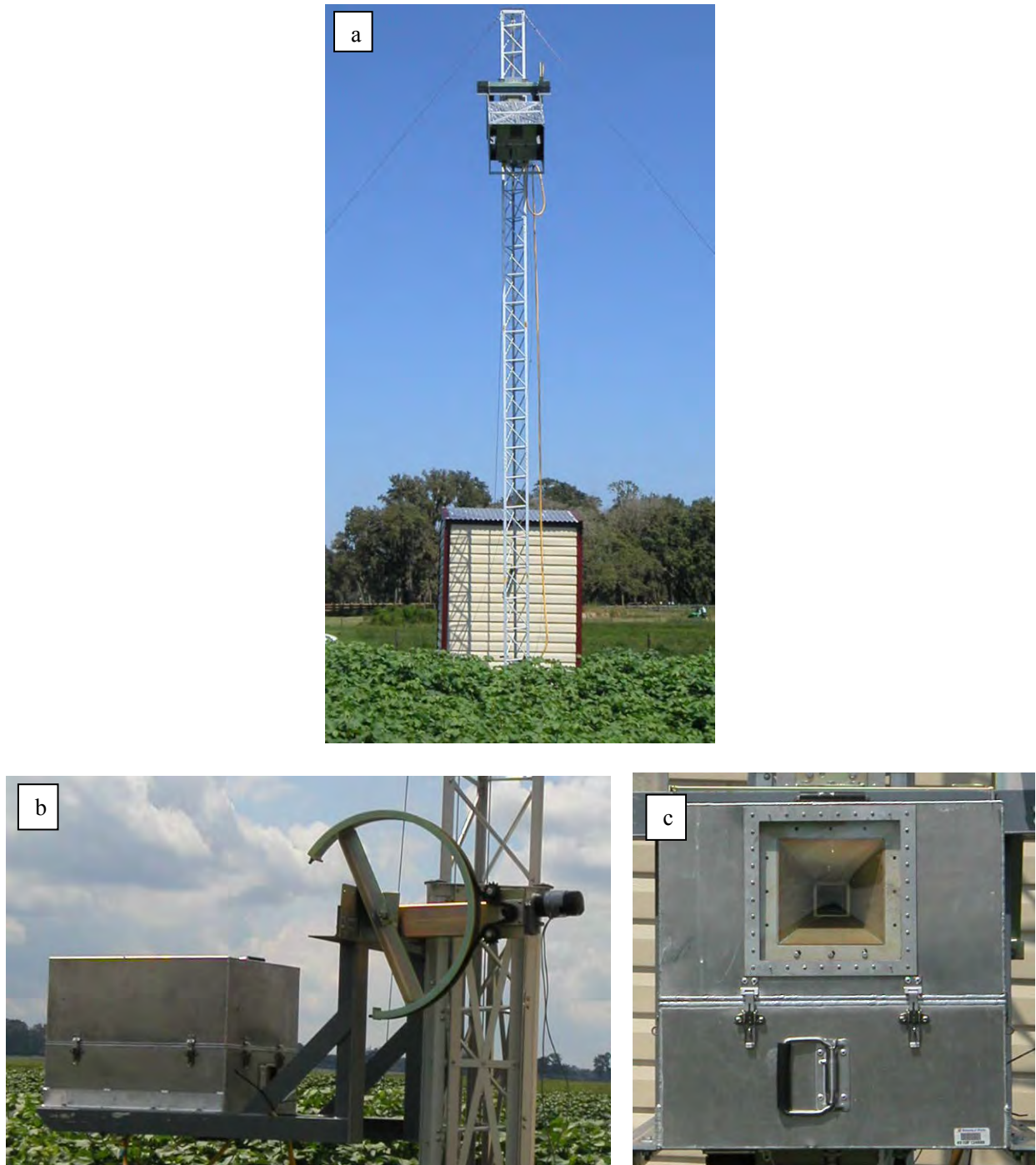


Figure 4. (a) The UFCMR system, (b) the side view of the UFCMR showing the rotary system, and (c) the front view of the UFCMR showing the receiver antenna
Credits: J. Casanova, University of Florida

4.1.2.1 Theory of operation

The UFCMR uses a thermoelectric cooler (TEC) for thermal control of the Radio Frequency (RF) stages for the UFCMR. This is accomplished by the Oven Industries “McShane” thermal controller. McShane is used to cool or heat by Proportional-Integral-Derivative (PID) algorithm with a high degree of precision at 0.01°C . The RF components are all attached to an aluminum plate that must have sufficient thermal mass to eliminate short-term thermal drifts. All components attached to this thermal plate, including the TEC, use thermal paste to minimize thermal gradients across junctions.

The majority of the gain in the system is provided by a gain and filtering block designed by the University of Michigan for the STAR-Light instrument (De Roo 2003). The main advantage of this gain block is the close proximity of all the amplifiers, simplifying the task of thermal control. This gain block was designed for a radiometer working at the radio astronomy window of 1400–1427 MHz, and so the receiver is a heterodyne type with downconversion from the C-band RF to L-band. To minimize the receiver noise figure, a C-band low-noise amplifier (LNA) is used just prior to downconversion. To protect the amplifier from saturation due to out-of-band interference, a relatively wide bandwidth, but low insertion loss, bandpass filter is used just prior to the amplifier. Three components are between the filter and the antenna: a switch for choosing polarization, a switch for monitoring a reference load, and an isolator to minimize changes in the apparent system gain due to differences in the reflections looking upstream from the LNA.

The electrical penetrations use commercially available weatherproof bulkhead connections (Deutsch connectors or equivalent). The heat sinks have been carefully located employing RTV (silicone sealant) to seal the bolt holes. The radome uses 15 mil polycarbonate for radiometric signal penetration. It is sealed to the case using a rubber gasket held down by a square retainer.

The first SubMiniature version A (SMA) connection is an electromechanical latching, driven by the Z-World control board switches between V- and H-polarization sequentially. The SMA second latching that switches between the analog signal from the first switch and the reference load signal from a reference load resistor sends the analog signal to an isolator, where the signals within 6.4–7.2 GHz in radiofrequency are isolated. Then the central frequency is picked up by a 6.7 GHz bandpass filter, which also protects the amplifier from saturation. A low-noise amplifier (LNA) is used to eliminate the noise figure and adjust gain. A mixer takes the input from the LNA and a local oscillator to output a 1.4 GHz signal to STAR-Light. After the power amplifier and filtering block (Star-Light back-end), the signal is passed through a square law detector and a post-detection amplifier (PDA). The UFCMR is equipped with a microcontroller that is responsible for taking measurements, monitoring the thermal environment, and storing data until a download is requested. A laptop computer is used for running the user interface named FluxMon to communicate with the radiometer through Radiometer Control Language (RadiCL). The radiometer is configured to maintain a particular thermal set point, and make periodic measurements of the brightness at both polarizations sequentially and the reference load. The data collected by the radiometer are not calibrated within the instrument, since calibration errors could corrupt an otherwise useful dataset. Figure 5 shows the block diagram of the UFCMR.

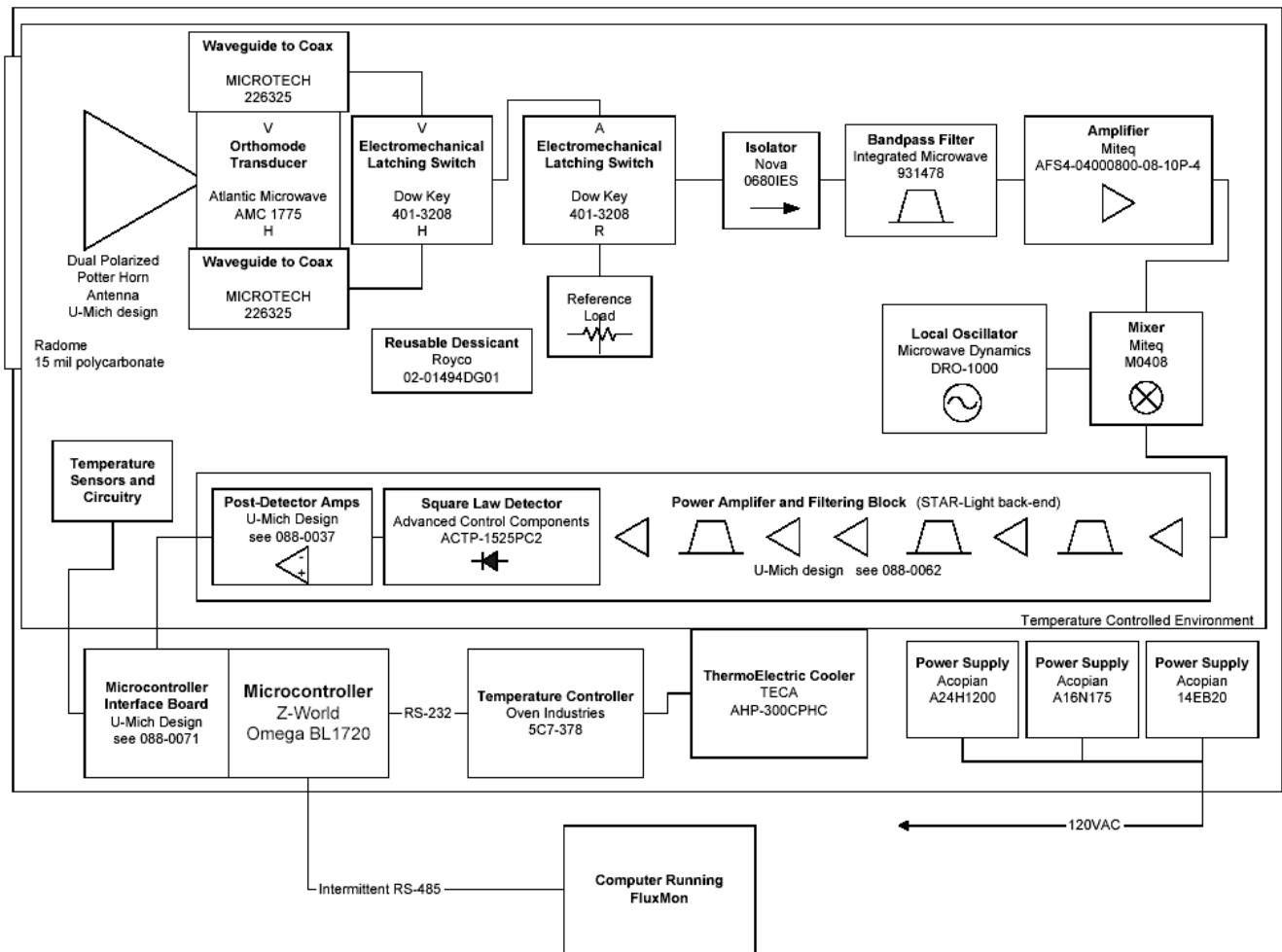


Figure 5. Block diagram of the University of Florida C-band Microwave Radiometer
Credits: De Roo (2002)

4.1.2 University of Florida L-band Microwave Radiometer (UFLMR)

Microwave brightness temperatures at 1.4 GHz ($\lambda = 21.0$ cm) were measured every 15 minutes using the University of Florida's L-band Microwave Radiometer system (UFLMR) (Figure 6[a]). The radiometer system consisted of a horizontally polarized total power radiometer operating at the center frequency of 1.4 GHz housed atop a 9.14 m tower installed on a 16' trailer bed. The UFLMR was designed and built by the Microwave Geophysics Group at the University of Michigan. It operates at the center frequency at 1.4 GHz, which is identical to the center frequency on the space-borne SMOS mission. The UFLMR observed the $5.54 \text{ m} \times 4.47 \text{ m}$ footprint from a height of 7.9375 m. The brightness temperatures were observed at an incidence angle of 40° . A rotary system was used to rotate the look-angle of the UFLMR for both field observations and sky measurements. The radiometer was calibrated at least every week with a measurement of sky as cold load. Figure 6(b) shows a close up of the rotary system and Figure 6(c) shows the antenna of the UFLMR. Table 2 lists the UFLMR specifications. Figure A-1 shows the horizontally polarized brightness temperatures observed by the UFLMR during MicroWEX-10 for the elephant grass field.

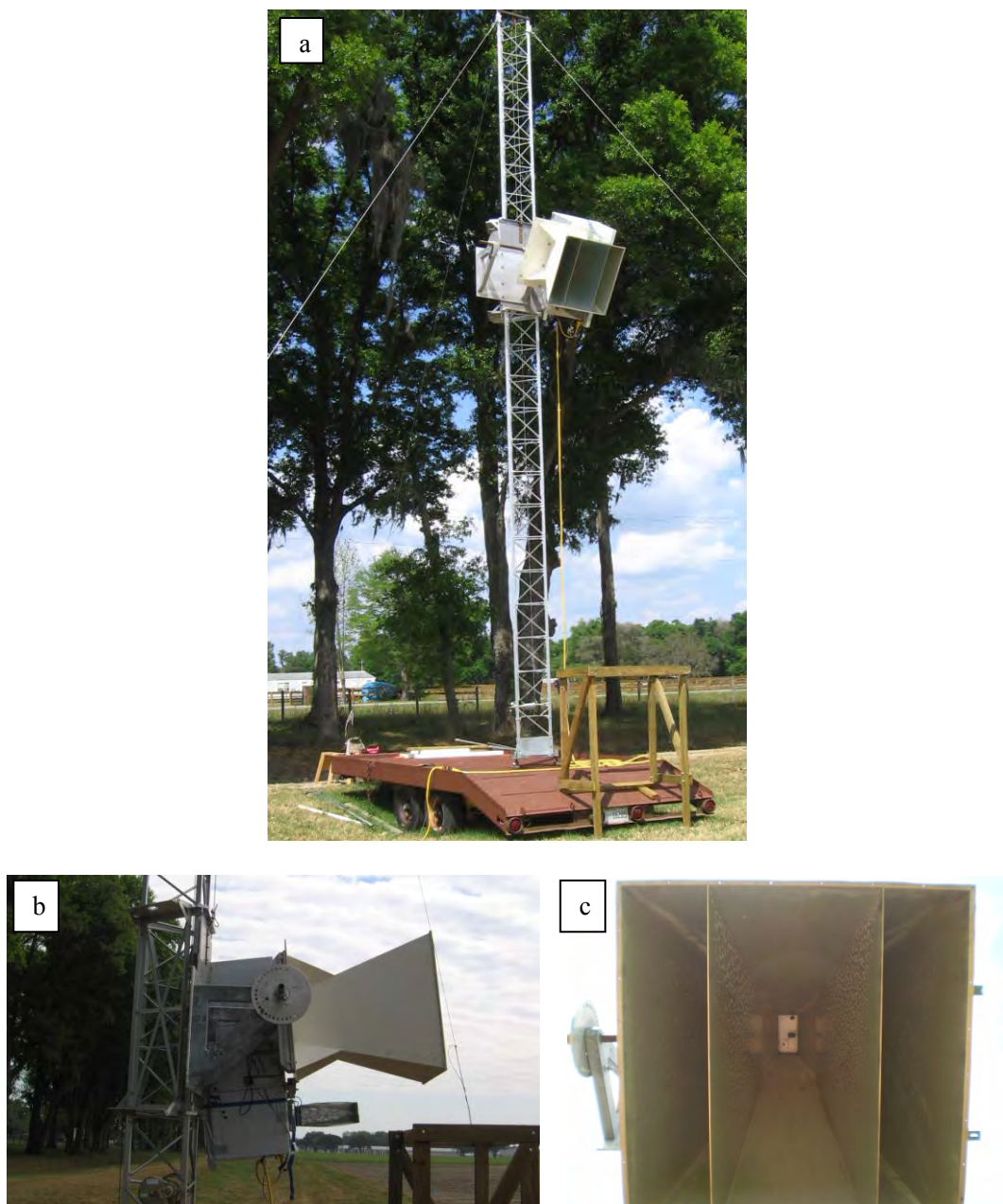


Figure 6. (a) The UFLMR system, (b) the side view of the UFLMR showing the rotary system, and (c) the front view of the UFLMR showing the receiver antenna
 Credits: J. Casanova, University of Florida

Table 2. UFLMR specifications

Parameter	Qualifier	Value
Frequency	Center	1.4 GHz
Bandwidth	3 dB	20 MHz
Beamwidth	3 dB H-pol elevation ^a	22.5°
	3 dB H-pol azimuth ^b	20.0°
Polarizations	Single	H
Receiver temp (T_{rec})		179 K
Noise Figure	From T_{rec}	2.1 dB
RF gain		79 dB
NE Δ T		0.5 K
^a sidelobes < -20 dB		
^b sidelobes < -30 dB		

4.1.2.1 Theory of operation

The UFLMR is similar to the UFCMR in many respects, using a thermoelectric cooler (TEC) for thermal control, a similar electromechanical switching mechanism, and a Z-World controller. The PDA is the same, and the software is a newer version of RadiCL. The RF block is designed for V- and H-pol switching. However, the UFLMR's employs only a single-polarization. As a result, only the H-pol signal is guided from antenna to coax to the RF block, and the V-pol input to the RF block is a cold load (ColdFet).

In the RF block, the first switch alternates between V- and H-pol and the second alternates between the reference load and the signal from the first switch. An isolator prevents reflections of the input signal. After the isolator, the signal goes through a bandpass filter and then an LNA, followed by a series of bandpass filters and power amplifiers before the square law detector and the PDA. The microcontroller logs voltage and physical temperature measurements. Figure 7 shows the block diagram of the UFLMR.

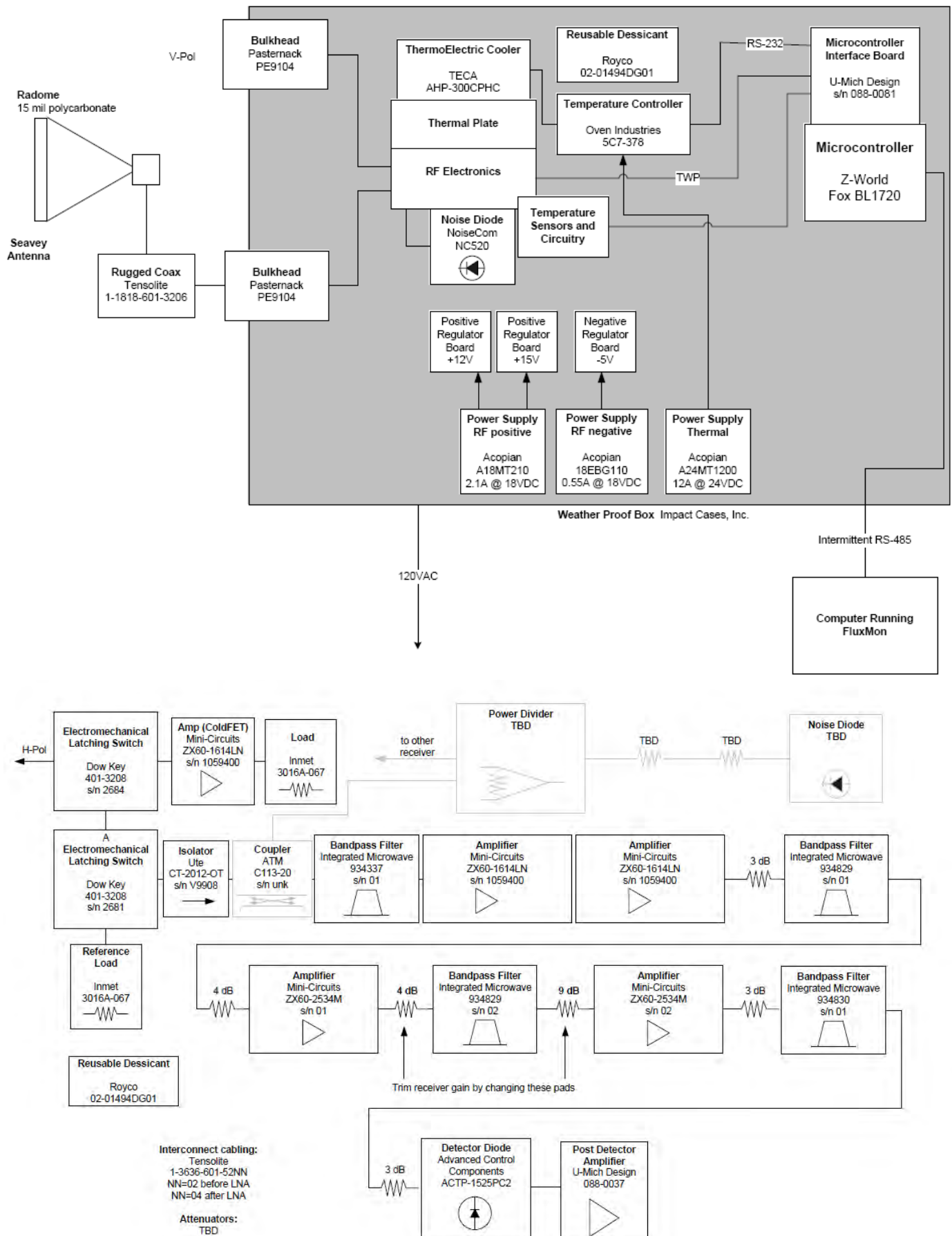


Figure 7. Block diagram of the University of Florida L-band Microwave Radiometer
Credits: De Roo (2010)

4.2 University of Michigan Radiometer

4.2.1 Truck Mounted Radiometer System - L-band (TMRS-L)

The Truck Mounted Radiometer System (TMRS) is a dual-polarized, multi-frequency radiometer system from the University of Michigan that measures microwave brightness temperatures. The radiometer system consisted of multiple dual polarization total power radiometers housed atop a bucket truck. In this experiment, only the L-band radiometer, operating at the center frequency of 1.4 GHz ($\lambda = 21.0$ cm), was used to measure every-15-minute data (Figure 8[a]) in the corn field. The TMRS was designed and built by the Microwave Geophysics Group at the University of Michigan. The height, incident angle, and footprint were identical to the UFLMR. A rotary system was used to rotate the look angle of the TMRS both for field observations and sky measurements. The radiometer was calibrated at least every week with a measurement of sky as cold load. Figure 8(b) shows the antenna and Figure 8(c) shows the close-up of the rotary system of the TMRS-L. Table 3 lists the specifications of the TMRS-L. Figure A-2 shows the V- and H-pol brightness temperatures observed by the TMRS-L during MicroWEX-10 for the corn field.

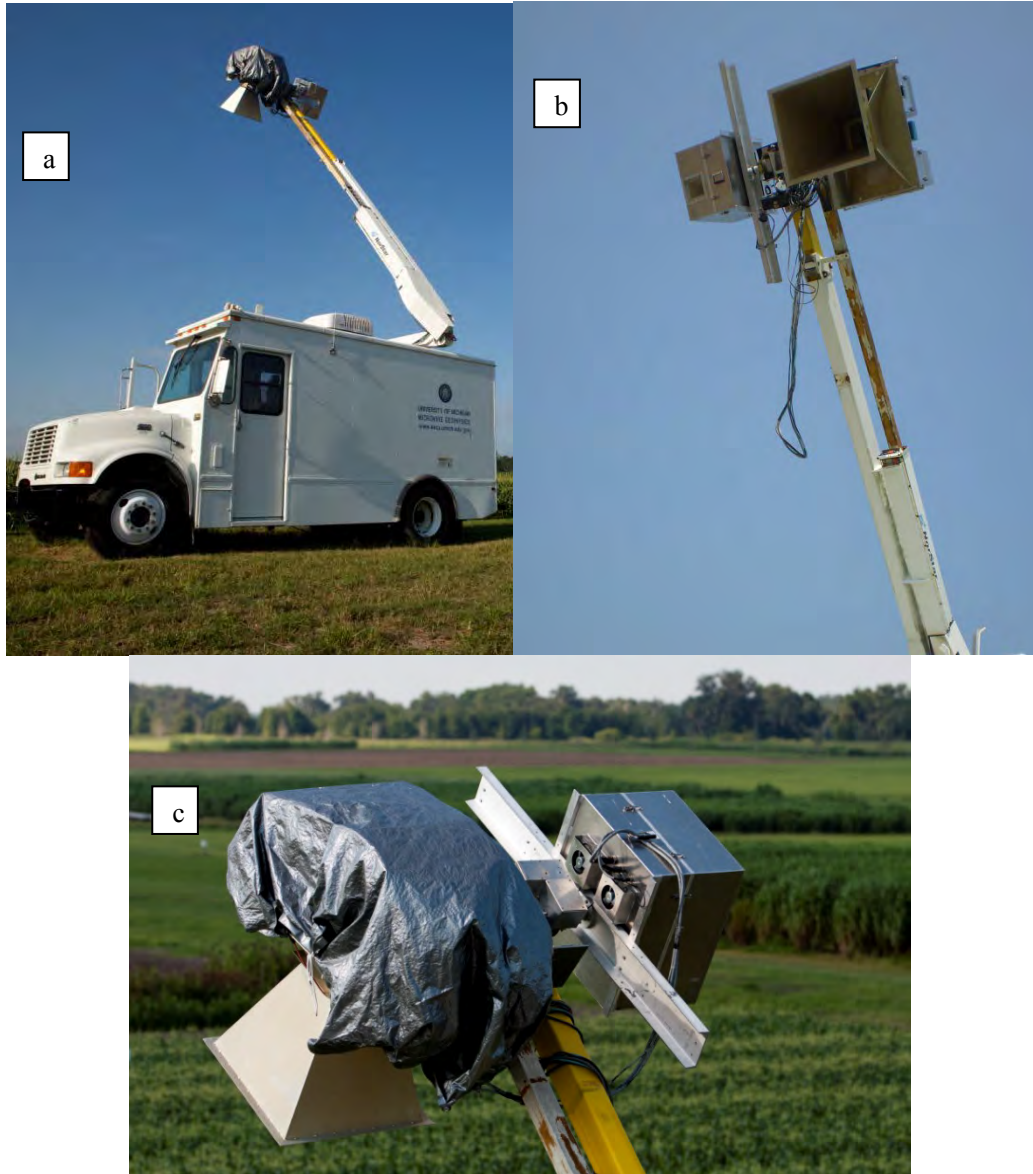


Figure 8. (a) The TMRS-L, (b) the front view of the TMRS-L showing the receiver antenna, and (c) the side view of the TMRS-L showing the rotary system

Credits: D. Preston, UF/IFAS

Table 3. TMRS-L specifications

Parameter	Qualifier	Value
Frequency	Center	1.4 GHz
Bandwidth	3 dB	20 MHz
Beamwidth	3 dB H-pol elevation ^a	22.5°
	3 dB H-pol azimuth ^b	20.0°
	3 dB V-pol elevation ^c	20.0°
	3 dB V-pol azimuth ^d	22.5°
Polarizations	Sequential	V/H
Receiver temp (T _{rec})		179 K
Noise Figure	From T _{rec}	2.1 dB
RF gain		79 dB
NEΔT		0.5 K
^a sidelobes < -20 dB ^b sidelobes < -30 dB ^c sidelobes < -30 dB ^d sidelobes < -20 dB		

4.2.1.1 Theory of operation

The TMRS-L is similar to the UFLMR and UFCMR in many respects, using a thermoelectric cooler (TEC) for thermal control, a similar electromechanical switching mechanism and a Z-World controller; the PDA is the same, and the software is an older version of RadiCL. The RF block is designed for V- and H-pol switching similar to the UFCMR.

In the RF block, the first switch alternates between V- and H-pol and the second alternates between the reference load and the signal from the first switch. An isolator prevents reflections of the input signal. After the isolator, the signal goes through a bandpass filter and then an LNA, followed by a series of bandpass filters and power amplifiers before the square law detector and the PDA. The microcontroller logs voltage and physical temperature measurements.

4.3 University of Florida Radar System

4.3.1 University of Florida L-band Automated Radar System (UF-LARS)

Observations of radar backscatter (σ^0) over 21 spatial samples were collected every 15 minutes using the University of Florida L-band Automated Radar System (UF-LARS) (Figure 9). The UF-LARS is mounted on a 25 m Genie manlift and is comprised of three major sub-systems: (1) the antenna and the RF (ARF) sub-system, (2) the electro-mechanical positioning (EMP) sub-system, and (3) the software control and data acquisition (SDA) sub-system. Figure 10 shows a simplified block diagram of the UF-LARS. The RF subsystem was based upon the established designs for ground-based scatterometers employing a vector network analyzer with simultaneous acquisition of V- and H- polarized returns. These components operate at a center frequency of 1250 MHz, with a bandwidth of 300 MHz and the one-way 3 dB beamwidth of 14.7° in the E-plane and 19.7° in the H-plane. The polarization isolation at the center frequency was > 37 dB for all principal planes and decreases to about 23 dB at the band edge of 1400 MHz. The EMP sub-system employs an embedded computer and is composed of three digital inclinometers, an elevation-over-azimuth controller, linear actuators, and a laser range finder. The elevation-over-azimuth controller was used to rotate the look-angle of the UF-LARS for both field observations and sky measurements. The antenna incidence angle was set to 40°. The SDA enabled system integration and automated data acquisition using a software control system designed in the Visual C++ environment. Radar calibration included sky measurements, a trihedral corner-reflector (Figure 9), and pole throughout the season. Table 4 summarizes the system specifications. More information regarding the UF-LARS can be found in Nagarajan et al. (2014). Figures A-3 and A-4 show the co-pol and cross-pol radar backscatter observed by the UF-LARS during MicroWEX-10 for the elephant grass and corn field, respectively.



Figure 9. UF-LARS mounted on the 25 m Genie platform. (Inset) Trihedral calibration target made of aluminum with an aperture length of 1.28 m.
Credits: Nagarajan et al. (2014)

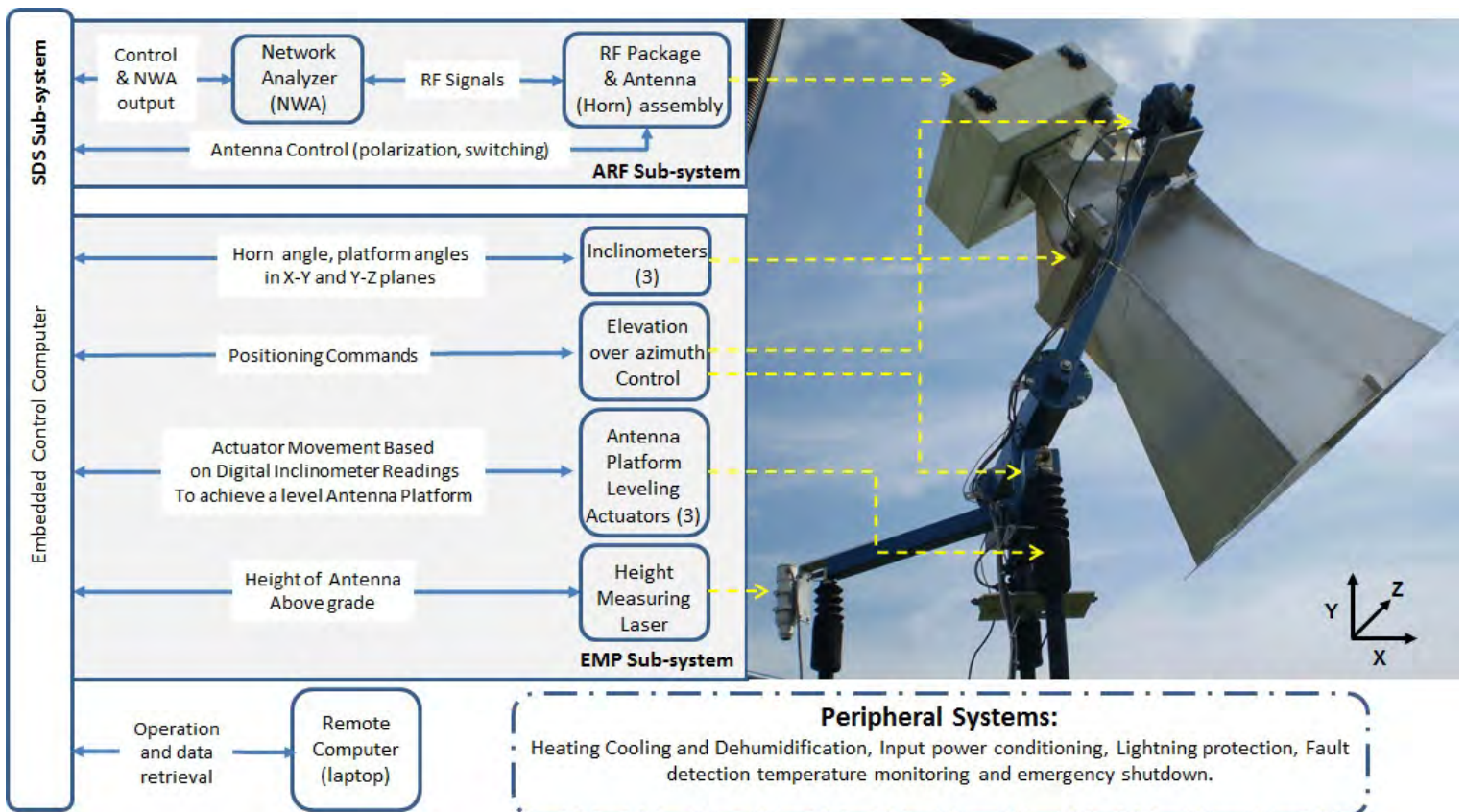


Figure 10. Sub-systems within the UF-LARS
Credits: Nagarajan et al. (2014)

Table 4. UF-LARS specifications

Parameter	Value
Center frequency	1.25 GHz
Bandwidth	300 MHz
Number of channels	4
Antenna HPBW	14.7° (E-plane)
	19.7° (H-plane)

4.4 University of Michigan Radar System

4.4.1 Microwave Observatory of Subcanopy and Subsurface (MOSS)

The Microwave Observatory of Subcanopy and Subsurface (MOSS) is an L-band tower-mounted radar (Figure 11[a]) from the University of Michigan that measures the scattering. Figure 11(b) shows the corner reflector; Figure 11(c) shows the antennae and top-mounted electronics of the radar system; and Figure 11(d) shows its ground-mounted electronics. This radar system operates at a center frequency of 1.14 GHz. It has two independent channels transmitting and receiving pulses of 50 ns yielding ~20 MHz bandwidth. Polarization of each channel is determined by the orientation of the antenna mounted. Cross-pol channels were measured by rotating one of the antennas. The look-angle of the antennas was ~40°, which is the same as the look angle used in the SMAP mission. The yagi antenna used has half-power beamwidths (HPBW) of ~32.4° in E-plane and ~41.4° in H-plane, which result in a minimum footprint size of 12 m × 18 m (50 m × 25 m assured during the measurements) at tower height of 12 m. To further focus the antenna beam in the vertical direction, the tower was raised stepwise from ~10 m to ~11.5 m during each measurement, and data were taken at more than 20 locations equally spaced with a quarter-wavelength interval. The synthesized beamwidth was ~15.3°. Calibration of the radar system had been done in the anechoic chamber at the University of Michigan. Sky calibration was taken before and after each full set of observations. Internal (the overall system except the antennae) calibration was done with every datatake, and a corner reflector was measured for absolute calibration in data post-processing. Observations of field scattering in L-band were obtained for the morning/evening during different stages of the corn growth including germination, before ear formation, and before harvest. Table 5 summarizes the system specifications.

Table 5. MOSS specifications

Parameter	Value
Center frequency	1.14 GHz
Bandwidth	20 MHz
Number of channels	4
Antenna HPBW	32.4° (E-plane)
	41.4° (H-plane)
Synthesized beamwidth	15.3°

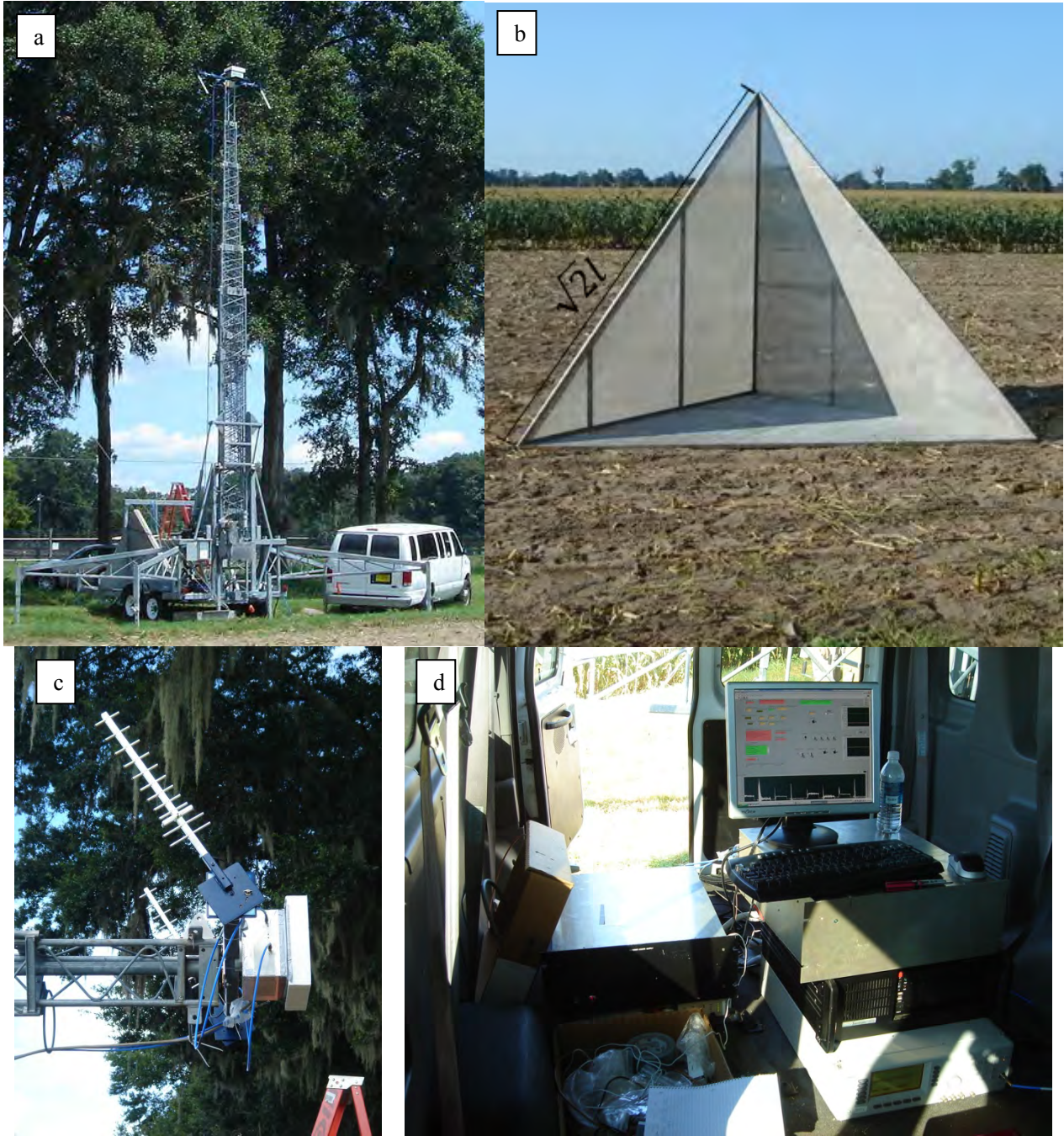


Figure 11. (a) The MOSS system, (b) corner reflector ($l = 2.4157$ m), (c) antennae and tower-mounted electronics, and (d) ground-mounted electronics
Credits: X. Duan, University of Michigan

4.4.1.1 Theory of operation

Figure 12 shows a high-level system block diagram of the radar. This radar system was designed for measurements at multiple frequencies. For this experiment the measurement frequency was specified to be 1.14 GHz. An arbitrary waveform generator is used to produce an L-band continuous wave signal for transmit. The transmit signal is routed through a switching network to either the V- (or 1-) or H- (or 2-) channels determined by the antenna orientation as mounted on the tower. The transmit/receive switches (fast switches) switch at 50 ns yielding ~ 20 MHz bandwidth is the radar single receive path. The network of switches that determine the transmit-and-receive paths are used to sequentially select the channel combinations (11 12 21 22). The received signal is filtered by the L-band filter in the

multi-frequency bank. The received signal is then mixed down to baseband and sampled in-phase and quadrature. The data are then stored on a PC for in-field and post analysis.

The spectral content of a returned signal from a point target is given as

$$E(\omega) = \frac{G \exp[-2i\omega r / c] W(\omega) H(\omega) \sigma(\omega)}{r^2}$$

where G is the two-way complex gain, $W(\omega)$ is the transmit pulse spectrum, $H(\omega)$ is the system frequency response and $\sigma(\omega)$ is the (potentially frequency dependent) radar cross-section. For nominal field operation, it is necessary to characterize the parameters G , $W(\omega)$, and $H(\omega)$ as a function of time and for each tower (antenna) position. The three steps to obtain these terms in full are the internal calibration loop; the “passive,” or corner reflector calibration; and the “active,” or transponder calibration. The internal calibration loop seen in Figure 12 characterizes the entire system except for the antennas. Therefore, it gives $W(\omega)$, $H(\omega)$, and all of G excluding the complex antenna gain. Internal calibration data are collected automatically at the beginning and end of every datatake (as detailed subsequently), and the internal calibration drift can be monitored on-screen. Figure A-5 shows the radar observations during MicroWEX-10.

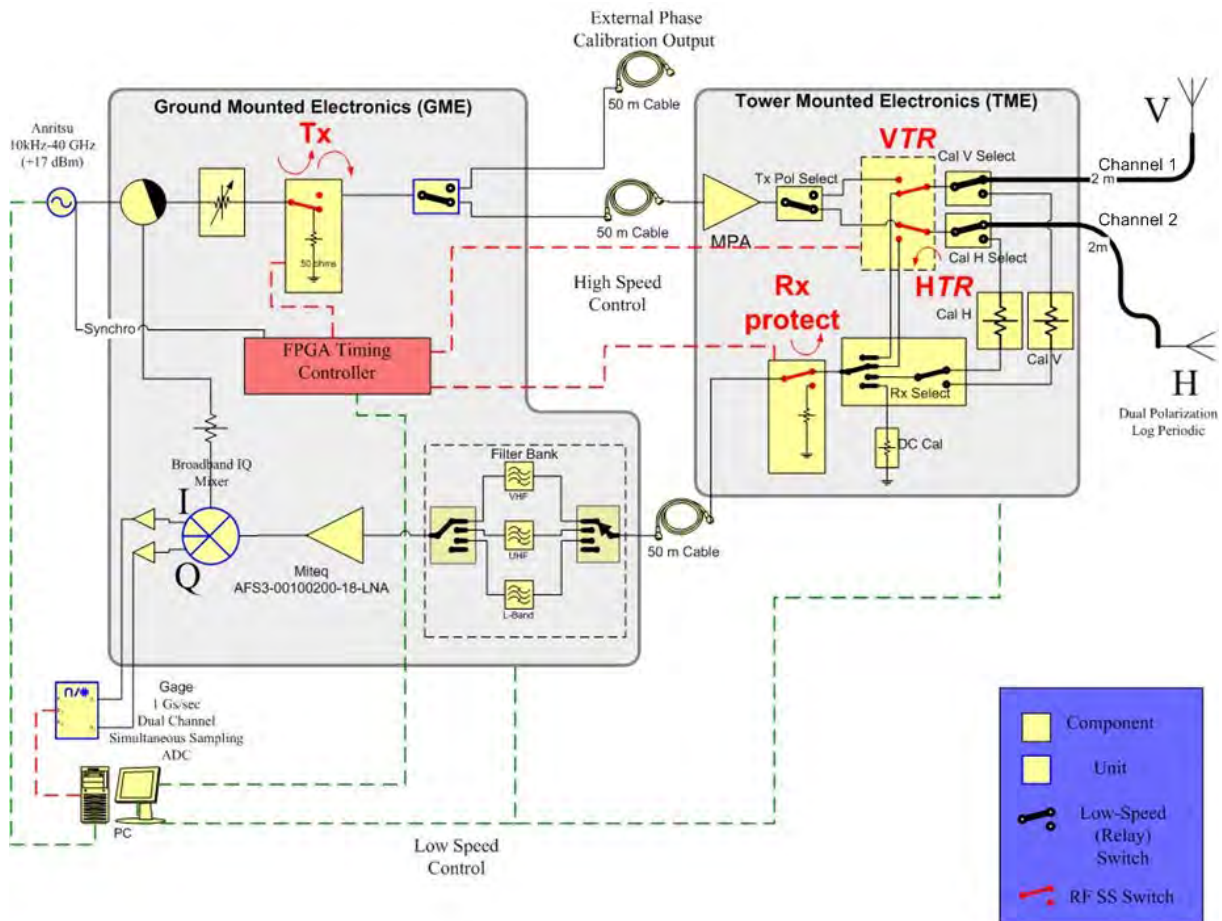


Figure 12. Block diagram of the University of Michigan’s Microwave Observatory of Subcanopy and Subsurface (MOSS).

Credits: X. Duan, University of Michigan

4.5 Net Radiometer

A Kipp and Zonen CNR-1 four-component net radiometer (Figure 13) was located in the elephant grass field, south of the C-band radiometer (as shown in Figure 3[a]), to measure up- and down-welling shortwave and longwave infrared radiation. The sensor consists of two pyranometers (CM-3) and two pyrgeometers (CG-3). The sensor was installed in the elephant grass field, south of the C-band radiometer, at the height of 2.95 m above ground and facing south on DoY 68 in 2011. On DoY 102 in 2011, the sensor was moved to a height of 4.84 m to stay above the plant canopy. Table 6 shows the list of specifications of the CNR-1 net radiometer. Figure A-6 shows the down- and up-welling solar (shortwave) and far infrared (longwave) radiation observed during MicroWEX-10.



Figure 13. CNR-1 net radiometer
Credits: J. Casanova, University of Florida

Table 6. Specifications of the CNR-1 net radiometer

Description	Value
Measurement spectrum: CM-3	305–2800 nm
Measurement spectrum: CG-3	5000–50000 nm
Response time	18 sec
Sensitivity	10–35 $\mu\text{V}/(\text{W}/\text{m}^2)$
Pt-100 sensor temperature measurement	DIN class A
Accuracy of the Pt-100 measurement	$\pm 2 \text{ K}$
Heating	Resistor 24 ohms, 6 VA at 12 volt
Maximum error due to heating: CM-3	10 W/m^2
Operating temperature	$-40^{\circ}\text{--}70^{\circ}\text{C}$
Daily total radiation accuracy	$\pm 10\%$
Cable length	10 m
Weight	4 kg
Source: Campbell Scientific (2006a)	

4.6 Air Temperature and Relative Humidity

Air temperature and relative humidity were measured every five minutes at the C-band station in the elephant grass field using a Campbell Scientific HMP45C Temperature and Relative Humidity Probe (Campbell Scientific 2006b). Figure A-7 shows the relative humidity and air temperature observations during MicroWEX-10.

4.7 Thermal Infrared Sensor

Two Apogee instruments IRR-PN thermal infrared sensors were installed during MicroWEX-10; one in the elephant grass and the other in the corn field site. Table 7 shows the list of specifications of the thermal infrared sensors.

Table 7. Specifications of the thermal infrared sensor (IRR-PN)

Description		Value
Field of view		18° half angle
Output	Target temp.	40 μ V per °C difference from sensor body
	Sensor body temp.	0–2500 mV
Accuracy	–10°C to 65°C	$\pm 0.2^\circ\text{C}$ absolute accuracy $\pm 0.1^\circ\text{C}$ uniformity $\pm 0.05^\circ\text{C}$ repeatability
	–40°C to 70°C	$\pm 0.5^\circ\text{C}$ absolute accuracy $\pm 0.3^\circ\text{C}$ uniformity $\pm 0.1^\circ\text{C}$ repeatability and uniformity
Optics		Germanium lens
Wavelength range		8–14 μm (corresponds to atmospheric window)
Response time		< 1 second to changes in target temperature
Input power		2.5 V excitation
Operating environment		–55°C–80°C; 0%–100% RH (non-condensing) Water resistant, designed for continuous outdoor use
Cable		4.5 meters twisted, shielded 4 conductor wire with Santoprene casing.
Dimensions		6 cm long by 2.3 cm diameter
Mass		190 g

4.7.1 Thermal Infrared Sensor (elephant grass)

The sensor was installed south of the C-band radiometer (as shown in Figure 3[a]) at a height of 2.5 m to observe skin temperature at nadir. On DoY 102 in 2011, the sensor was raised to 4.8 m. Figure A-8 shows the thermal infrared temperatures observed during MicroWEX-10.

4.7.2 Thermal Infrared Sensor (sweet corn)

The sensor was installed south of the radar and radiometer footprints (as shown in Figure 3[b]) at a height of 2.245 m to observe skin temperature at nadir. Figure A-9 shows the surface thermal infrared temperature observed during MicroWEX-10.

4.8 Soil Temperature Probes

Lab made temperature probes, based on Campbell Scientific 107-1 temperature sensor, were used to measure soil temperature.

4.8.1 Soil Temperature Probes (elephant grass)

Thirty-nine temperature probes were placed at depths of 2, 4, 8, 16, 32, 64, 100, 120, and 150 cm measuring every five minutes. At the C-band and L-band stations, the depths included replicates at 2, 4, 8, 16, and 32 cm. The radar station included two replicates at 2, 4, and 8 cm. Figure A-10 shows the soil temperatures observed at the depths of 2, 4, 8, 16, 32, 64, 120, and 150 cm at the L-band station during MicroWEX-10. Figure A-11 shows the soil temperatures at the same depths at the C-band station during MicroWEX-10. Figure A-12 shows the soil temperatures observed at the depths of 2, 4, 8, 16, 32, 64, and 100 cm at the radar station during MicroWEX-10.

4.8.2 Soil Temperature Probes (sweet corn)

Twenty-six temperature probes were placed at depths of 2, 4, 8, 16, 32, 64, and 100 cm measuring every five minutes. The north and the south station included 2 replicates at 2, 4, and 8 cm. Figure A-13 and Figure A-14 show the soil temperatures observed at the depths of 2, 4, 8, 16, 32, 64, and 100 cm at the north and south station, respectively, during MicroWEX-10.

4.9 Soil Moisture Probes

Campbell Scientific time-domain water content reflectometers (CS616) were used to measure soil volumetric water content. The calibration coefficients were obtained from laboratory calibration and are listed in Table 8.

Table 8. The calibration coefficients for the CS616 probe

Coefficient	Value
C_0	1.5377
C_1	0.1814
C_2	-0.0070
C_3	0.0001

4.9.1 Soil Moisture Probes (elephant grass)

Thirty-nine reflectometers were placed at depths of 2, 4, 8, 16, 32, 64, 100, 120, and 150 cm measuring every five minutes. At the C-band and L-band stations, the depths included replicates at 2, 4, 8, 16, and 32 cm. The radar station included two replicates at 2, 4, and 8 cm. Figure A-15 shows the volumetric soil moisture contents observed at the depths of 2, 4, 8, 16, 32, 64, 120, and 150 cm at the L-band station during MicroWEX-10. Figure A-16 shows the volumetric soil moisture contents observed at the same depths at the C-band station during MicroWEX-10. Figure A-17 shows the volumetric soil moisture contents observed at the depths of 2 cm, 4 cm, 8 cm, 16 cm, 32 cm, 64 cm, and 100 cm at the Radar station during MicroWEX-10.

4.9.2 Soil Moisture Probes (sweet corn)

Twenty-six reflectometers were placed at depths of 2, 4, 8, 16, 32, 64, and 100 cm measuring every five minutes. The north and the south station included two replicates at 2, 4, and 8 cm. Figure A-18 and Figure A-19 shows the volumetric soil moisture contents observed at the depths of 2, 4, 8, 16, 32, 64, and 100 cm at the north and south station, respectively, during MicroWEX-10.

4.10 Precipitation

Precipitation and overhead irrigation was determined using six tipping-bucket rain gauges with locations shown in Figure 3(a) and (b).

4.10.1 Precipitation (elephant grass)

Two tipping-bucket rain gauges, in line with the outer edge of the L-band radiometer footprint were installed on DoY 129 in 2011 at a height of 20 cm above the ground to catch both precipitation and irrigation. Figure A-20 shows the observed precipitation and overhead irrigation.

4.10.2 Precipitation (sweet corn)

Four tipping-bucket rain gauges, in line with the outer edge of the Michigan radiometer footprint and at the southeast and southwest corners of the field were installed on DoY 193 in 2011 at a height of 20 cm. The rain gauges were raised to a height of 3 m above the ground on DoY 224 in 2011 to stay above the height of the corn canopy. Figure A-21 shows the observed precipitation.

4.11 Drip Irrigation

Drip-tape with a diameter of 15.9 mm ($\frac{5}{8}$ inch) and emitters every 30.5 cm (12 inches) was installed on DoY 151 in 2011 in the elephant grass field (Figure 14). The specified flow rate was 0.5 gpm/100 ft. In the north side of the field, where intensive monitoring was typically conducted, three drip tapes per row were installed (Figure 14). In other areas of the field, one drip tape per row was installed. Drip irrigation occurred on DoY 209, DoY 217, DoY 220, DoY 230, DoY 245, DoY 256, DoY 278, and DoY 280 in 2011. On DoY 4 and DoY 5 in 2012, measurements were taken using a flow meter in six locations of the field. Figure A-22 shows the observed flow measurements.



Figure 14. Irrigation via drip-tape
Credits: D. Preston, UF/IFAS

5. VEGETATION SAMPLING AT THE ELEPHANT GRASS SITE

Vegetation properties in four spatially distributed sampling locations, as shown in Figure 3(a), were measured from DoY 74 until DoY 312 in 2011 during the field experiment. The first sampling occurred in all four locations of the field on DoY 74 in 2011. Starting on DoY 111 in 2011 biweekly sampling occurred until DoY 279 in 2011 with a sampling in the northern sections of the field on DoY 312 and DoY 342 in 2011. A vegetation sampling consisted of measurements of clump height and width, as well as tiller height, width, biomass, LAI, and geometric description of the plant. Vertical distribution of moisture in the canopy was also measured when the canopy reached 4.5 m. Two sampling locations were located where Merkron was planted in the north end of the field, while the other sampling locations included N-51 in the southwest location and N-13 in the southeast location of the field. Each sampling included one row of elephant grass in the four sampling locations. The sampling length started between two clumps and ended at the next midpoint between clumps that was greater than or equal to 4 m from the starting point.

5.1 Clump and Tiller Count

The clumps and tillers were counted for each sampling length in each of the four sampling areas. Before DoY 181 in 2011, when the tillers were not uniform in height, three representative clumps were chosen to determine the percentages of small, medium, and large tillers in the sampling area. Figure A-23 and A-24 show the clumps and tillers per square meter.

5.2 Clump Height and Width

Maximum clump height and width were measured by placing a tape measure at the soil surface adjacent to the stems to the maximum height of the clump. The clump width, parallel to the row, was measured at the base of the clump. Before DoY 209 in 2011, all clump heights and widths were measured in the sampling area described in 5.1. From DoY 209 in 2011 until the end of the season, measurement of the maximum clump height was taken from 1–3 sample clumps. Figures A-25 and A-26 show the average of the maximum clump heights and widths during MicroWEX-10.

5.3 Tiller Height and Width

One to three representative tillers were selected from the 10 sample tillers to obtain heights and widths. Tiller height and width were measured by placing a tape measure at the soil surface adjacent to the stem up to the maximum height of the crop. The maximum width of the tiller (parallel or perpendicular to the row) was also measured. Figures A-27 and A-28 show the maximum tiller height and width during MicroWEX-10.

5.4 Wet and Dry Biomass

Using the sampling area, 10 tillers each of representative small, medium, and large were chosen from the three clumps in section 5.1. Each tiller was cut at the base, separated into leaves and stems, and weighed immediately. The samples were dried in the oven at 60°C for one week for leaves and two weeks for stems. Figure A-29 shows the wet and dry biomass (in kg/m²) observed during MicroWEX-10 for the four sampling areas.

5.5 LAI

LAI was measured with destructive sampling implementing Equation 1. Using the 1–3 tillers selected in section 5.3, the leaves were separated from the stems. The length and width of the green leaves were measured. The specific leaf area (SLA) in Equation 1 was calculated, assuming a leaf as an ellipse (Boote 1994). The green leaves, senesced leaves, and the stems were then dried in an oven at 60°C for 48–72 hours to measure the dry weight of the leaves and the dry biomass of the sample. The ratio of the leaf dry weight to the sample dry biomass was used to calculate the fraction of leaf (F_{LEAF}). The total dry biomass (DM) was obtained in section 5.4.

$$LAI = DM \cdot F_{LEAF} \cdot SLA \quad (\text{Equation 1})$$

The LAI obtained is shown in Figure A-30.

5.6 Vertical Distribution of Moisture in the Canopy

The vertical distribution measurement was conducted on DoY 270 in 2011 during MicroWEX-10. The sampling consisted of one representative tiller from the northwest area. The tiller was cut at the base and laid with the leaves arranged to closely match their natural orientation in the field as shown in Figure 15. The tiller was cut every 20 cm. The sample in each layer was weighed, both fresh and after drying in the oven at 60°C for 48 hours. Figure A-31 shows the wet and dry weights as a function of crop height during MicroWEX-10.



Figure 15. Tiller sample marked and ready to be subdivided into 20 cm layers
Credits: T. Bongiovanni, UF/IFAS

5.7 Geometric description

A geometric description of the tiller consisted of the leaf height from the ground and the maximum length and width of each green leaf of the 1–3 representative tillers in section 5.3. The stem circumference was measured by using a string to wrap around the base and around the tip of the plant to calculate the diameter of the stem. The stem length was measured from the base of the tiller to the base of the last leaf. Figure A-32 (a–b) shows the height of each leaf. The leaf length and width are shown in Figures A-33 (a–b) and A-34 (a–b). The stem length and diameter observed are shown in Figure A-35 and A-36.

6. VEGETATION SAMPLING AT THE SWEET CORN SITE

Vegetation properties in two sampling locations as shown in Figure 3(b) were measured weekly during the field experiment. A vegetation sampling consisted of measurements of height, width, biomass, LAI, geometric description of the plant, and vertical distribution of moisture in the canopy. The crop density derived from the stand density (6.3 plants per m²) and row spacing (36") was measured at the first sampling (DoY 196). The first two vegetation sampling on DoY 196 and DoY 200 in 2011 did not include measurements of moisture distribution in the canopy or stem diameter. After the initial two vegetation samplings, seven vegetation samplings were conducted on DoY 207, DoY 214, DoY 221, DoY 229, DoY 236, DoY 243, and DoY 250 in 2011.

6.1 Height and Width

Crop height and width were measured by placing a measuring stick at the soil surface adjacent to the stem up to the maximum height of the crop. The maximum canopy width of the plant (parallel or perpendicular to the row) was also measured. Four representative plants were selected to obtain heights and widths inside each vegetation sampling area. Figure A-37 shows the average maximum crop heights and widths during MicroWEX-10.

6.2 Wet and Dry Biomass

Each sampling included one row of corn in the four sampling locations. The sampling length started between two plants and ended at the next midpoint between plants that was greater than or equal to one meter away from the starting point. The plants within this length were cut at the base, separated into leaves, stems, and ears, and weighed immediately. The samples were dried in the oven at 60°C for one week and weighed. Figure A-38 shows the wet and dry biomass observed during MicroWEX-10 for the four sampling areas.

6.3 LAI

Destructive LAI was measured by taking two representative plants in the sampling area and separating the leaves. The leaves and the rest of the plant were then dried in an oven at 60°C for one week to measure the dry weight of the leaf and the dry biomass of the sample. The ratio of the leaf dry weight to the dry biomass was used to calculate the fraction of leaf (F_{LEAF}) in Equation 1. The length and width of each individual leaf of the four sample plants were also measured. Assuming a leaf as an ellipse, the area of the leaves was summed and divided by the dry mass of the leaves to calculate the specific leaf area (SLA) in Equation 1. The total dry biomass (DM) was found using the procedure in 5.2. Equation 1 was then used to determine the destructive LAI (Boote 1994). The LAI obtained is shown in Figure A-39.

6.4 Vertical Distribution of Moisture in the Canopy

The wet and dry biomass of discrete vertical layers of individual corn plants was measured. Seven samplings were conducted during MicroWEX-10. Each sampling was conducted by selecting a representative plant at each sampling location. The plants were taken out of the ground with the roots still attached and taken indoors to prevent moisture loss. Each plant sample was carefully laid out on a metal sheet with grid spacing of 2 cm. The leaves were arranged to closely match their natural orientation in the field. The stem was cut every 10 cm as shown in Figure 16. The sample in each layer was weighed, both fresh and after drying in the oven at 60°C for 48 hours. Figure A-40 shows the wet and dry weights as a function of crop height during MicroWEX-10.



Figure 16. Subdividing plant samples into 10 cm layers
Credits: D. Preston, UF/IFAS

6.5 Geometric description

A geometric description of the plant consisted of the maximum length and width of each leaf of the sample plants, as shown in Figure 17. The stem circumference was measured by using a string to wrap around the base and around the tip of the plant to calculate the diameter of the stem. The ear length was measured while still in the husk from the base of the cob near the stem to the top, and the maximum circumference of the ear was measured by using a string. The stem length and diameter observed are shown in Figure A-41. Figure A-42 shows the height of each leaf. The leaf length and width are shown in Figures A-43 and A-44. The ear height, length, and diameter are shown in Figure A-45. The ear and leaf angles were measured from a digital photograph of a single plant taken while still in the field at each sampling area using a reference length such as a meter stick. The angle between the leaf and the stem (θ_1), the angle of the leaf fold (θ_2), and the ear angle (θ_e) were measured using an angle gage, as shown in Figure 18. See Figures A-46 and A-47 for the value of θ_1 and θ_2 . Figure A-48 shows the ear angle for each ear.

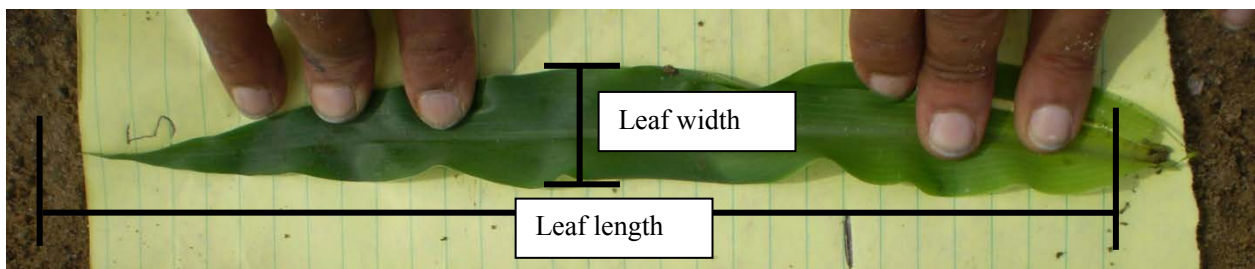


Figure 17. Leaf length and width
Credits: D. Preston, UF/IFAS

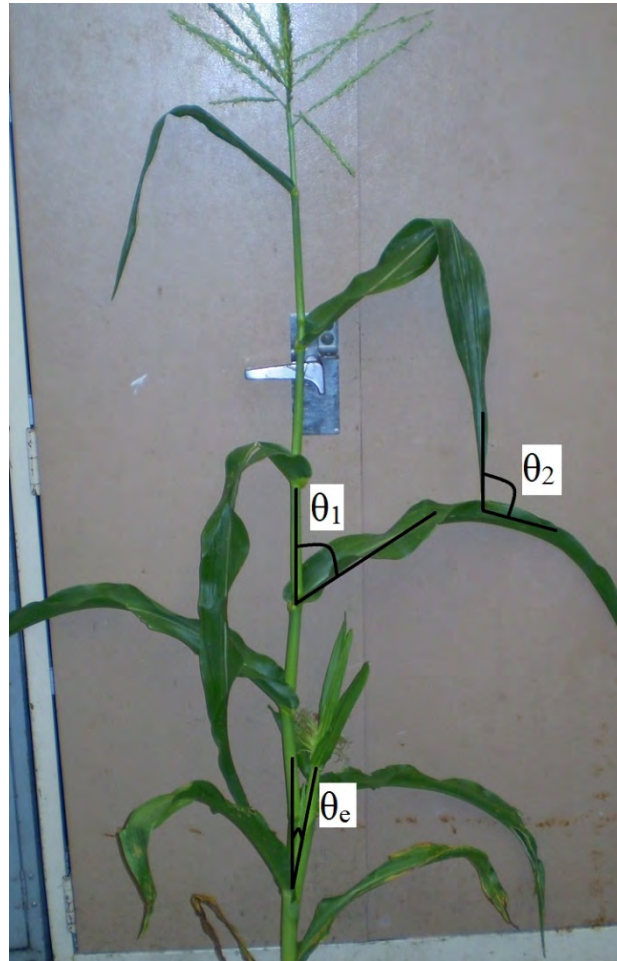


Figure 18. Leaf angles and ear angle location
Credits: R.Terwilliger, UF/IFAS

7. WELL SAMPLING

7.1 Water level measurement

The water level measurement was processed by the Levellogger from Solinst Canada Ltd. The Levelloggers were installed at the northern wells in the elephant grass field and set to automatically record the water level every 30 minutes. The data were downloaded onto a laptop during the well sampling. Figure A-49 shows the water table elevation and depth during MicroWEX-10.

8. SOIL SAMPLING

8.1 Soil Analysis

Soil sampling from two locations in the corn field and two locations in the elephant grass field was done on DoY 174 in 2011 and from four locations of the elephant grass field on DoY 208 in 2011. Samples included organic matter, texture analysis, and full (10, 18, 32, 56, 100, 316, 1000, and 1500 kPa) and partial (10 and 1500 kPa) moisture curves from depths of 1–10, 10–40, 40–90, and 90–120 cm for the corn field and 0–15, 15–40, 40–70, and 70–100 cm for the elephant grass site (Figure A-50). The texture analysis was conducted at the elephant grass field site for depths of 0–10 cm for two locations and 0–15 cm for four locations of the field (Table 9). The texture analysis was conducted at the corn field site for depths of 0–10 cm in two locations of the field (Table 10). Organic matter, bulk density, and saturated hydraulic conductivity in the elephant grass field was conducted for depths of 0–15, 15–40, 40–70, and 70–100 cm for four locations in the field. Organic matter and saturated hydraulic conductivity in the corn field was conducted for depths of 0–10, 10–40, and 40–90 cm for one location and 0–10, 10–40, 40–90, and 90–120 cm for the other location in the field. Bulk density in the corn field was conducted twice for depths of 0–10, 10–40, and 40–90 cm for one location and 0–10, 10–40, 40–90, and 90–120 cm for the other location in the field.

Table 9. The soil physical properties for elephant grass field site (percentages are given on a weight basis)

Elephant Grass Soil Physical Properties												
	Sand (%)		Silt (%)		Clay (%)		OM (%)		KSAT (cm/hr)		Bulk Density (g/cm ³)	
Depth	Avg	SD	Avg	SD	Avg	SD	Avg	SD	Avg	SD	Avg	SD
0–10	94.360	0	2.000	0	3.64	0	-	-	-	-	-	-
0–15	92.443	0.688	2.668	0.471	4.890	0.500	2.268	0.676	527	456	1.416	0.165
15–40	-	-	-	-	-	-	2.248	0.662	102	43	1.630	0.088
40–70	-	-	-	-	-	-	1.310	0.633	276	82	1.497	0.194
70–100	-	-	-	-	-	-	1.115	0.630	277	73	1.395	0.112

Table 10. The soil physical properties for the corn field site (percentages are given on a weight basis)

Corn Soil Physical Properties												
	Sand (%)		Silt (%)		Clay (%)		OM (%)		KSAT (cm/hr)		Bulk Density (g/cm ³)	
Depth	Avg	SD	Avg	SD	Avg	SD	Avg	SD	Avg	SD	Avg	SD
0–10	93.525	1.181	2.335	0.474	4.140	0.707	1.505	0.049	100	36	1.515	0.178
10–40	-	-	-	-	-	-	1.625	0.233	95	45	1.689	0.033
40–90	-	-	-	-	-	-	0.620	0.113	127	0	1.544	0.164
90–120	-	-	-	-	-	-	0.790	-	152	-	1.632	0.085

8.2 Soil Surface Roughness

Soil roughness was measured near the radiometer footprints in the corn field on DoY 160, 162, 182, 200, 227, and 231 in 2011 with a traditional grid board method (Table 11). The 2D surface profiles in directions parallel and perpendicular to the row structure were measured using a 2 m long grid board. Jang et al. (2005) describes the grid board method in detail. Table 12 lists the root mean square height and correlation length measurements parallel and perpendicular to the row structure.

Table 11. Soil surface roughness measurements using 2 m long grid board








DoY (2011)	Parellel to row structure	Perpendicular to row structure
160 Before Plowing	-	
160 After Plowing	-	
162	-	
182 Before Plowing		
182 After Plowing		
200		
227		
231		

Table 12. Soil surface roughness measurements of root mean square height (s) and correlation length (cl)

DoY	Parallel to row structure		Perpendicular to row structure	
	s (cm)	cl (cm)	s (cm)	cl (cm)
160 Before Plowing	-	-	0.78	7.40
160 After Plowing	-	-	1.30	6.91
162	-	-	1.60	7.62
182 Before Plowing	0.25	20.44	0.66	20.92
182 After Plowing	0.90	13.40	1.74	8.76
200	0.41	13.69	1.07	12.57
227	0.86	11.95	0.62	13.88
231	0.42	9.95	0.69	14.98

9. OBSERVATIONS

For the microwave radiometric observations at C-band, the horizontally polarized brightness temperatures were found to be more sensitive to soil moisture than vertically polarized brightness temperatures during the short vegetation cover periods (Figure A-1). As the vegetation grew, it effectively masked the contribution of microwave emission from soil resulting in sensitivity decrease at both polarizations. Due to its higher penetration capability, the observations at lower frequencies (longer wavelengths), such as the L-band, were more sensitive to soil moisture during the growing season than at the higher frequencies of C-band (Figure A-2). The σ_{VV}^0 was more sensitive to the vertical structure of growing vegetation in the mid- and late-stages of crop growth (Figure A-3–A-4).

The first row in Figure A-5 shows the measurements of the field of germinating corn. The signature of the return signal does not change much from the bare soil measurements, as expected. The second row in Figure A-5 presents the measurements of the field when the corn grew approximately 1 meter tall before earing. More features appear in the return signals even after 600 ns. Both the HH and VV measurements show larger ground return signals. The cross polarization components are also measured, showing similar signature as the co-pol components. This becomes clearer in the third row of Figure A-5, showing the measurements of the corn field right before harvest.

The average down-welling shortwave radiation average was 206.22 W/m² during the growing season while the average up-welling shortwave radiation was 38.93 W/m² (Figure A-6). The average relative humidity was 79.89% while the average air temperature was 294.76 K (Figure A-7). The average thermal infrared temperature was 287.70 K and 300.78 K for the elephant grass and corn field, respectively (Figure A-8–A-9). The rain gauges below the canopy in the elephant grass field tended to give diverse readings, which could be due to canopy cover (Figure A-20–A-21). Figure A-22 shows that the flow meter measurements of the drip tape were highest at the main line and decreased as the drip tape went into the field. The water table gradually decreased as the year progressed (Figure A-49). The field capacity (10 kPa) for the elephant grass field site was higher than the corn site; however, the wilting point (1500 kPa) was similar (Figure A-50).

During the beginning of the season when vegetation was low, diurnal variations in soil temperature were maximum, while later in the season the diurnal variations were minimal. Diurnal variations for soil temperatures at 64 cm and below were minimal throughout the season (Figure A-10–A-14). The change in soil moisture in the deeper layers was minimal during light rains (Figure A-15–A-19).

The average clump density for the elephant grass was 0.9 clump/m² (Figure A-23). The tiller density started high before decreasing and reaching equilibrium (Figure A-24). The maximum height of the canopy was the highest at the NW vegetation sampling area, reaching 5.3 m, while the NE and SW area were the lowest, with a maximum height of 4.2 m (Figure A-25). The average clump width was 0.42 m (Figure A-26). The maximum height of the sample tillers was the highest at the NW vegetation sampling area, reaching 5.4 m, while the NE area was the lowest, with a maximum height of 4.0 m (Figure A-27). The widest maximum width of the sample tiller was an average of 2.22 m for the SW vegetation sampling areas (Figure A-28). The biomass of the plant increased before reaching a maximum and then decreased slightly (Figure A-29). The LAI increased before reaching a maximum of 12.7 m²/m², and then decreased due to leaf senescence (Figure A-30). The moisture per 10 cm section in the plant remained relatively constant due to the stem until there was a decrease with the lowest amount of moisture located at the top of the plant (Figure A-31). The maximum number of leaves in the NE vegetation sampling area was 38 leaves, while the SE vegetation sampling area had a maximum of 62 leaves due to the increased number of tillers (Figure A-32). The maximum leaf length was 1.46 m (Figure A-33) and the maximum leaf width was 0.055 m (Figure A-34). The length of the stem increased until DoY 200 when it leveled out (Figure A-35). The average minimum diameter was 0.012 m, while the average maximum diameter was 0.018 m (Figure A-36).

The maximum height of the sweet corn was the same for both vegetation sampling area, reaching 1.7 m (Figure A-37). The maximum width of the sweet corn plant was 0.95 m at the north vegetation sampling areas (Figure A-37). The biomass of the plant continued to increase in the south sampling area while the biomass in the north sampling area reaching an equilibrium after DoY 236 in 2011 (Figure A-38). The LAI increased before reaching a maximum of 3 m²/m², and then decreasing slightly due to leaf senescence (Figure A-39). During ear formation the moisture per 10 cm section in the plant was higher at the ear location (Figure A-40). The length of the stem increased until DoY 236 in 2011 when it leveled out (Figure A-41). The average minimum diameter was 0.009 m while the average maximum diameter was 0.023 m (Figure A-41). The maximum number of leaves in the south vegetation sampling area was 20 (Figure A-42). The maximum leaf length was 0.84 m (Figure A-43) and the maximum leaf width was 0.095 m (Figure A-44). Each plant had 1–2 ears, with the highest ear not exceeding 0.60 m above the base (Figure A-45). The ear located highest on the plant was bigger in both length and diameter than the other ears on the plant (Figure A-45). For the leaf angles, θ_1 ranged from 0°–90° from the vertical (Figure A-46) while θ_2 ranged from 90°–180° (Figure A-47). The ear angle, θ_e , was larger for the bigger ears (Figure A-48).

10. ELEPHANT GRASS FIELD LOG

Note: Time is in Eastern Standard Time.

March 1 (DoY 60)

	Buried L-band station sensor 2–32 cm north pit
	Marked vegetation sampling areas in 60'–75' (10 rows × 75')
	L-band radiometer was mounted (looking angle 45°)
	Marked L-band footprint

March 2 (DoY 61)

8:50	Attached guy wires to C-band
	Installed L-band station pole

March 4 (DoY 63)

	Timer of L-band radiometer fixed
--	----------------------------------

March 7 (DoY 66)

9:45	Buried L-band station sensor 2–150 cm south pit
------	---

March 9 (DoY 68)

	Installed CNR at 2.95 m
	Installed TIR pole
	Installed low rain gauges
	Buried C-band station soil sensors

March 15 (DoY 74)

	Elephant grass vegetation sampling
--	------------------------------------

March 22 (DoY 81)

	Took L-band radiometer out of field to burn
	Removed sensors from field

April 12 (DoY 102)

	Reburied sensors
--	------------------

April 18 (DoY 108)

	L-band radiometer mounted (looking angle 40°)
--	---

April 21 (DoY 111)

	Elephant grass vegetation sampling NE and NW
--	--

April 25 (DoY 115)

9:45	L-band radiometer calibration
------	-------------------------------

May 4 (DoY 124)

10:00	L-band radiometer calibration
-------	-------------------------------

May 5 (DoY 125)

	Elephant grass vegetation sampling NE, NW, SE, and SW
--	---

May 6 (DoY 126)

	C-band radiometer mounted (angle 90°)
--	---------------------------------------

May 9 (DoY 129)

	C-band radiometer error msg: overheat shutdown
	Hooked by C-band radiometer rotator
	Installed NE and NW rain gauges

May 11 (DoY 131)

14:50	L-band radiometer calibration
-------	-------------------------------

May 12 (DoY 132)

14:50	C-band radiometer troubleshooting
-------	-----------------------------------

May 13 (DoY 133)

	Rebooted C-band radiometer
	Adjusted gain and offset for C-band radiometer

May 16 (DoY 136)

10:35	L-band radiometer calibration
	Adjusted gain and offset for C-band radiometer
	C-band radiometer calibration

May 17 (DoY 137)

10:35	L-band radiometer calibration
-------	-------------------------------

May 19 (DoY 139)

10:35	L-band radiometer calibration
	Elephant grass vegetation sampling NE, NW, SE, and SW

May 24 (DoY 144)

14:30	C-band radiometer calibration
15:20	L-band radiometer calibration
	TIR pole knocked down
	Measured CNR height: 4.84 m

May 31 (DoY 151)

	Installed drip tape
	Lowered CNR
	Raised CNR

June 1 (DoY 152)

9:40	C-band radiometer calibration
10:20	L-band radiometer calibration
12:00	Lowered CNR

June 2 (DoY 153)

	Elephant grass vegetation sampling NE, NW, SE, and SW
10:00	Raised CNR
12:00	Lowered CNR

June 3 (DoY 154)

	Raised CNR
--	------------

June 7 (DoY 158)

10:35	C-band radiometer calibration
11:20	L-band radiometer calibration
10:00	Lowered CNR

June 8 (DoY 159)

13:30	Raised CNR
-------	------------

June 9 (DoY 160)

10:15	C-band radiometer calibration
11:03	L-band radiometer calibration

June 16 (DoY 167)

9:10	C-band radiometer calibration
10:05	L-band radiometer calibration
	Elephant grass vegetation sampling NE, NW, SE, and SW

June 23 (DoY 174)

9:25	C-band radiometer calibration
10:20	L-band radiometer calibration

June 29 (DoY 180)

10:00	L-band radiometer calibration
10:50	C-band radiometer calibration

June 30 (DoY 181)

8:30	Elephant grass vegetation sampling NE, NW, SE, and SW
------	---

July 7 (DoY 188)

11:25	C-band radiometer calibration
12:20	L-band radiometer calibration

July 14 (DoY 195)

10:30	C-band radiometer calibration
11:16	L-band radiometer calibration
	Elephant grass vegetation sampling NE, NW, SE, and SW

July 21 (DoY 202)

9:20	C-band radiometer calibration
10:05	L-band radiometer calibration

July 26 (DoY 207)

	Replaced C-band station 8 cm and 32 cm thermistors with new model in north pit
	Fixed two TDRs on C-band station

July 27 (DoY 208)

	Soil sampling in elephant grass field in skip row
--	---

July 28 (DoY 209)

8:50	Elephant grass vegetation sampling NE, NW, SE, and SW
9:00	C-band radiometer calibration
10:05	L-band radiometer calibration
9:25	Drip tape turned on

August 2 (DoY 214)

	Replaced C-band station 2, 4, and 16 cm thermistors with new model in north pit
	Connected C-band-thermistors

August 4 (DoY 216)

9:17	L-band radiometer calibration
10:17	C-band radiometer calibration
	Replaced L-band station 64 and 120 cm thermistors
	C-band 32 cm thermistor output writing to wrong array

August 5 (DoY 217)

7:30	Drip irrigation ~ 5 hrs
	Fixed hole in drip irrigation at C-band north pit

August 8 (DoY 220)

	Drip irrigation ~ 24 hrs
--	--------------------------

August 11 (DoY 223)

	Elephant grass vegetation sampling NE, NW, SE, and SW
--	---

August 12 (DoY 224)

9:16	L-band radiometer calibration
9:32	C-band radiometer calibration
	Power failure in evening

August 18 (DoY 230)

	Drip Irrigation
9:06	C-band radiometer calibration
9:36	L-band radiometer calibration

August 25 (DoY 237)

	Elephant grass vegetation sampling NE, NW, SE, and SW
	C-band was set to incident angle of 52° changed back to 45°

August 26 (DoY 238)

8:47	C-band radiometer calibration
9:18	L-band radiometer calibration
	Moved radar to elephant grass field

August 28 (DoY 240)

	Radar stopped
--	---------------

August 29 (DoY 241)

	Restarted radar
	Cleared skip row to get to radar center
	Buried sensors for radar station

August 30 (DoY 242)

	Stopped radar to look for laser height
	Restarted radar

August 31 (DoY 243)

	Set up pole with board for height measurement
14:45	Radar stopped working

September 1 (DoY 244)

	Radar calibration
--	-------------------

September 2 (DoY 245)

	Brought radar down to work on restart
	Drip irrigation

September 6 (DoY 249)

	Power failure
--	---------------

September 7 (DoY 250)

9:35	C-band radiometer calibration
10:15	L-band radiometer calibration
	Switched UPS battery
	Moved radar to corn field

September 8 (DoY 251)

	Elephant grass vegetation sampling NW and SW
--	--

September 13 (DoY 256)

	Drip irrigation ~5 hrs
	Wired in radar station, started program

September 15 (DoY 258)

9:20	C-band radiometer calibration
9:50	L-band radiometer calibration
	Moved radar to elephant grass field
	Fixed thermistors on L-band station- found corrosion

September 20 (DoY 263)

9:28	Michigan radiometer calibration
	Moved Michigan radiometer to elephant grass field
	Power failure on C-band and L-band radiometer

September 21 (DoY 264)

9:24	C-band radiometer calibration
9:50	L-band radiometer calibration
10:20	Michigan radiometer calibration

September 22 (DoY 265)

	Elephant grass vegetation sampling NW and SW
--	--

September 27 (DoY 270)

9:27	L-band radiometer calibration
10:20	C-band radiometer calibration
	Michigan radiometer power failure
	Unplugged Michigan radiometer's UPS
	Michigan radiometer calibration
	Radar stopped

September 30 (DoY 273)

	Michigan radiometer power failure
--	-----------------------------------

October 3 (DoY 276)

	Changed the GFI breaker to normal for Michigan radiometer
--	---

October 5 (DoY 278)

	Drip irrigation ~5 hrs
--	------------------------

October 6 (DoY 279)

11:32	L-band radiometer calibration
	C-band radiometer calibration
	Michigan radiometer calibration
	Elephant grass vegetation sampling NW and SW

October 7 (DoY 280)

	Drip irrigation ~5 hrs
--	------------------------

October 10 (DoY 283)

	Power failure Restarted radiometers
--	--

October 11 (DoY 284)

	Restarted radar
--	-----------------

October 13 (DoY 286)

	Radar failed
	Michigan radiometer calibration
9:25	L-band radiometer calibration
10:12	C-band radiometer calibration

October 17 (DoY 290)

14:57	Michigan radiometer calibration
-------	---------------------------------

October 20 (DoY 293)

9:47	Michigan radiometer calibration
9:50	L-band radiometer calibration
10:47	C-band radiometer calibration

October 24 (DoY 297)

14:50	Michigan radiometer calibration
-------	---------------------------------

October 27 (DoY 300)

9:35	C-band radiometer calibration
9:53	Michigan radiometer calibration
	Power for truck failed
	L-band radiometer calibration

October 28 (DoY 301)

14:46	Michigan radiometer calibration
	Michigan radiometer rotator failed

November 3 (DoY 307)

9:58	L-band radiometer calibration
10:35	C-band radiometer calibration

November 8 (DoY 312)

	Elephant grass vegetation sampling NE and NW
--	--

November 10 (DoY 314)

9:06	C-band radiometer calibration
9:47	L-band radiometer calibration

November 17 (DoY 321)

	Radar stopped
1:55	L-band radiometer calibration
2:32	C-band radiometer calibration
	South flowering completed
	North ready to flower
	Fixed station time
	Michigan rotator fixed
	Michigan radiometer calibration

November 22 (DoY 326)

9:10	Michigan radiometer calibration
9:10	L-band radiometer calibration
9:47	C-band radiometer calibration

November 25 (DoY 329)

	Radar not moving
17:33	Connected and restarted radar

December 6 (DoY 340)

	Radar not moving
10:00	L-band radiometer calibration
10:05	Michigan radiometer calibration
10:32	C-band radiometer calibration
11:32	Restarted radar

December 8 (DoY 342)

	Elephant grass vegetation sampling NE and NW
	Started to remove sensors

December 19 (DoY 353)

9:18	C-band radiometer calibration
10:02	L-band radiometer calibration
	Uninstalled C-band radiometer

January 4 (DoY 4)

	Drip tape initial measurements
--	--------------------------------

January 5 (DoY 5)

	Drip tape measurements
	Uninstalled radar

January 25 (DoY 25)

	Burned field
--	--------------

11. SWEET CORN FIELD LOG

June 2 (DoY 153)

8:30	Sensors for bare soil installed in corn field—3 pits, 13 sensors total
------	--

June 5 (DoY 156)

8:30	UM bare soil measurements
------	---------------------------

June 9 (DoY 160)

12:30	Sensors taken out of field (TDR at NE 4 cm and thermistor at NE 8 cm were disturbed upon arrival)
	Field plowed
	Sensors reinstalled into bare soil field

June 24 (DoY 175)

8:30	Upon arrival 2 cm and 4 cm TDR and thermistor in SW pit were disturbed (possible animal)
	TDRs for SE pit were switched out for longer TDRs

June 28 (DoY 179)

8:30	Moved bare soil stations
------	--------------------------

July 1 (DoY 182)

8:30	Moved bare soil stations due to flooding on northwest of corn field
15:30	Data collection begins
	Soil roughness measurements using grid board
18:00	Power failure Michigan radiometer

July 4 (DoY 185)

17:30	Power outage for UF radar
-------	---------------------------

July 5 (DoY 186)

10:00	Power restarted on Michigan radiometer
	Removed sensors for planting
	Thermal infrared: 2 m 24.5 cm
	Michigan radiometer boom angle 53°, incident angle 40°
	Corn planting

July 6 (DoY 187)

17:30	South station installed
-------	-------------------------

July 7 (DoY 188)

	Michigan radiometer calibration
--	---------------------------------

July 11 (DoY 192)

	Emergence of corn
	Herbicide spray
	Wire north station

July 12 (DoY 193)

	Installed rain gauges
--	-----------------------

July 13 (DoY 194)

	North station complete
	University of Michigan arrives
	Two TDRs not working

July 14 (DoY 195)

	Radar motor installed
--	-----------------------

July 15 (DoY 196)

	Corn vegetation sampling
--	--------------------------

July 17 (DoY 198)

	University of Michigan leaves
--	-------------------------------

July 18 (DoY 199)

	Troubleshooting two TDRs
	Michigan radiometer calibration

July 19 (DoY 200)

	Corn vegetation sampling
	Moved rain gauges
	Radar calibration
	Soil roughness measurements using grid board

July 20 (DoY 201)

7:41	Radar stopped due to power fluctuation
14:56	Restarted radar

July 22 (DoY 203)

	Radar stopped due to A/C unit
9:26	Restarted radar

July 25 (DoY 206)

	West hobos not communicating
--	------------------------------

July 26 (DoY 207)

5:56	Radar stopped
	Corn vegetation sampling
10:00	North station sensors ran over by mower
11:56	Restarted radar
	Replaced C-band station 8 cm and 32 cm thermistors with new model in north pit
	Fixed two TDRs on C-band station

July 27 (DoY 208)

8:26	Restarted radar due to slow movement
9:06	North station repaired

July 29 (DoY 210)

13:00	Corn fertilizer application
-------	-----------------------------

August 1 (DoY 213)

4:41	Radar stopped
10:26	Restarted radar
	Michigan radiometer = adjusted H-pol

August 2 (DoY 214)

	Replaced C-band station 2, 4, and 16 cm thermistors with new model in north pit
	Connected C-band thermistors
	Michigan radiometer = adjusted H-pol
	Michigan truck boom not working

August 3 (DoY 215)

	Michigan truck boom fixed
	Michigan radiometer calibration

August 7 (DoY 219)

20:00	Radar stopped due to power surge
-------	----------------------------------

August 8 (DoY 220)

12:32	Restarted radar
-------	-----------------

August 9 (DoY 221)

8:41	Restarted radar for correct time-offset
	Corn vegetation sampling in south

August 10 (DoY 222)

	Corn vegetation sampling in north
--	-----------------------------------

August 11 (DoY 223)

	Checked Michigan radiometer
--	-----------------------------

August 12 (DoY 224)

10:30	Michigan radiometer calibration
	Corn is tasseling
	10 ft rain gauge poles installed to stay above the canopy
	SW and NE pits redug; replaced NE 8 cm thermistor
	Power failure in evening

August 14 (DoY 226)

	Michigan radiometer calibration
--	---------------------------------

August 15 (DoY 227)

	Michigan radiometer calibration
	Soil roughness measurements using grid board
	Coax cable replaced for Michigan radiometer H-pol
	Power supply installed for Michigan radiometer

August 16 (DoY 228)

	Downloaded Michigan radiometer
	Ear formation beginning
15:48	Power failure on Michigan radiometer due to power cable getting run over by irrigation system

August 17 (DoY 229)

	Corn silking ~15%
	Michigan radiometer calibration

August 18 (DoY 230)

	Michigan radiometer calibration
--	---------------------------------

August 19 (DoY 231)

	Soil roughness measurements using grid board
	Michigan radiometer calibration

August 23 (DoY 235)

10:03	Michigan radiometer calibration
-------	---------------------------------

August 24 (DoY 236)

9:17	Michigan radiometer calibration
------	---------------------------------

August 25 (DoY 237)

	Michigan radiometer cannot communicate with software
--	--

August 26 (DoY 238)

	Moved radar to elephant grass field
--	-------------------------------------

September 2 (DoY 245)

	Connector port is fixed on Michigan radiometer
	Restarted Michigan radiometer

September 6 (DoY 249)

	Power failure
--	---------------

September 7 (DoY 250)

11:05	Michigan radiometer calibration
	Moved radar to corn field

September 8 (DoY 251)

11:17	Michigan radiometer calibration
-------	---------------------------------

September 9 (DoY 252)

10:05	Michigan radiometer calibration
	Harvested south side of field

September 12 (DoY 255)

10:07	Michigan radiometer calibration
	Harvested north side of field

September 15 (DoY 258)

10:42	Michigan radiometer calibration
	Coax cable replaced for Michigan radiometer V-pol
	Moved radar to elephant grass field

September 16 (DoY 259)

14:41	Michigan radiometer calibration
-------	---------------------------------

September 20 (DoY 263)

9:28	Michigan radiometer calibration
	Moved Michigan radiometer to elephant grass field
	Power failure on C-band and L-band radiometer

12. REFERENCES

Apogee Instruments, Inc. *Infrared Radiometer Owner's Manual, Model: IRR-PN*. Logan, UT: Apogee Instruments Inc., 2007.

Boote, K. J. "Data Requirements for Model Evaluation and Techniques for Sampling Crop Growth and Development." In: DSSAT version 3.5, Volume 4. ed. Gerrit Hoogenboom, Paul W. Wilken, and Gordon Y. Tsuji. Honolulu, HI: University of Hawaii, 1994, 215–229.

Campbell Scientific. *CNRI Net Radiometer Instruction Manual*. Logan, UT: Campbell Scientific Inc., 2006a.

Campbell Scientific. *Campbell Scientific Model HMP45C Temperature and Relative Humidity Probe Instruction Manual*. Logan, UT: Campbell Scientific Inc., 2006b.

De Roo, R. D. *University of Florida C-band Radiometer Summary*. Space Physics Research Laboratory, University of Michigan, Ann Arbor, Michigan, March, 2002.

De Roo, R. D. *TMRS-3 Radiometer Tuning Procedures*. Space Physics Research Laboratory, University of Michigan, Ann Arbor, Michigan, March, 2003.

De Roo, R. D. Personal communication, 2010.

Jang, M. Y., K. C. Tien, J. J. Casanova, and J. Judge, "Measurements of soil surface roughness during the fourth microwave water and energy balance experiment: April 18 through June 13, 2005." Gainesville: University of Florida

Institute of Food and Agricultural Sciences. Center of Remote Sensing. UF/IFAS EDIS Circular 1483. <http://edis.ifas.ufl.edu/AE363>, 2005.

Nagarajan, K., P. W. Liu, R. D. DeRoo, J. Judge, R. Akbar, P. Rush, S. Feagle, D. Preston, and R. Terwilleger. "Automated L-Band Radar System for Sensing Soil Moisture at High Temporal Resolutions." *IEEE Geosci. and Remote Sens. Letters*, 11(2), 2014

13. ACKNOWLEDGEMENTS

The authors would like to acknowledge Mr. James Boyer and his team at the PSREU, Citra, Florida, for excellent field management. MicroWEX-10 was supported by grant from NASA-THP (Grant number: NNX09AK29G).

A. FIELD OBSERVATIONS

Figure Captions

Figure A-1 Microwave brightness at C-band at Vertical and Horizontal polarization and L-band at Horizontal polarization—UFCMR and UFLMR (elephant grass).....	44
Figure A-2 Microwave brightness at L-band at Vertical and Horizontal polarization—TMRS-L (sweet corn).....	45
Figure A-3 Radar backscatter at Co-Pol- and Cross-Pol—UF-LARS (elephant grass).....	46
Figure A-4 Radar backscatter at Co-Pol- and Cross-Pol—UF-LARS (sweet corn).....	47
Figure A-5 UM Radar observations (sweet corn)—MOSS: germinating, growing ~1 meter tall, and before harvest	48
Figure A-6 Down- and up- welling shortwave and longwave radiation (elephant grass).....	49
Figure A-7 Relative humidity and air temperature	50
Figure A-8 Surface temperature (TIR) (elephant grass).....	51
Figure A-9 Surface temperature (TIR) (sweet corn).....	52
Figure A-10 L-band station soil temperature	53
Figure A-11 C-band station soil temperature.....	54
Figure A-12 Radar station soil temperature	55
Figure A-13 North station soil temperature	56
Figure A-14 South station soil temperature.....	57
Figure A-15 L-band station soil moisture.....	58
Figure A-16 C-band station soil moisture	59
Figure A-17 Radar station soil moisture.....	60
Figure A-18 North station soil moisture.....	61
Figure A-19 South station soil moisture	62
Figure A-20 Rainfall and overhead irrigation (elephant grass).....	63
Figure A-21 Rainfall and overhead irrigation (sweet corn).....	64
Figure A-22 Flow meter measurements in gal/min where (0,0) is point A in Figure 3(a).....	65
Figure A-23 Clumps in one square meter.....	66
Figure A-24 Tillers in one square meter.....	67
Figure A-25 Averages and standard deviations of the maximum clump height	68
Figure A-26 Averages and standard deviations of the base width	69
Figure A-27 Maximum height of sample tillers.....	70
Figure A-28 Maximum width of sample tillers.....	71
Figure A-29 Wet and dry canopy biomass	72
Figure A-30 Canopy LAI.....	73
Figure A-31 Vertical distribution of wet and dry biomass	74
Figure A-32 Leaf height	75
Figure A-33 Leaf length.....	77
Figure A-34 Leaf width	79
Figure A-35 Stem length	81
Figure A-36 Stem diameter	82
Figure A-37 Average crop height and width (sweet corn).....	83
Figure A-38 Wet and dry canopy biomass (sweet corn).....	84
Figure A-39 Canopy LAI (sweet corn).....	85
Figure A-40 Vertical distribution of wet and dry biomass	86
Figure A-41 Stem length and diameter	87
Figure A-42 Leaf height	88
Figure A-43 Leaf length.....	89
Figure A-44 Leaf width	90
Figure A-45 Ear height, length, and diameter	91
Figure A-46 Leaf angle (θ_1)	92
Figure A-47 Leaf angle (θ_2)	93
Figure A-48 Ear angle (θ_e)	94
Figure A-49 Water table depth and elevation above sea level	95
Figure A-50 Water retention curve	96

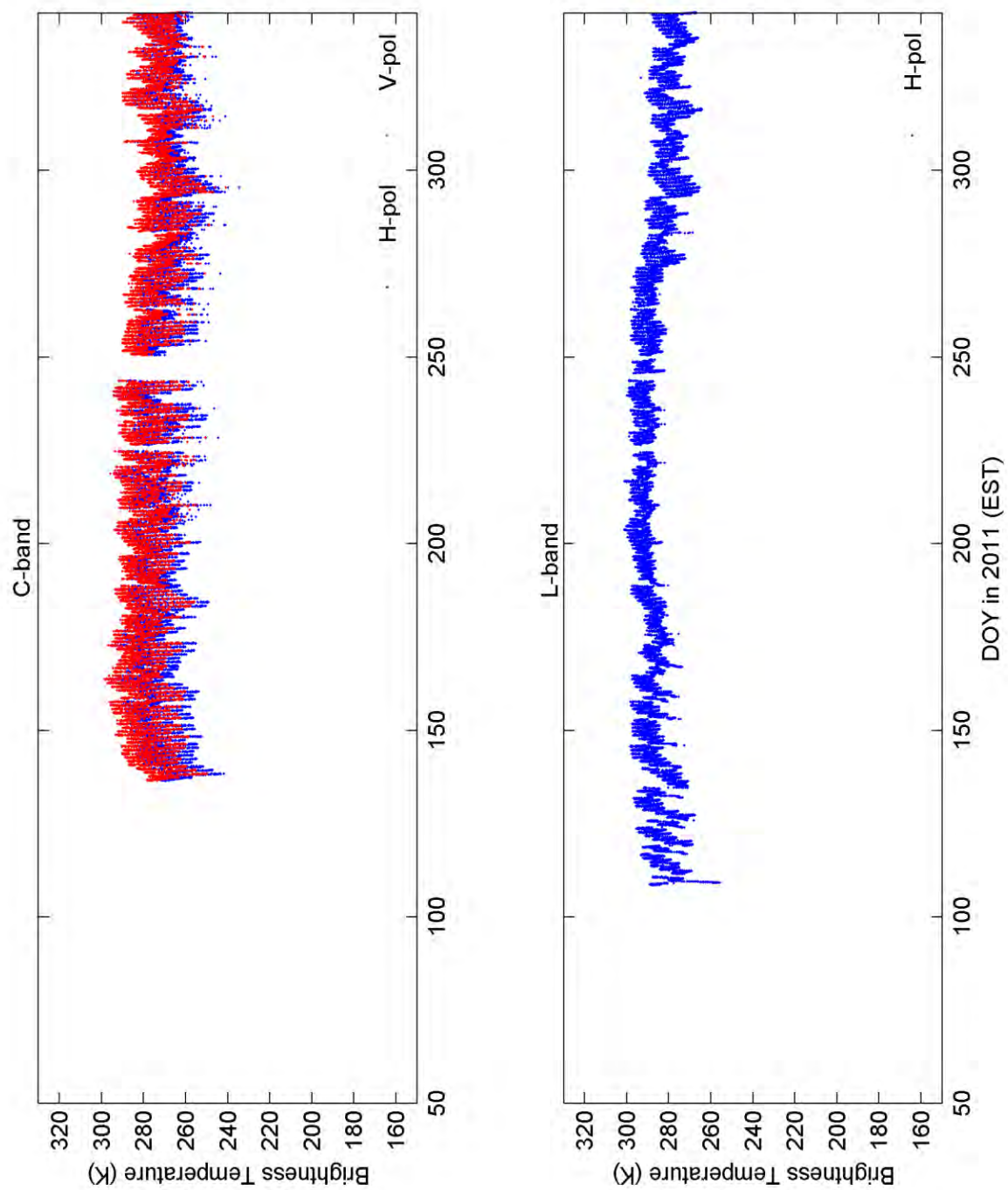


Figure A-1. Microwave brightness at C-band at vertical and horizontal polarization and L-band at horizontal polarization—UFCMR and UFLMR (elephant grass)

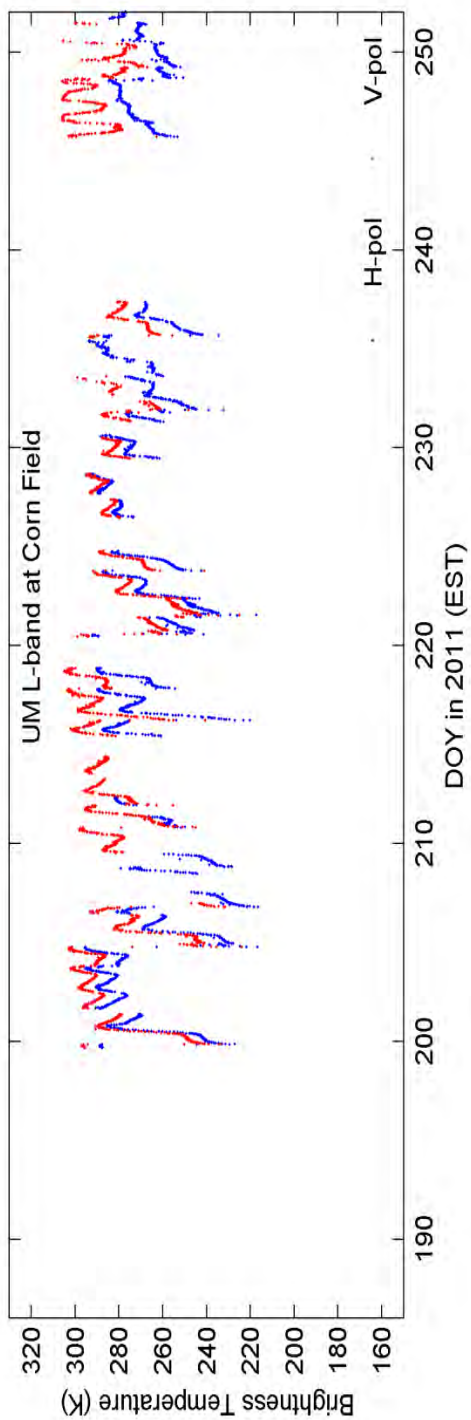


Figure A-2. Microwave brightness at L-band at vertical and horizontal polarization—TMRS-L (sweet corn)

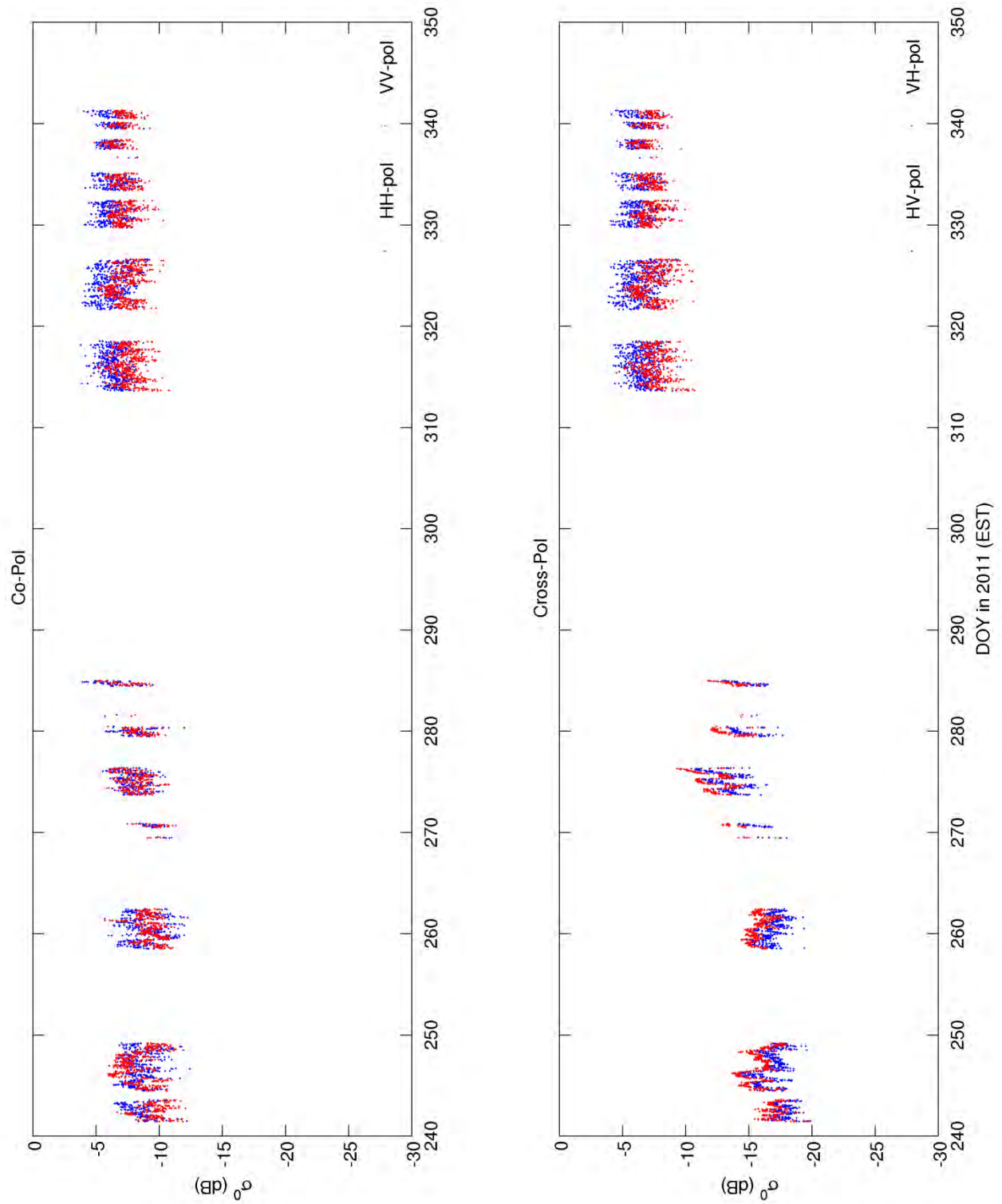


Figure A-3. Radar backscatter at Co-Pol- and Cross-Pol—UF-LARS (elephant grass)

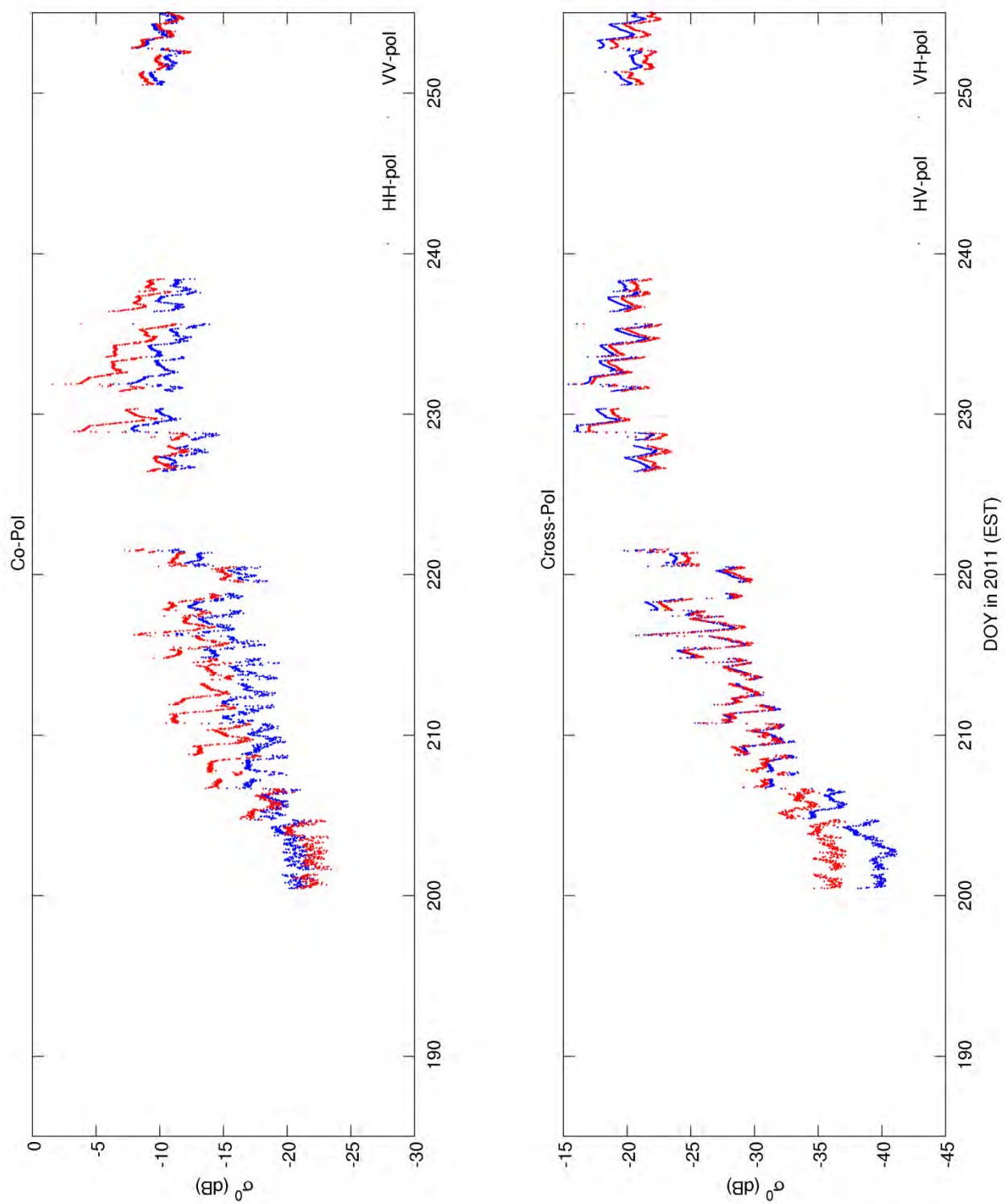


Figure A-4. Radar backscatter at Co-Pol- and Cross-Pol—UF-LARS (sweet corn)

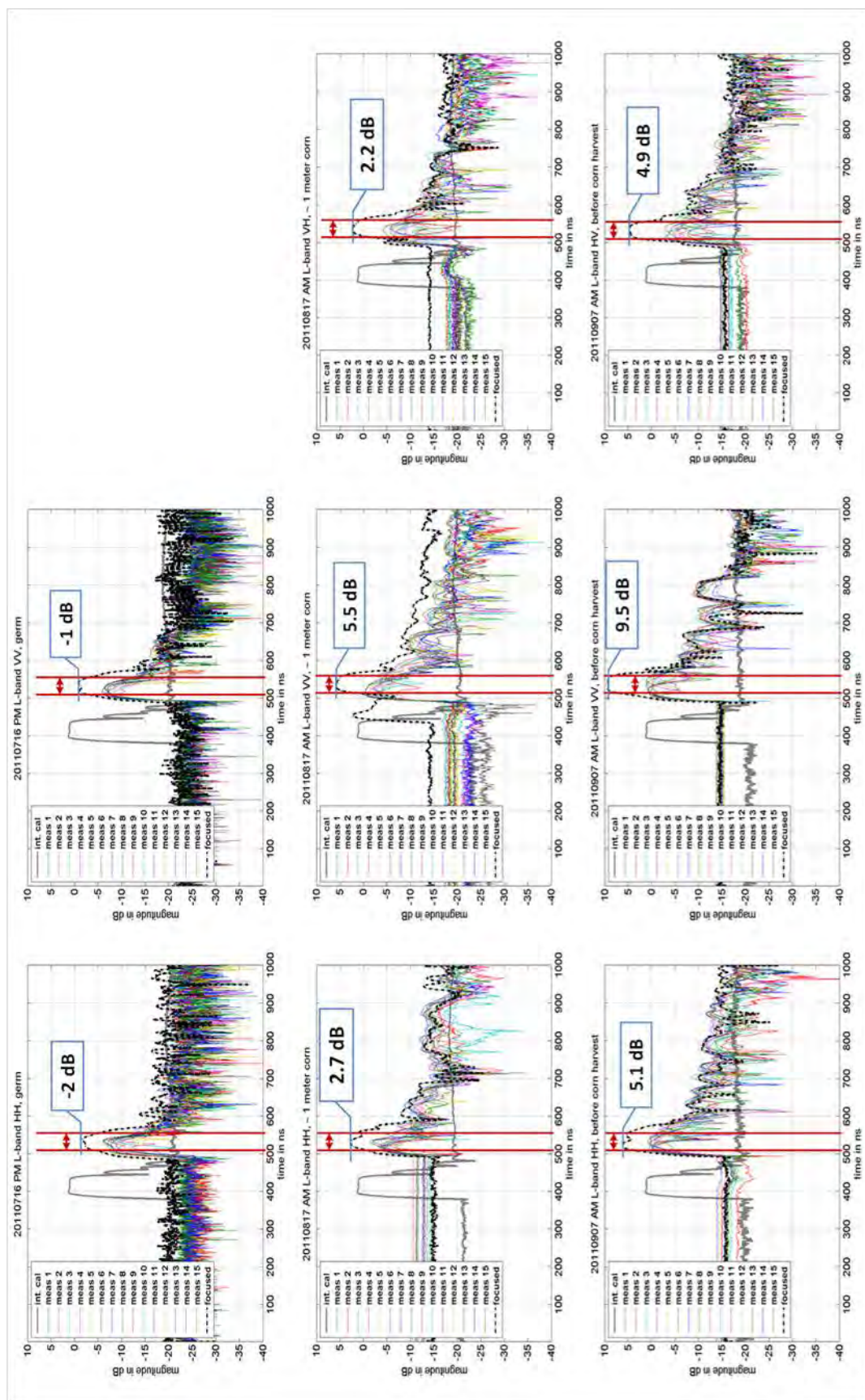


Figure A-5. UM Radar observations (sweet corn)—MOSS: germinating (row 1), growing ~1 meter tall (row 2), and before harvest (row 3)

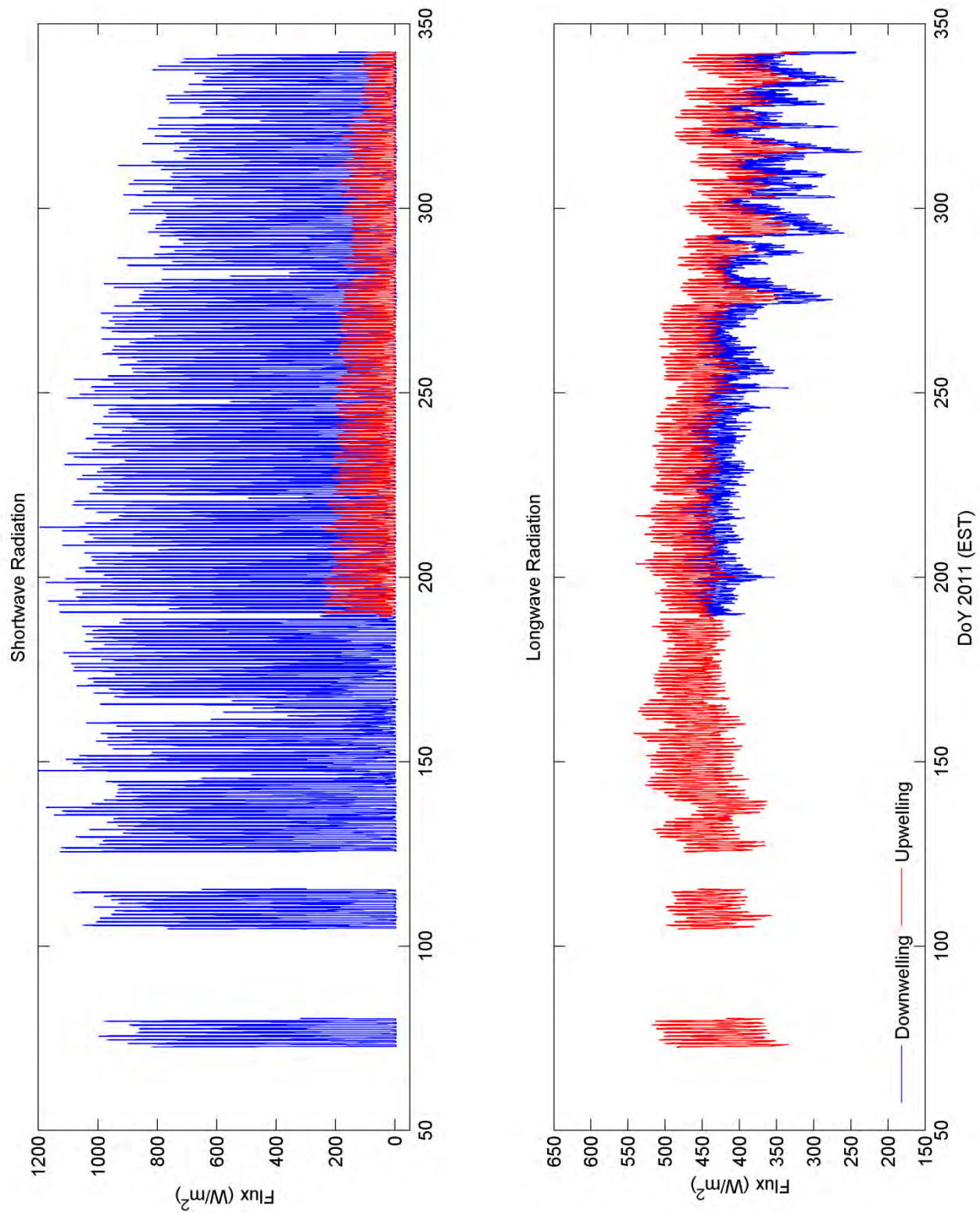


Figure A-6. Down- and up-welling shortwave and longwave radiation

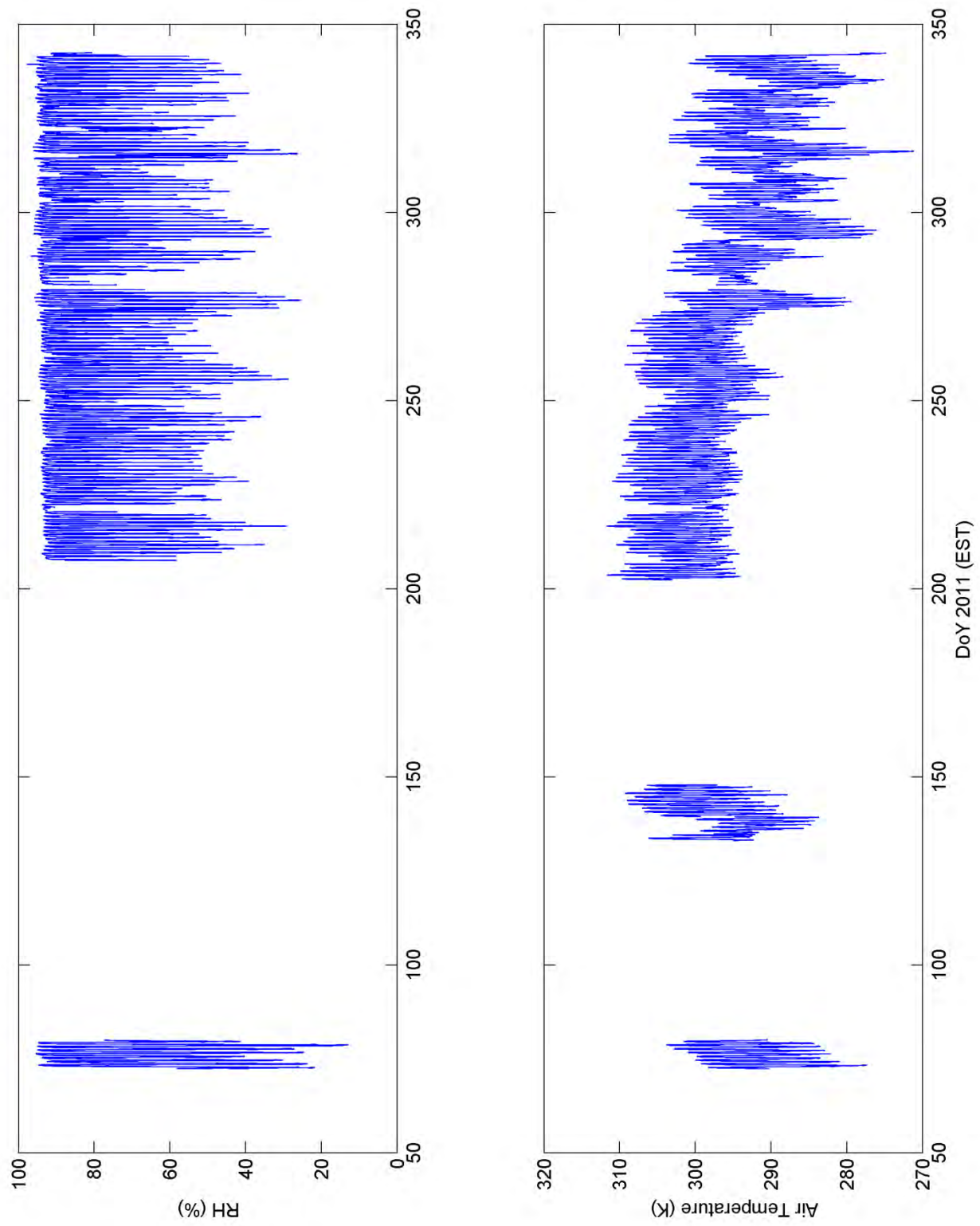


Figure A-7. Relative humidity and air temperature

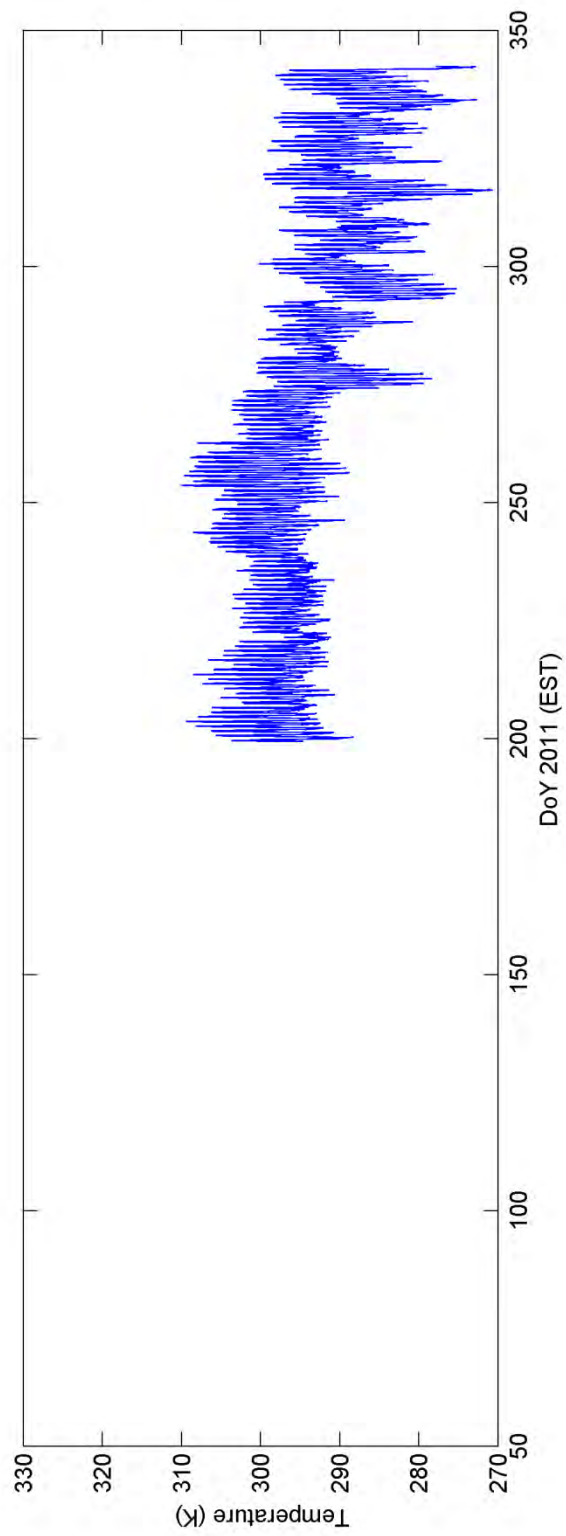


Figure A-8. Surface temperature (TIR) (elephant grass)

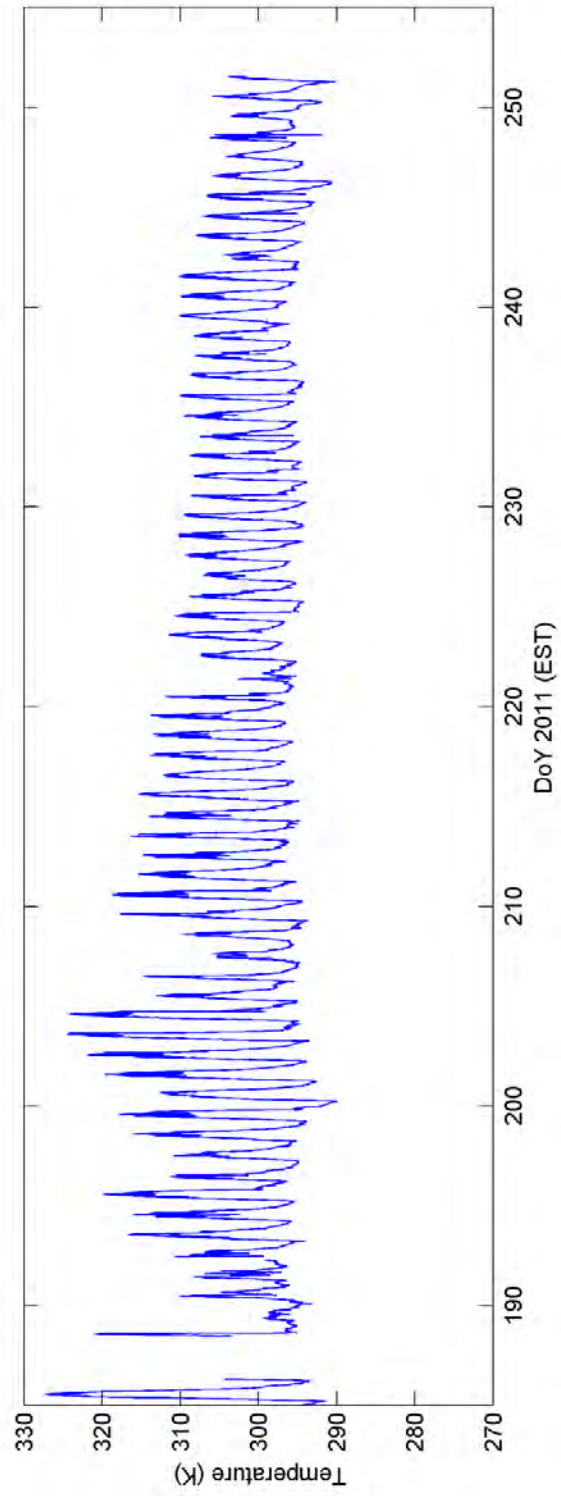


Figure A-9. Surface temperature (TIR) (sweet corn)

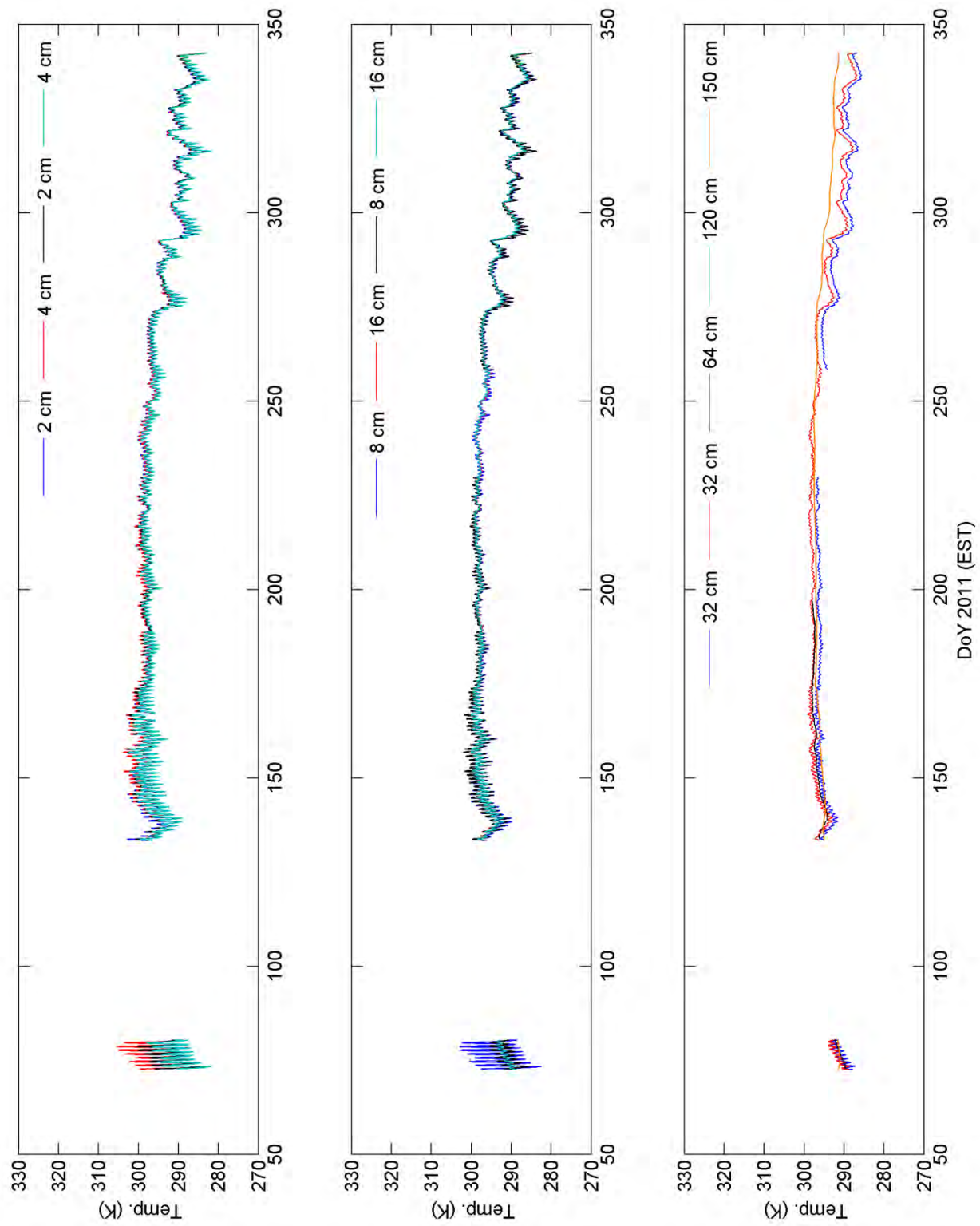


Figure A-10. L-band station soil temperature

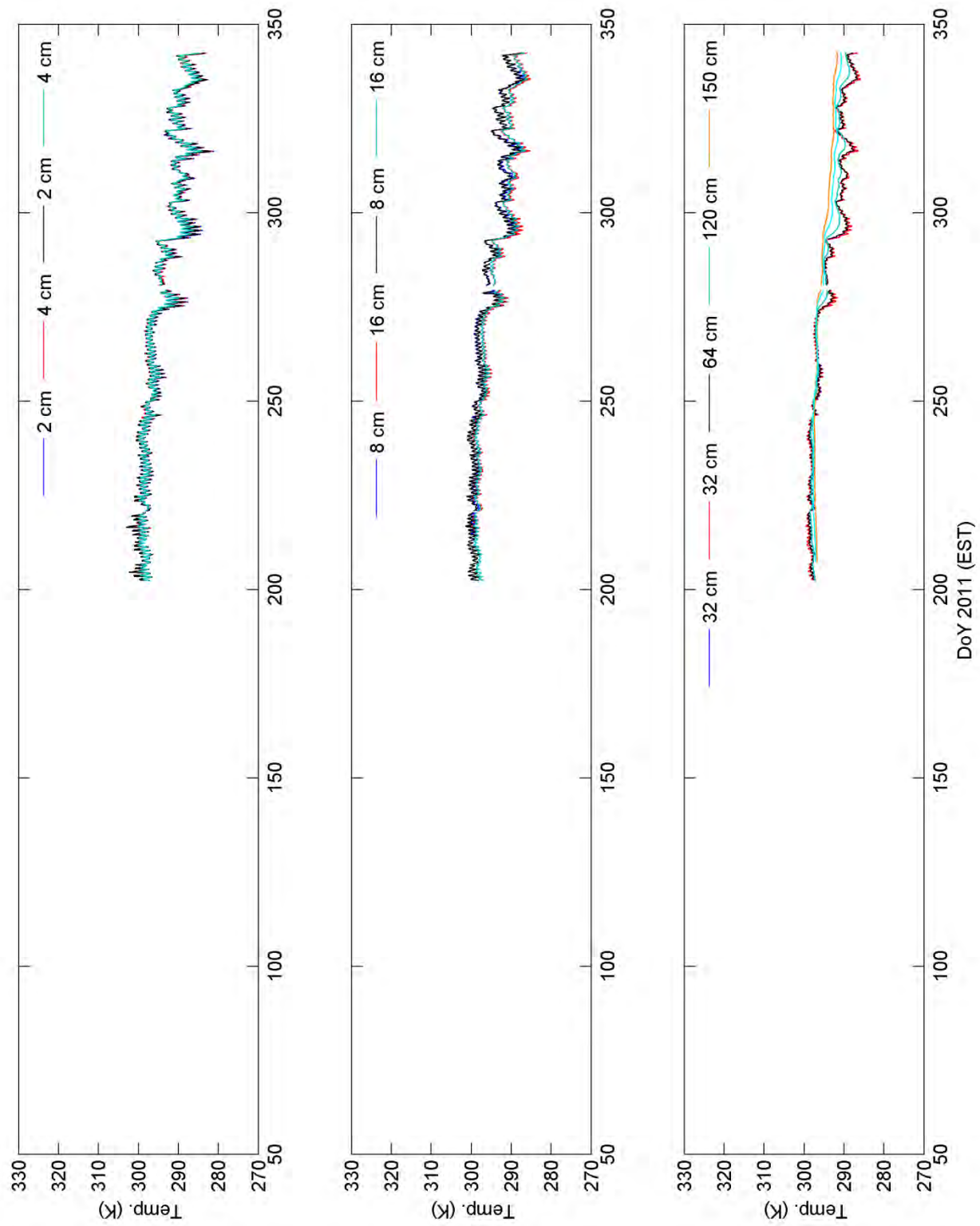


Figure A-11. C-band station soil temperature

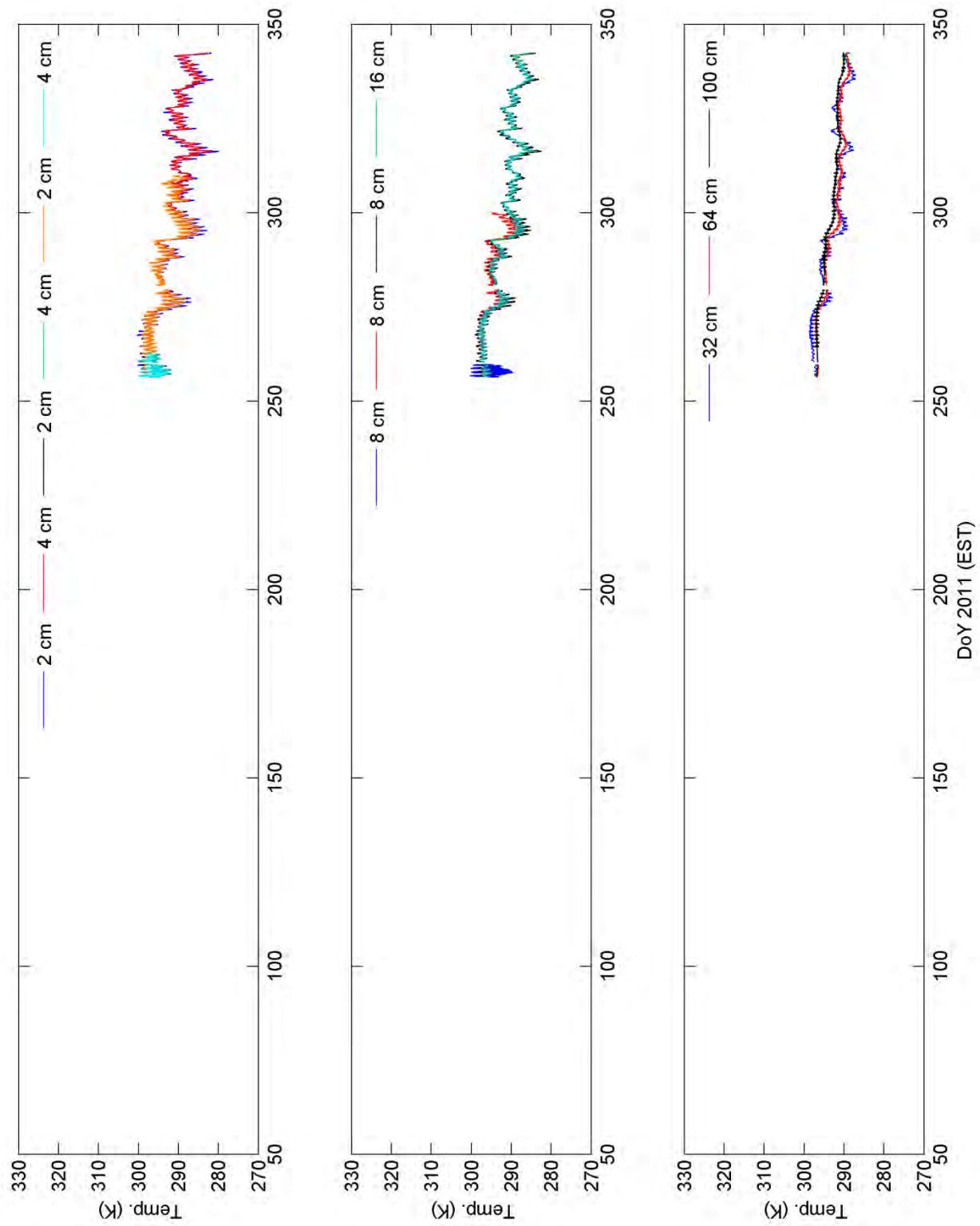


Figure A-12. Radar station soil temperature

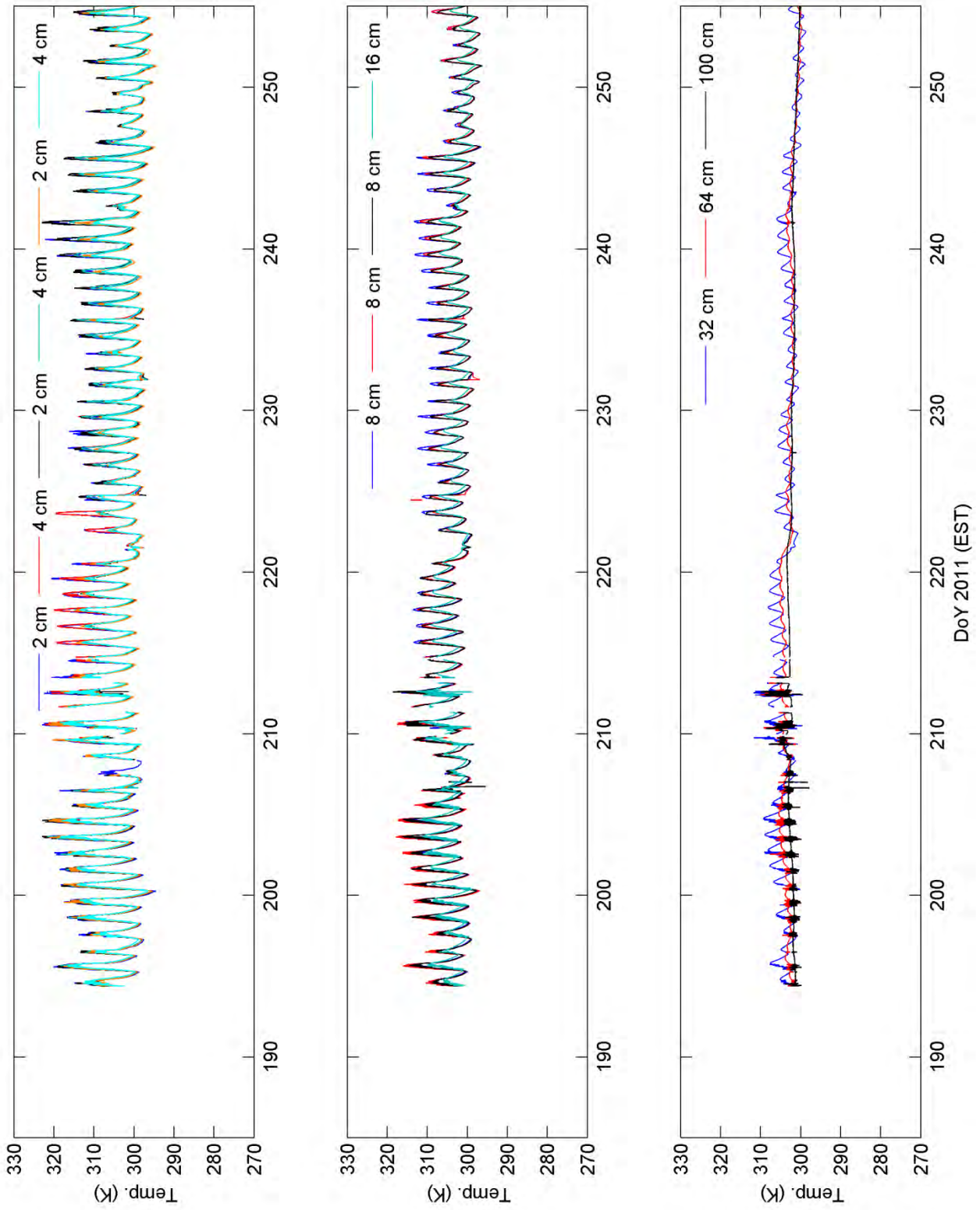


Figure A-13. North station soil temperature

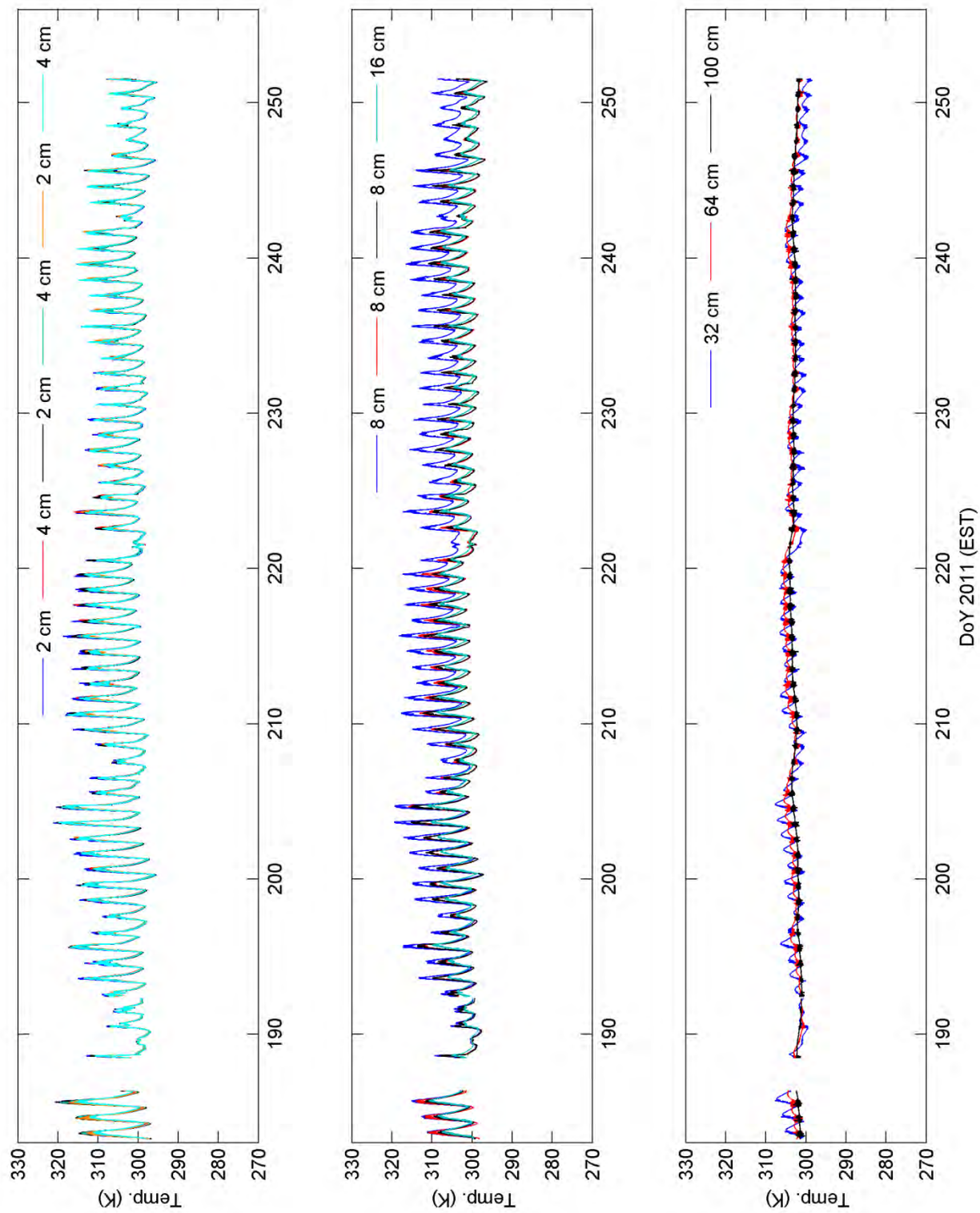


Figure A-14. South station soil temperature

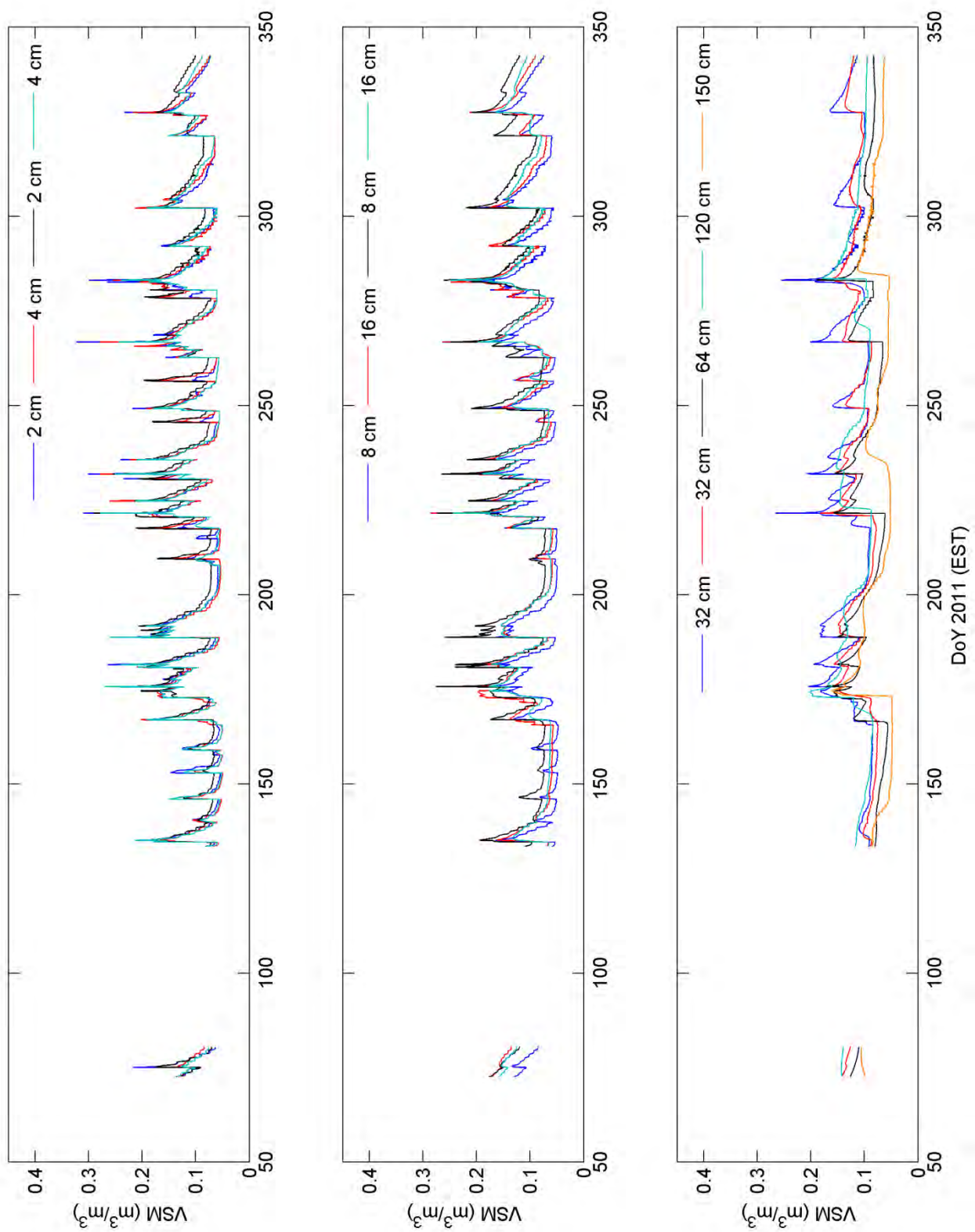


Figure A-15. L-band station soil moisture

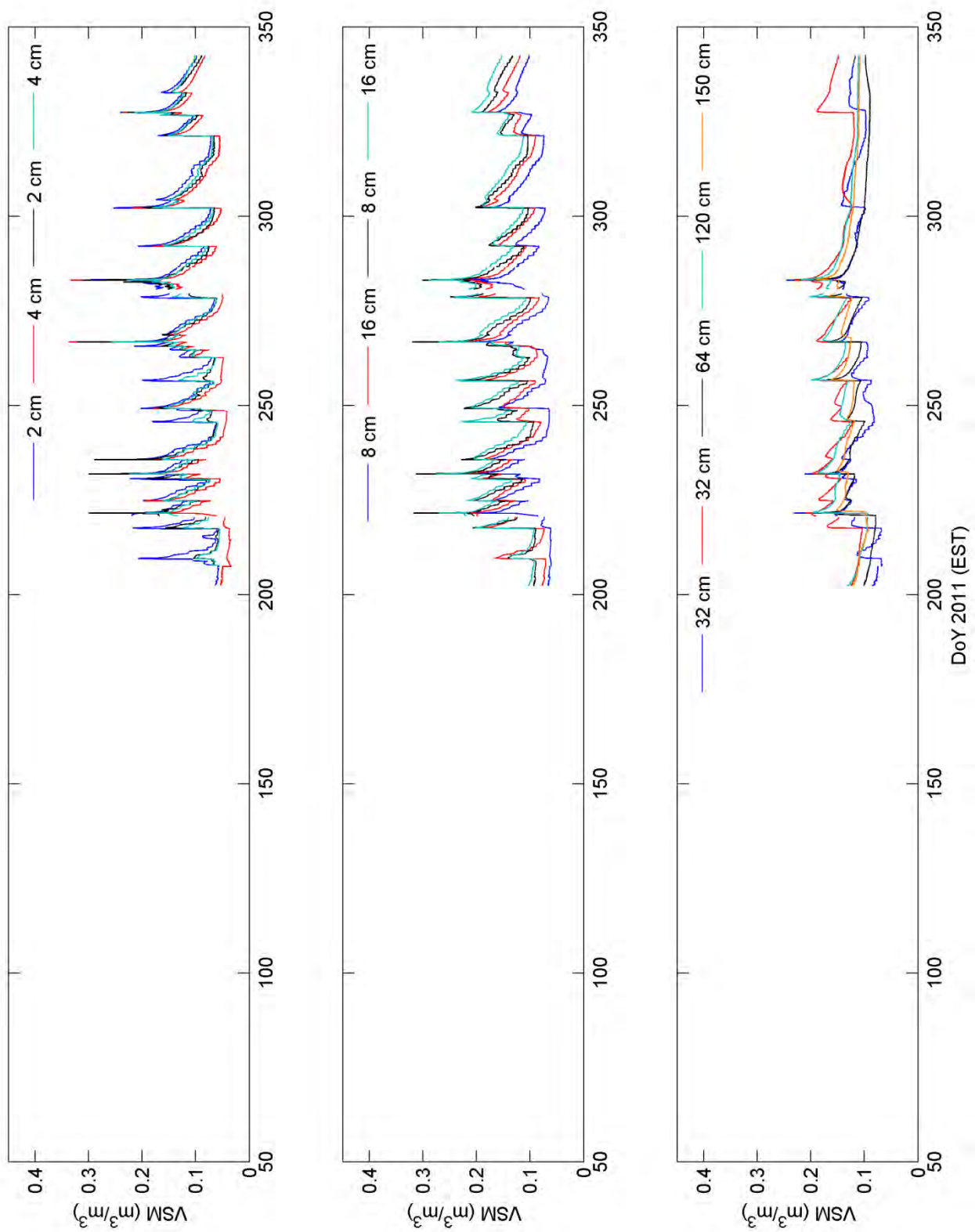


Figure A-16. C-band station soil moisture

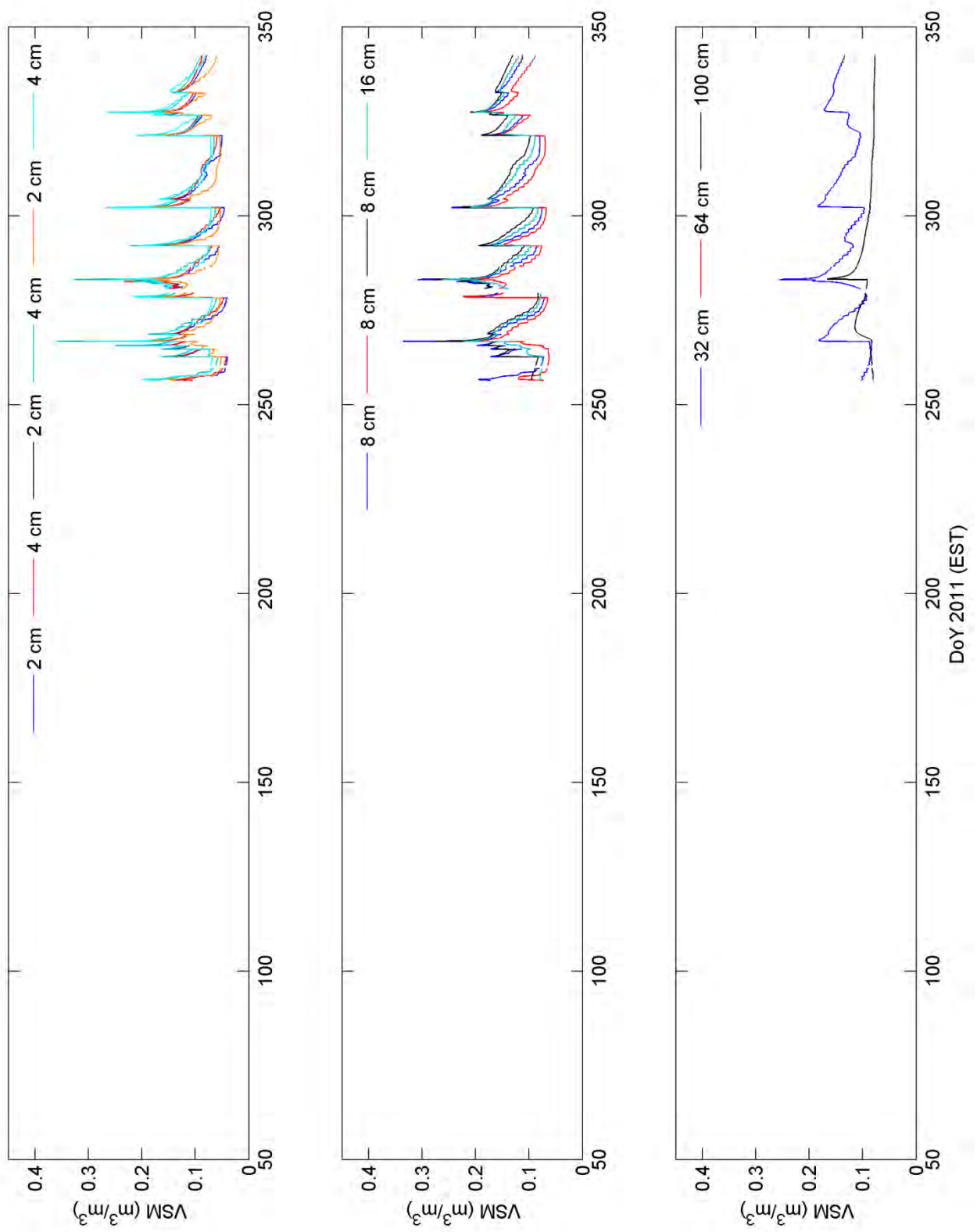


Figure A-17. Radar station soil moisture

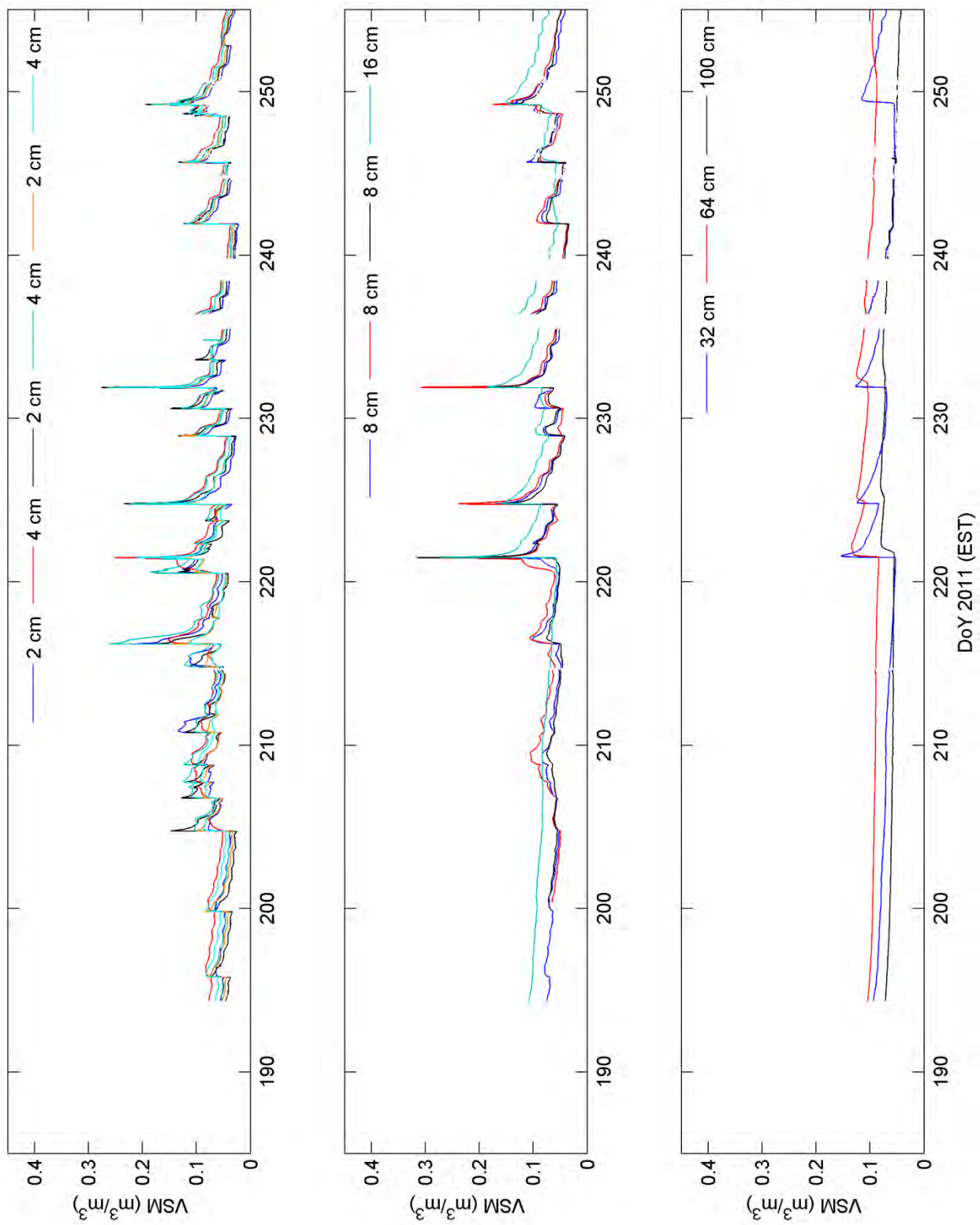


Figure A-18. North station soil moisture

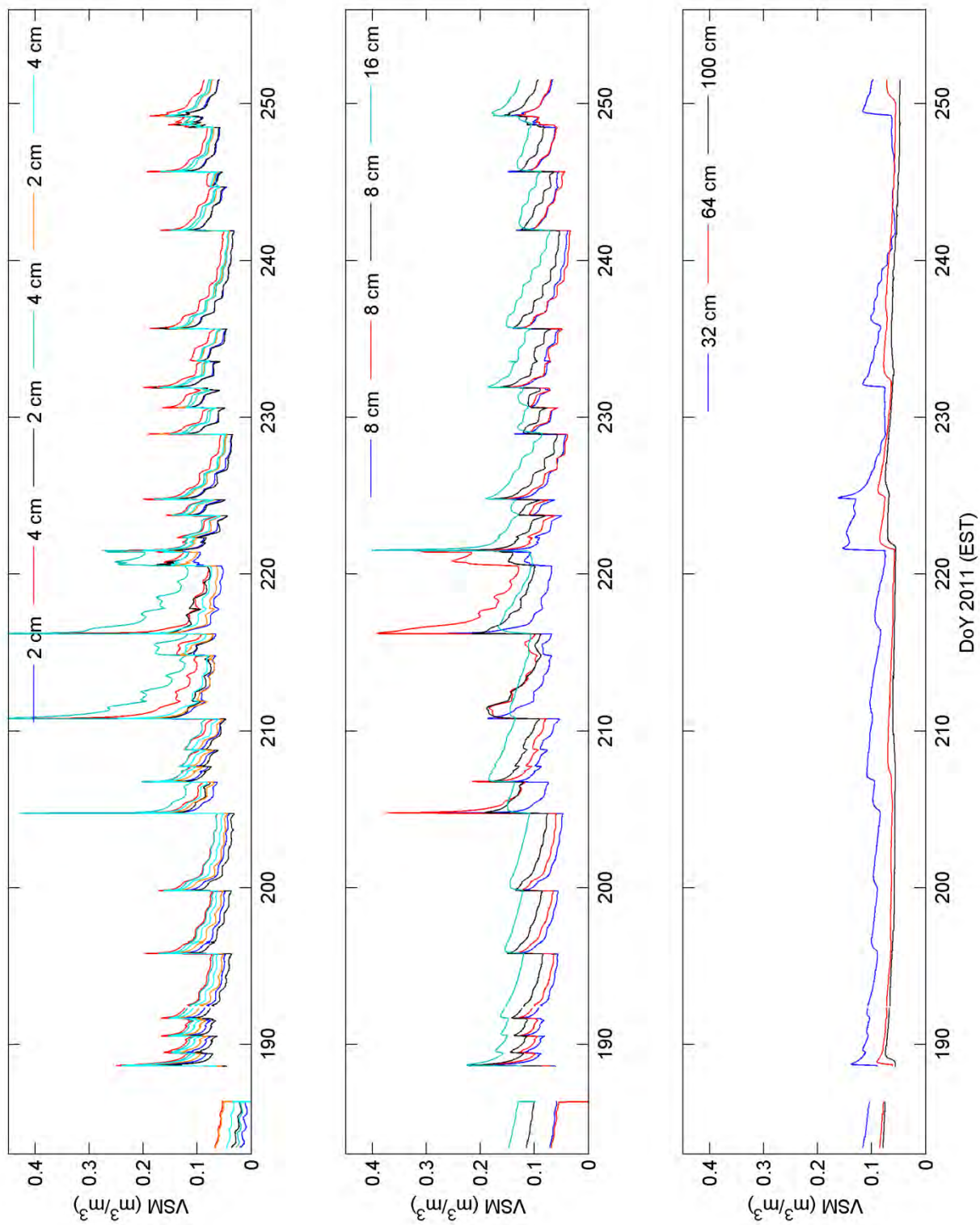


Figure A-19. South station soil moisture

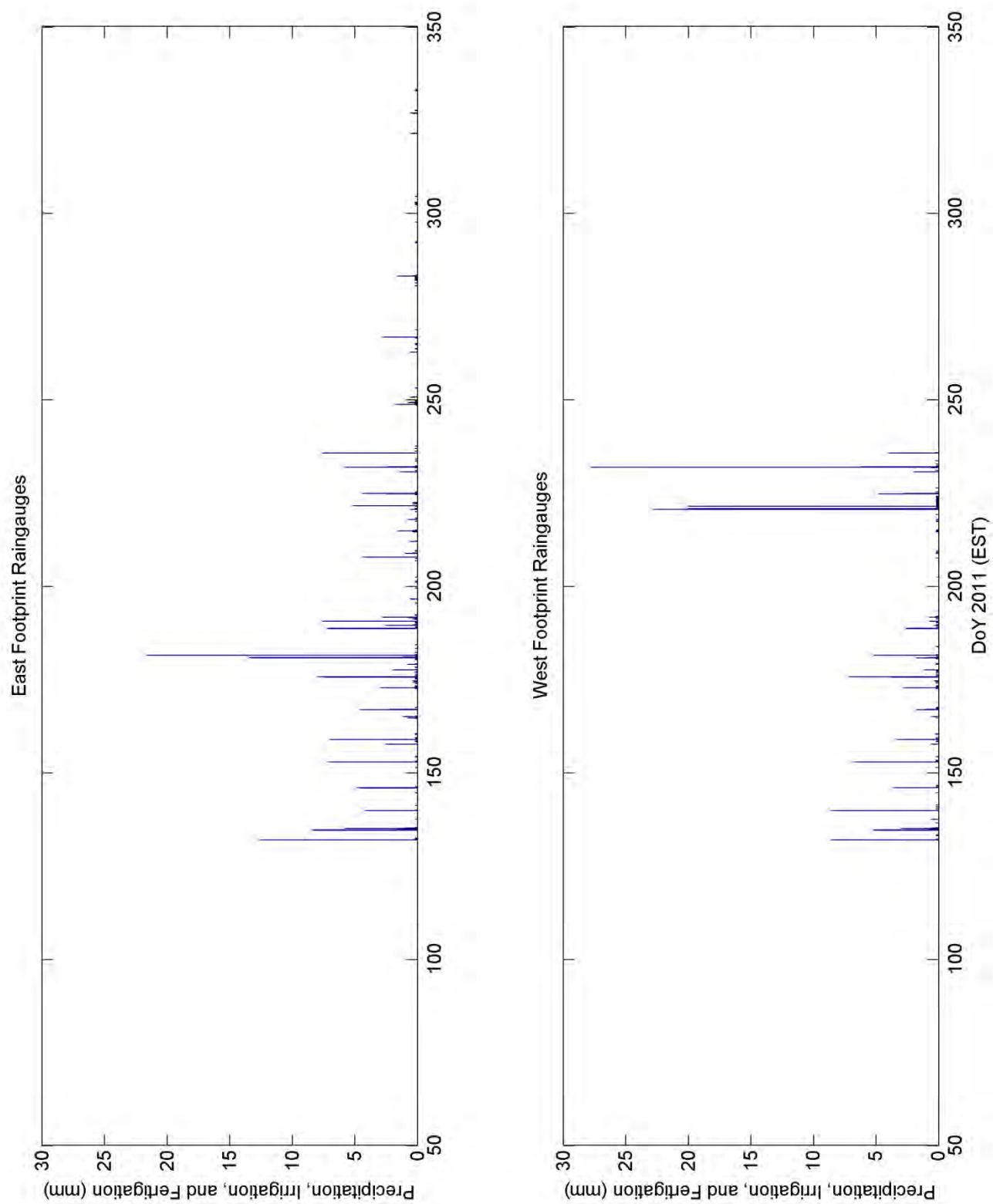


Figure A-20. Rainfall and overhead irrigation (elephant grass)

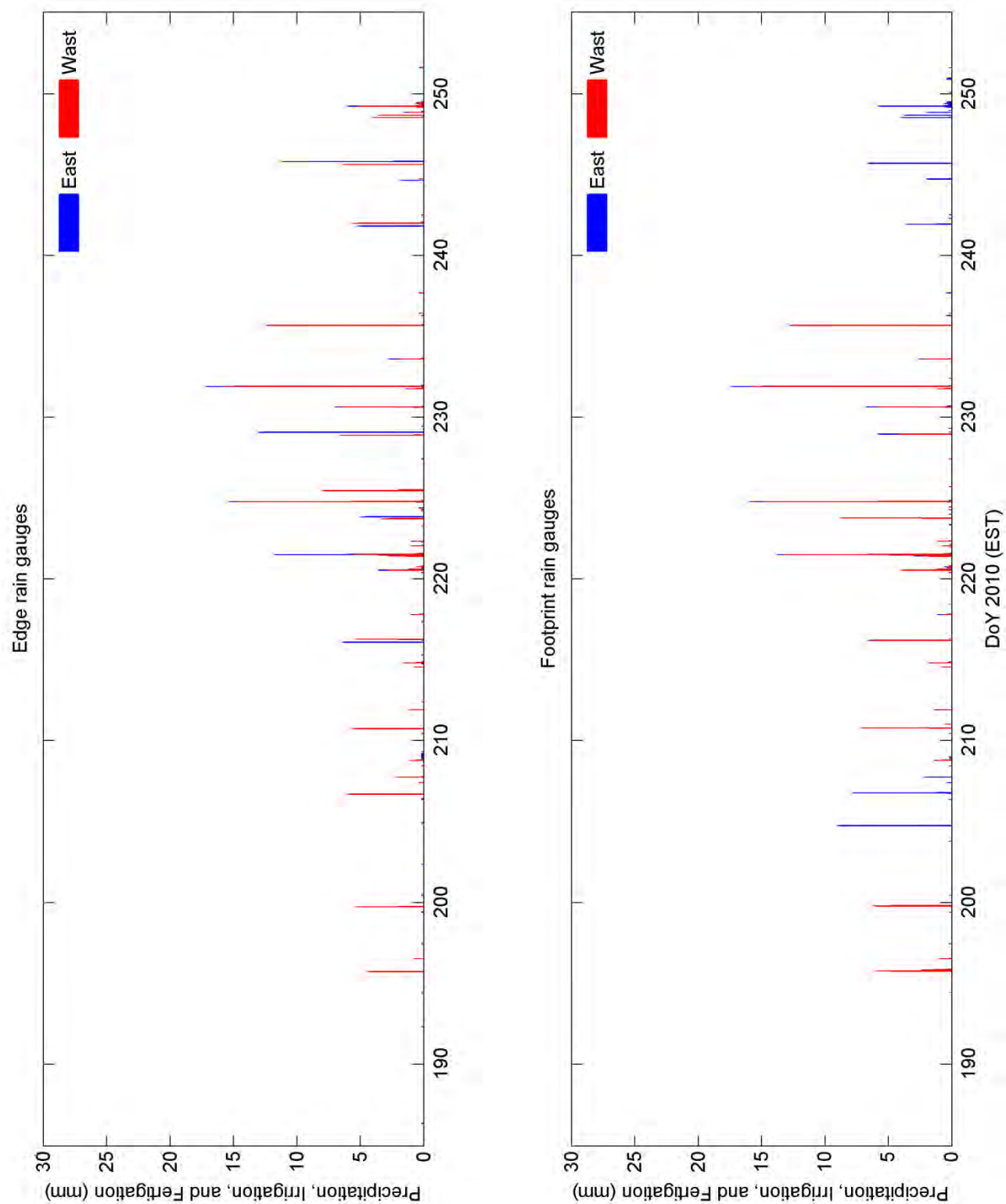


Figure A-21. Rainfall and overhead irrigation (sweet corn)

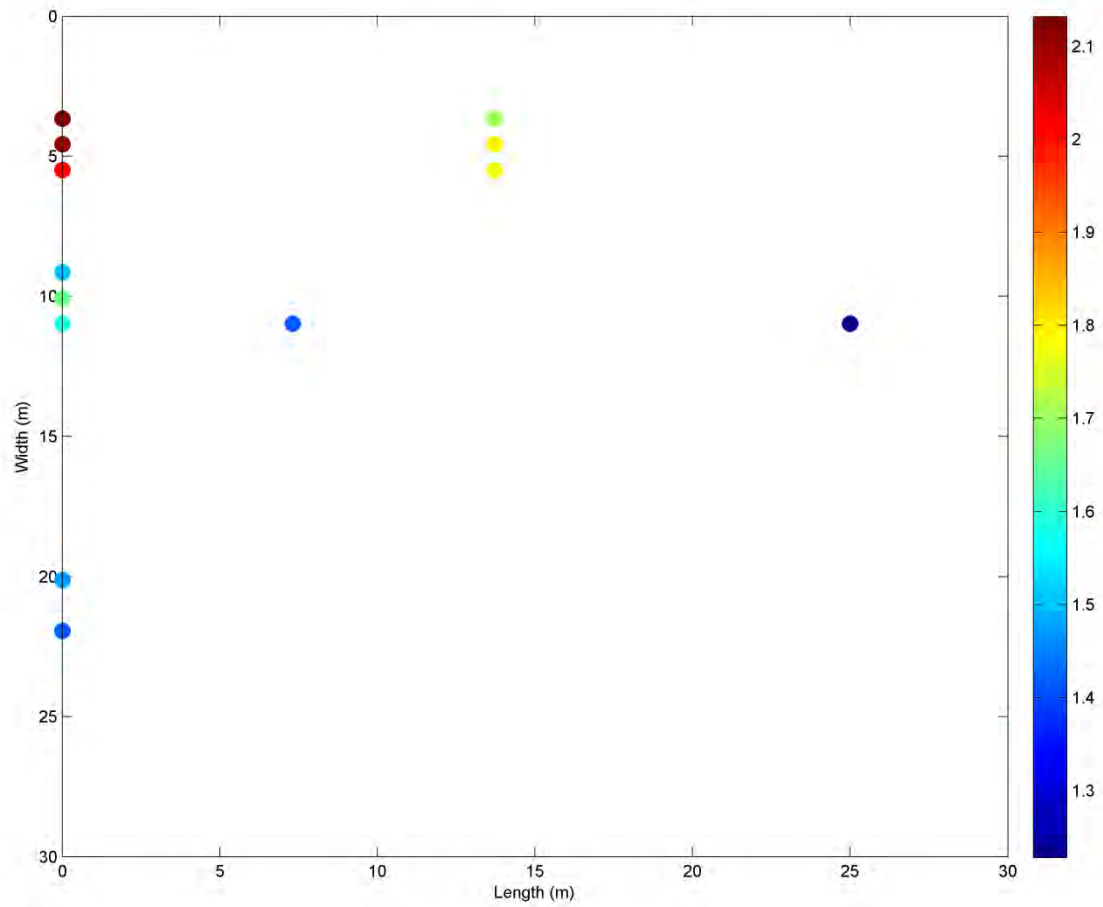


Figure A-22. Flow meter measurements in gal/min where (0, 0) is point A in Figure 3(a)

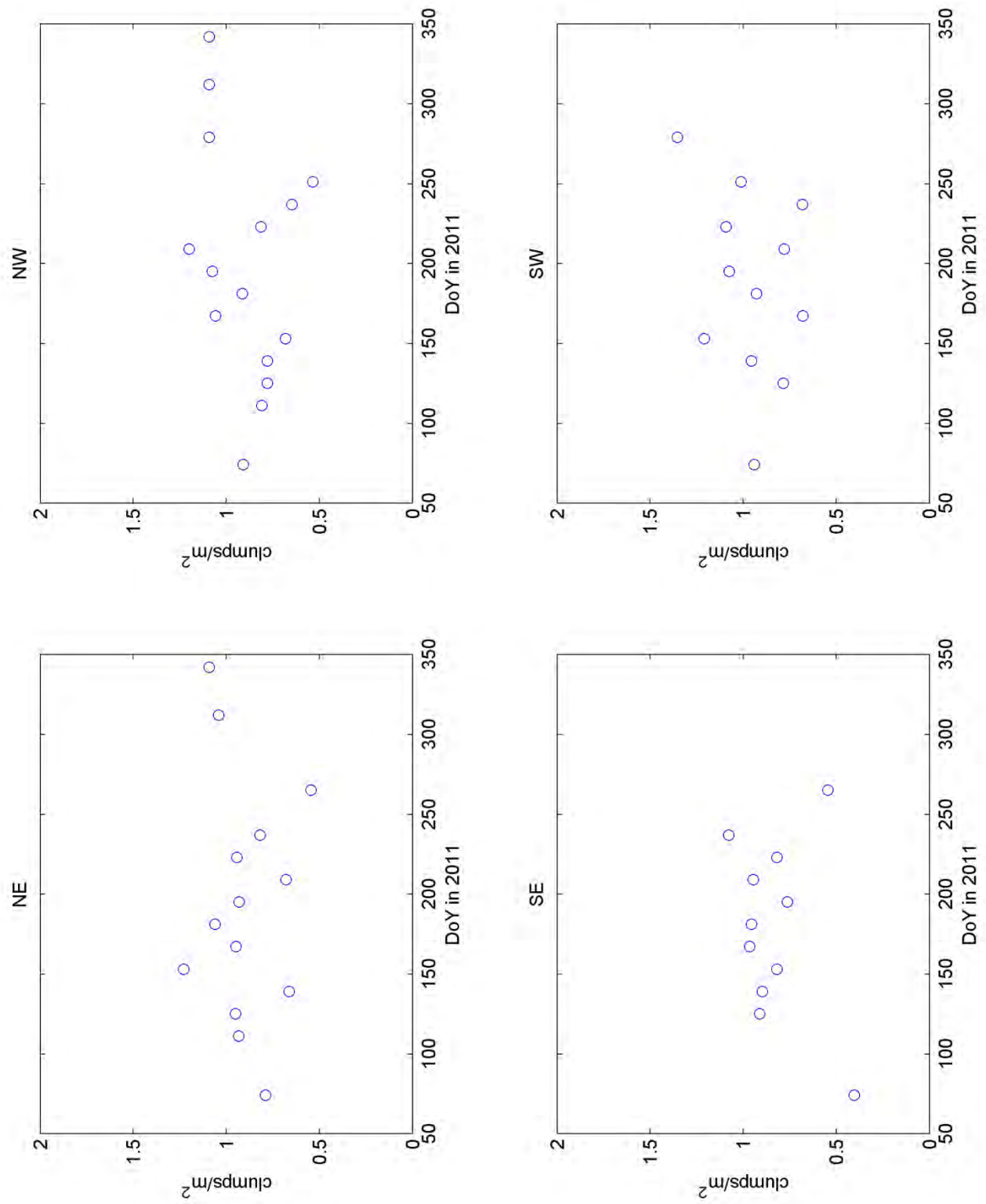


Figure A-23. Clumps in one square meter

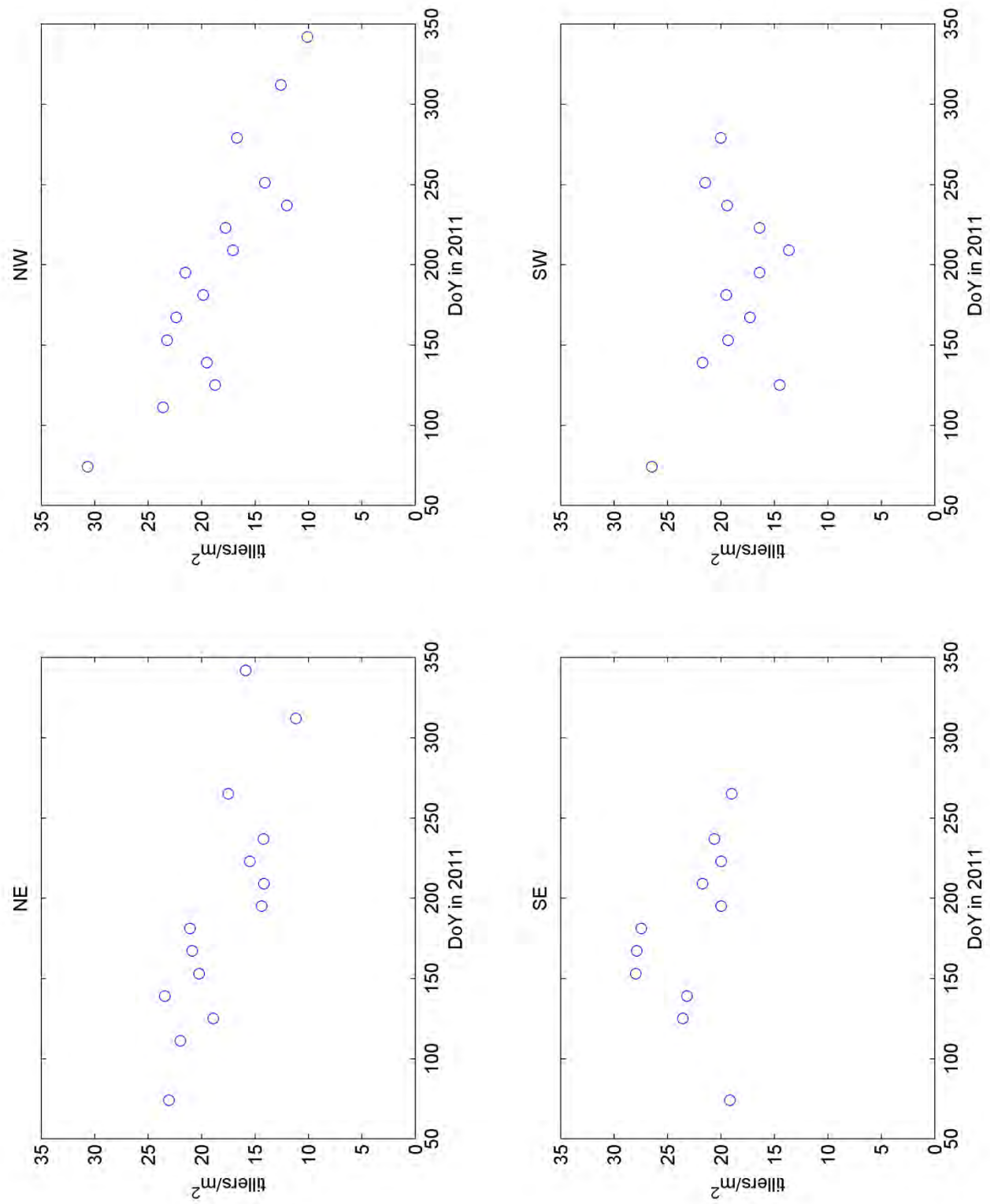


Figure A-24. Tillers in one square meter

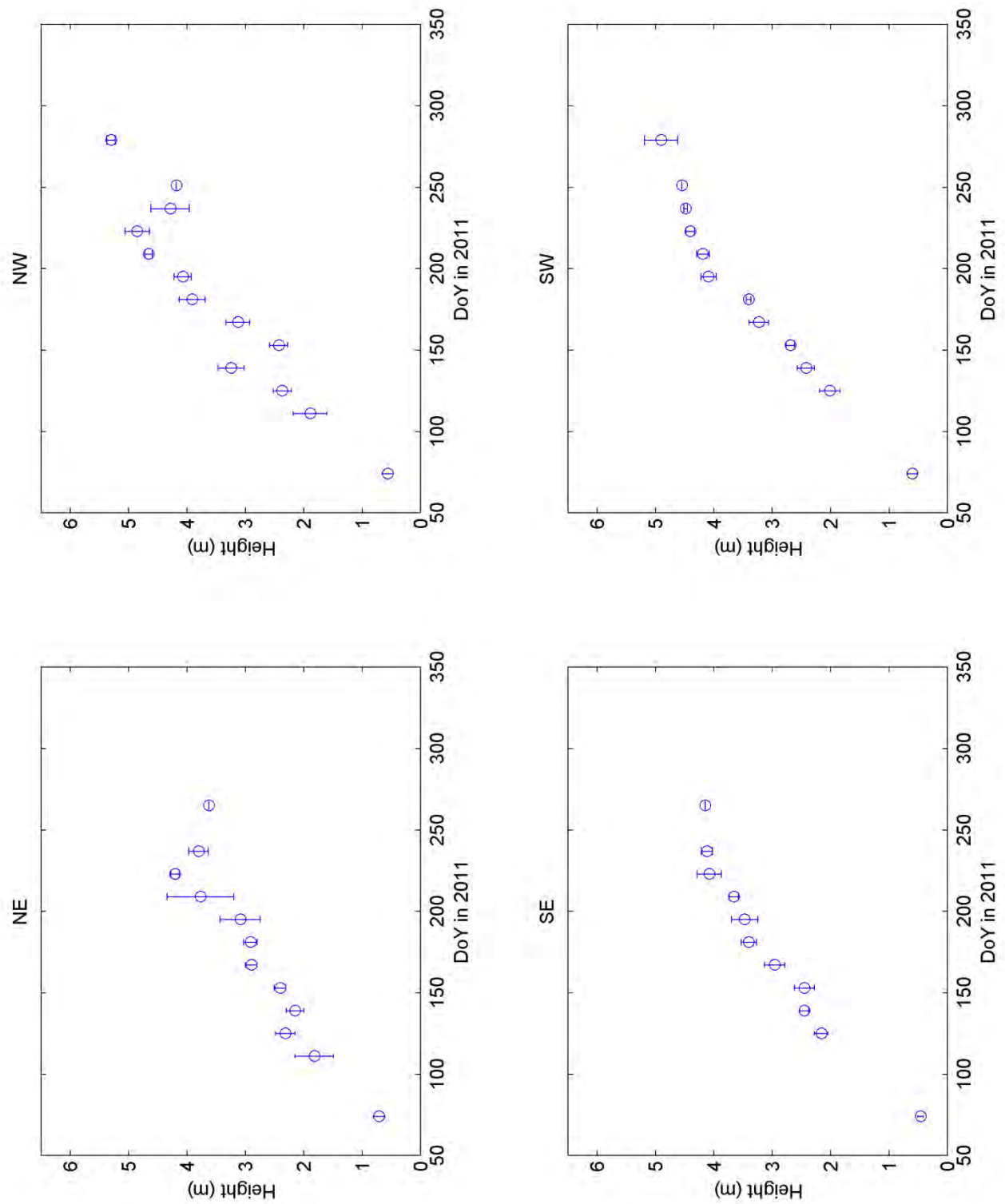


Figure A-25. Averages and standard deviations of the maximum clump height

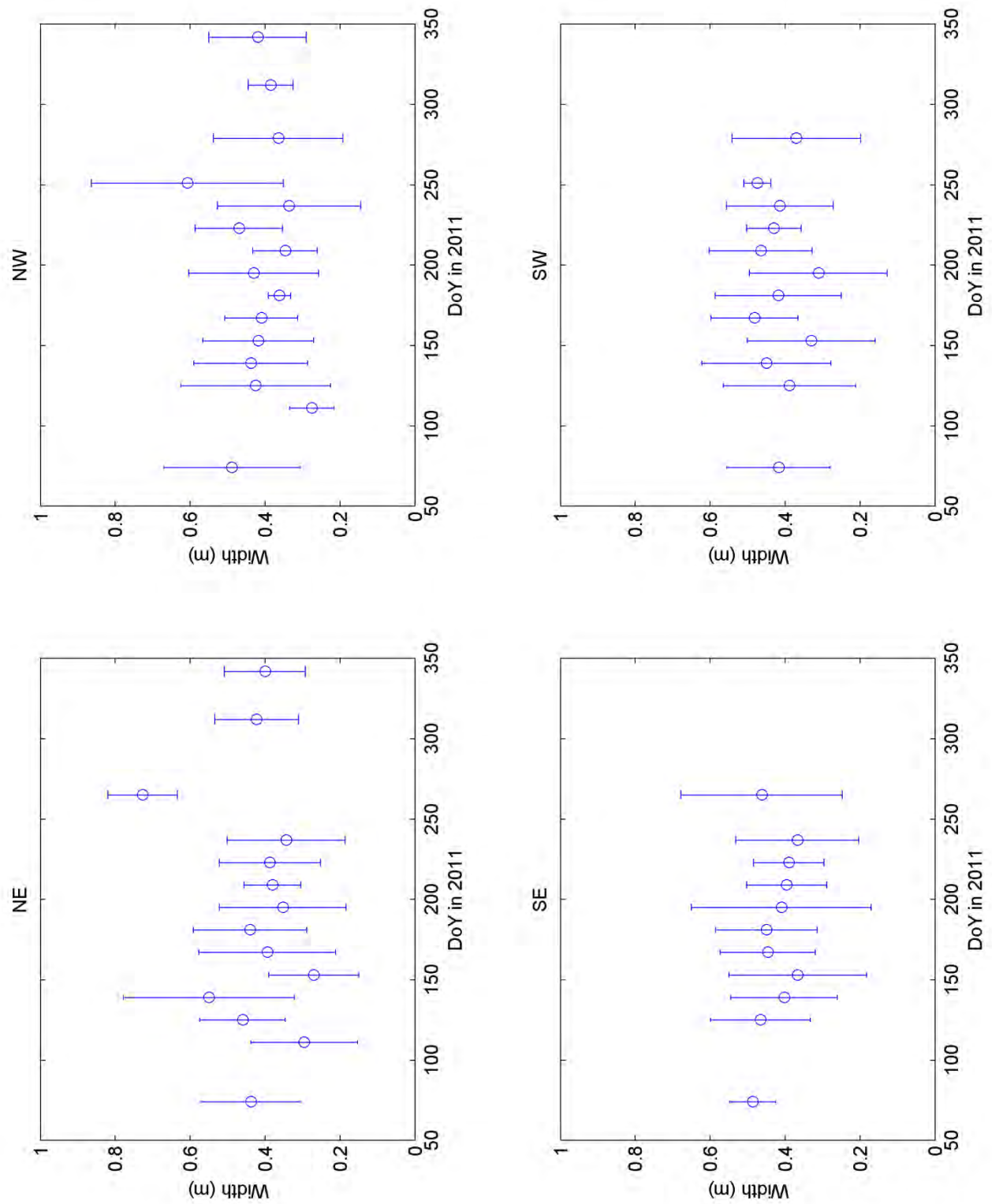


Figure A-26. Averages and standard deviations of the base width

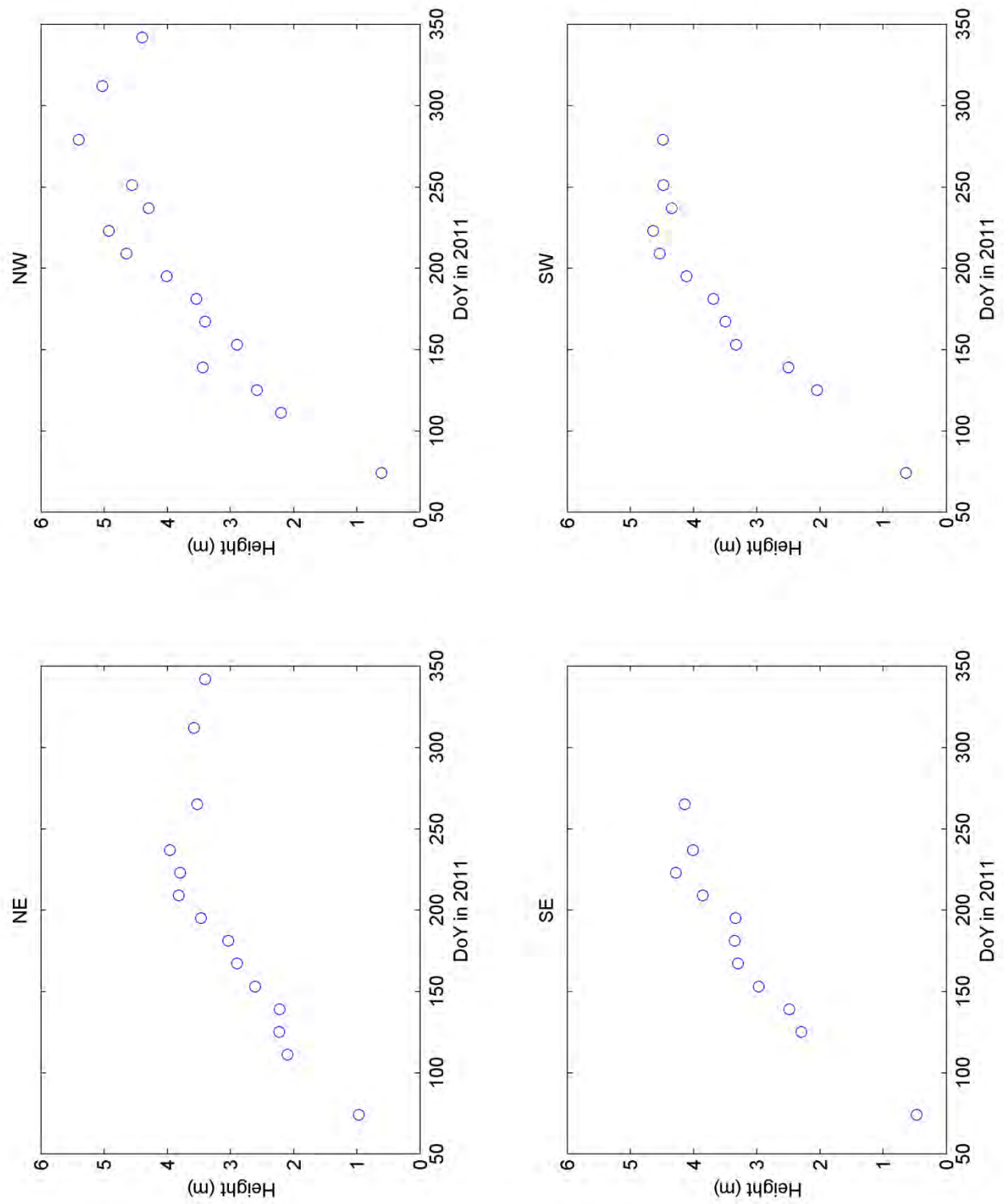


Figure A-27. Maximum height of sample tillers

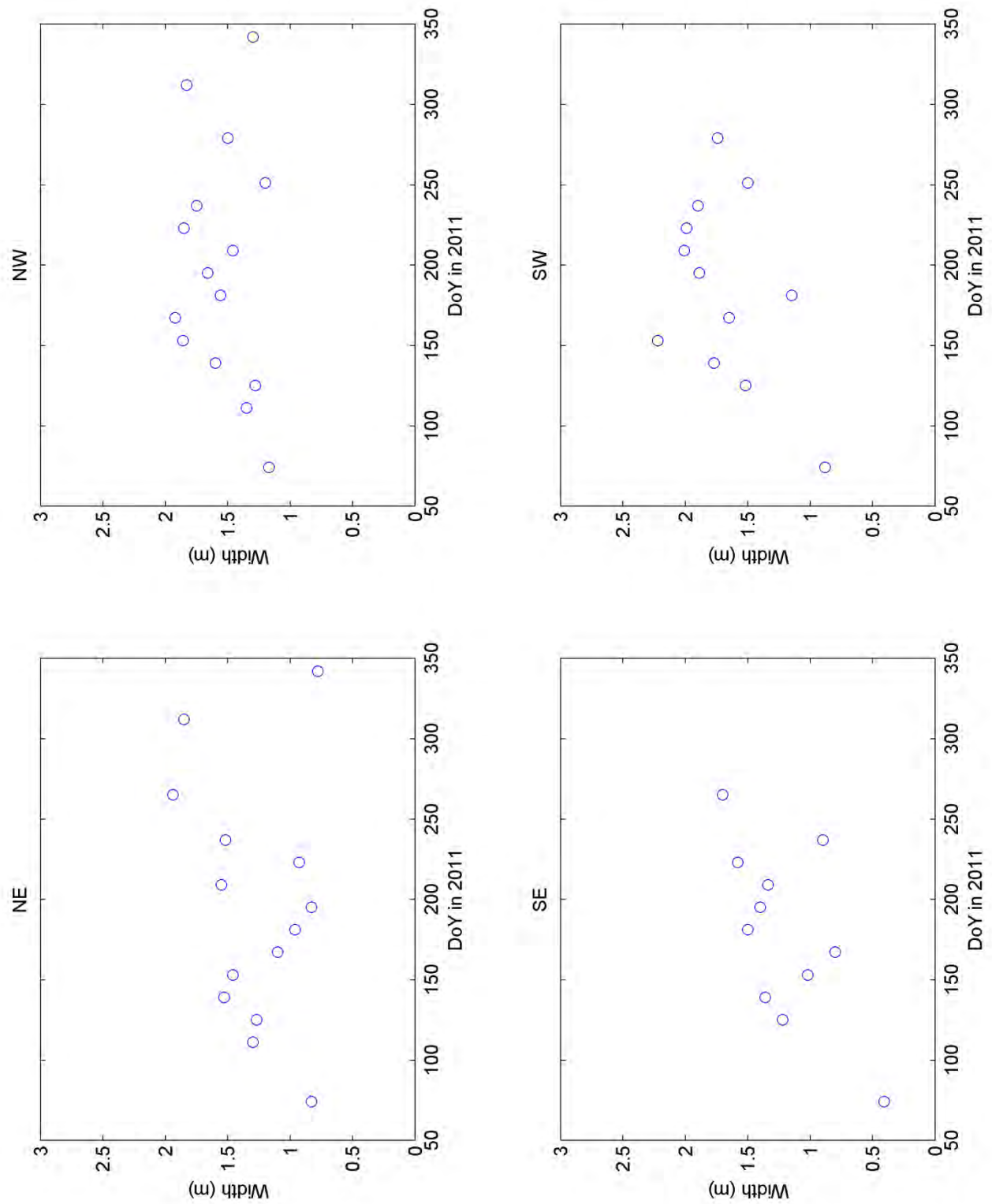


Figure A-28. Maximum width of sample tillers

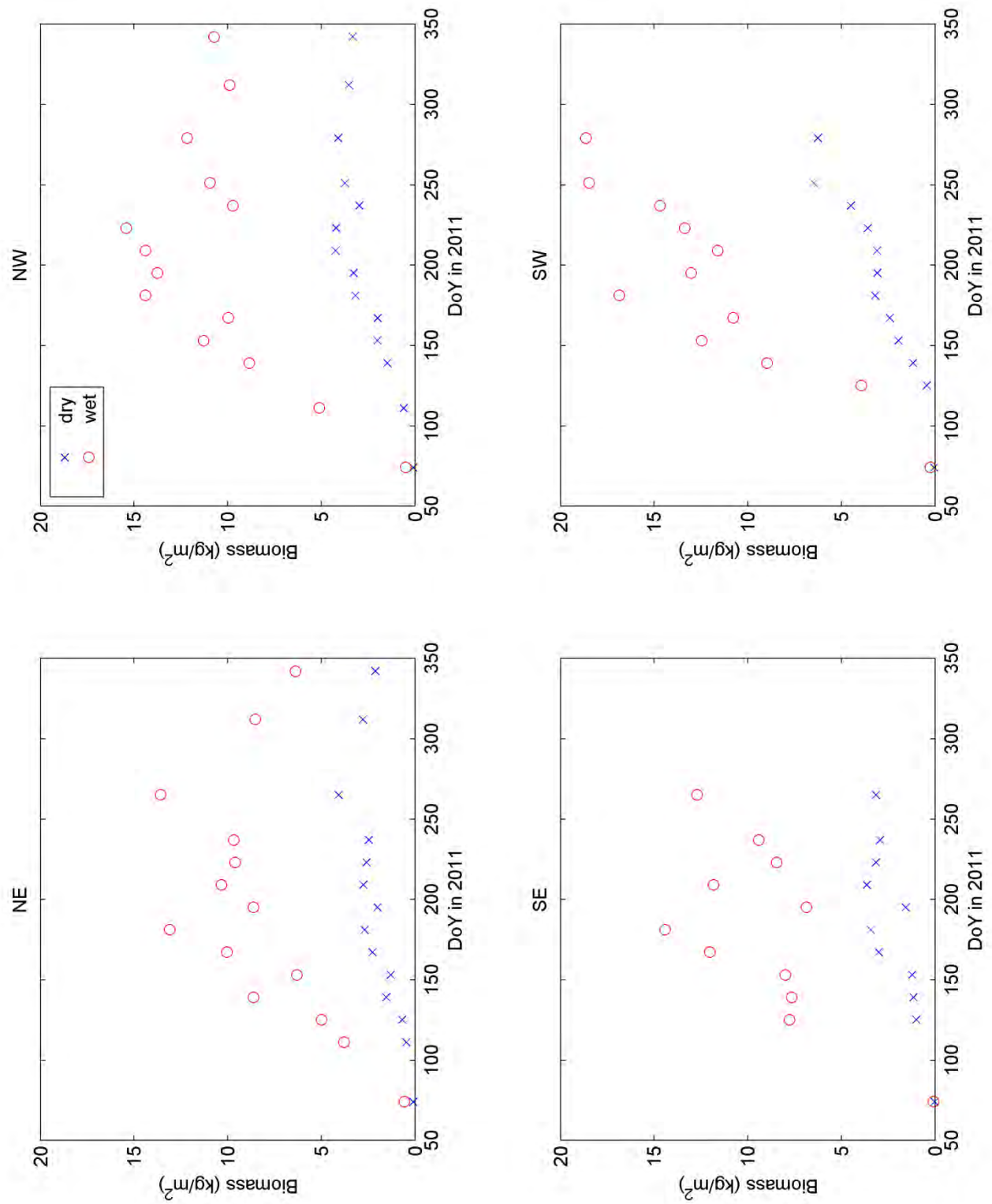


Figure A-29. Wet and dry canopy biomass

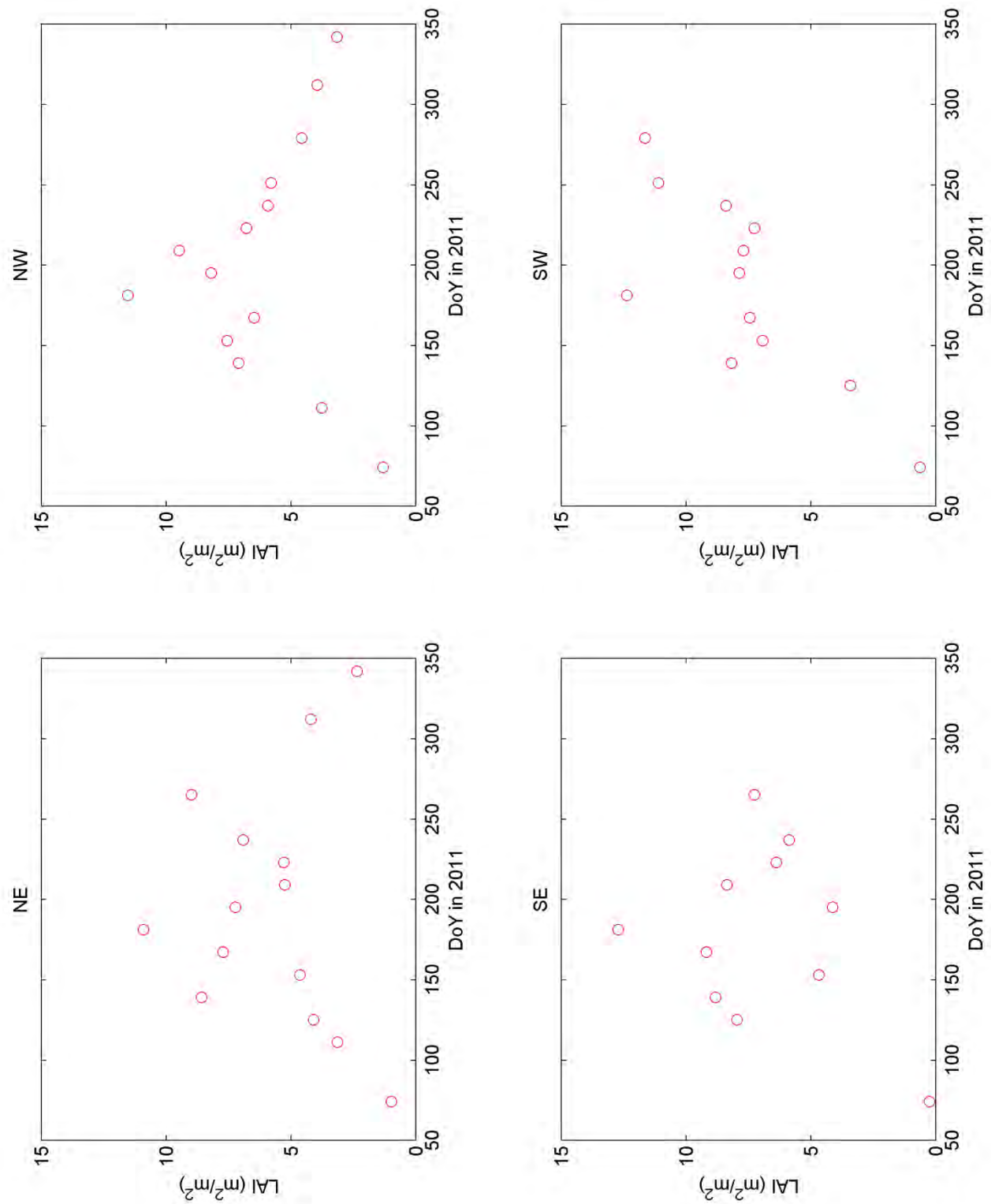


Figure A-30. Canopy LAI

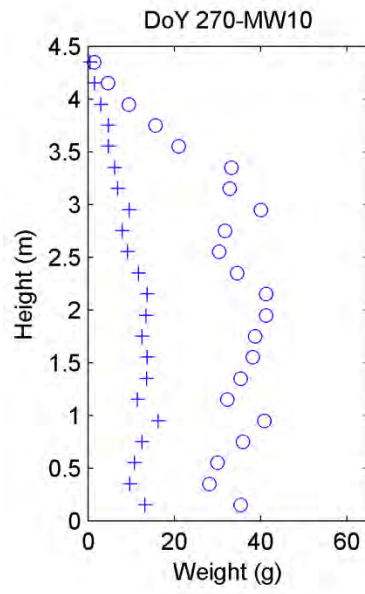


Figure A-31. Vertical distribution of wet and dry biomass

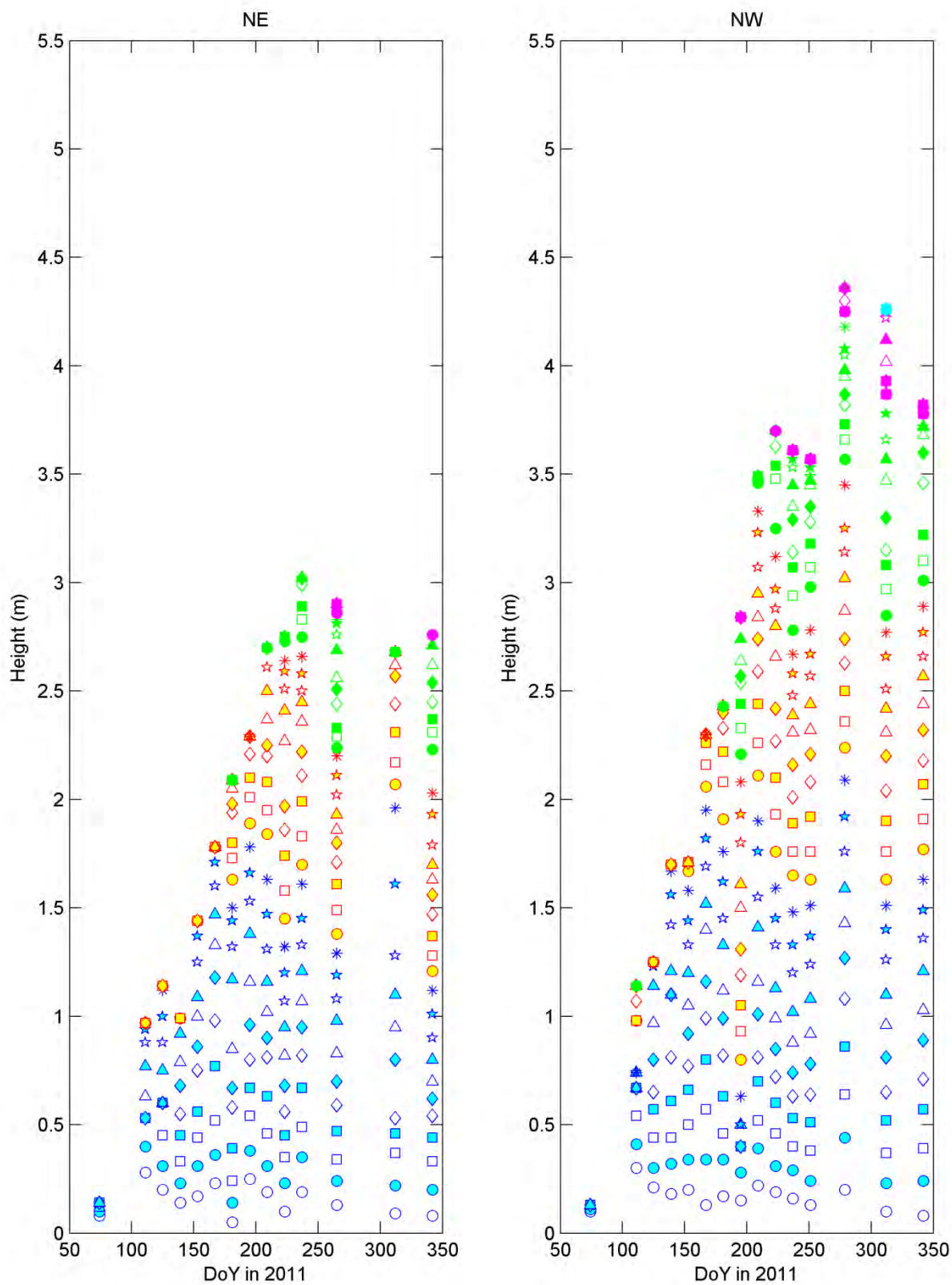


Figure A-32(a). Leaf height

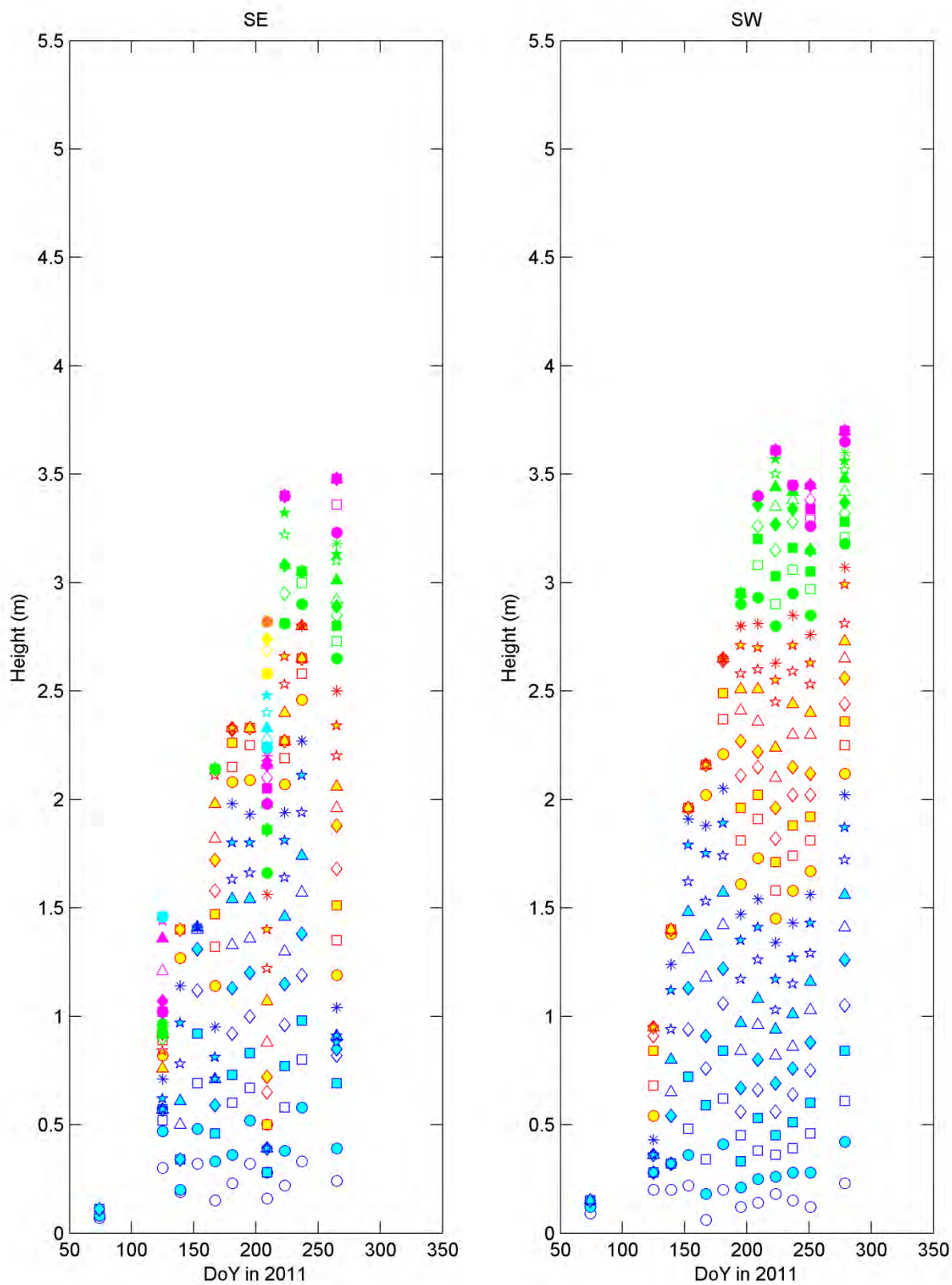


Figure A-32(b). Leaf height

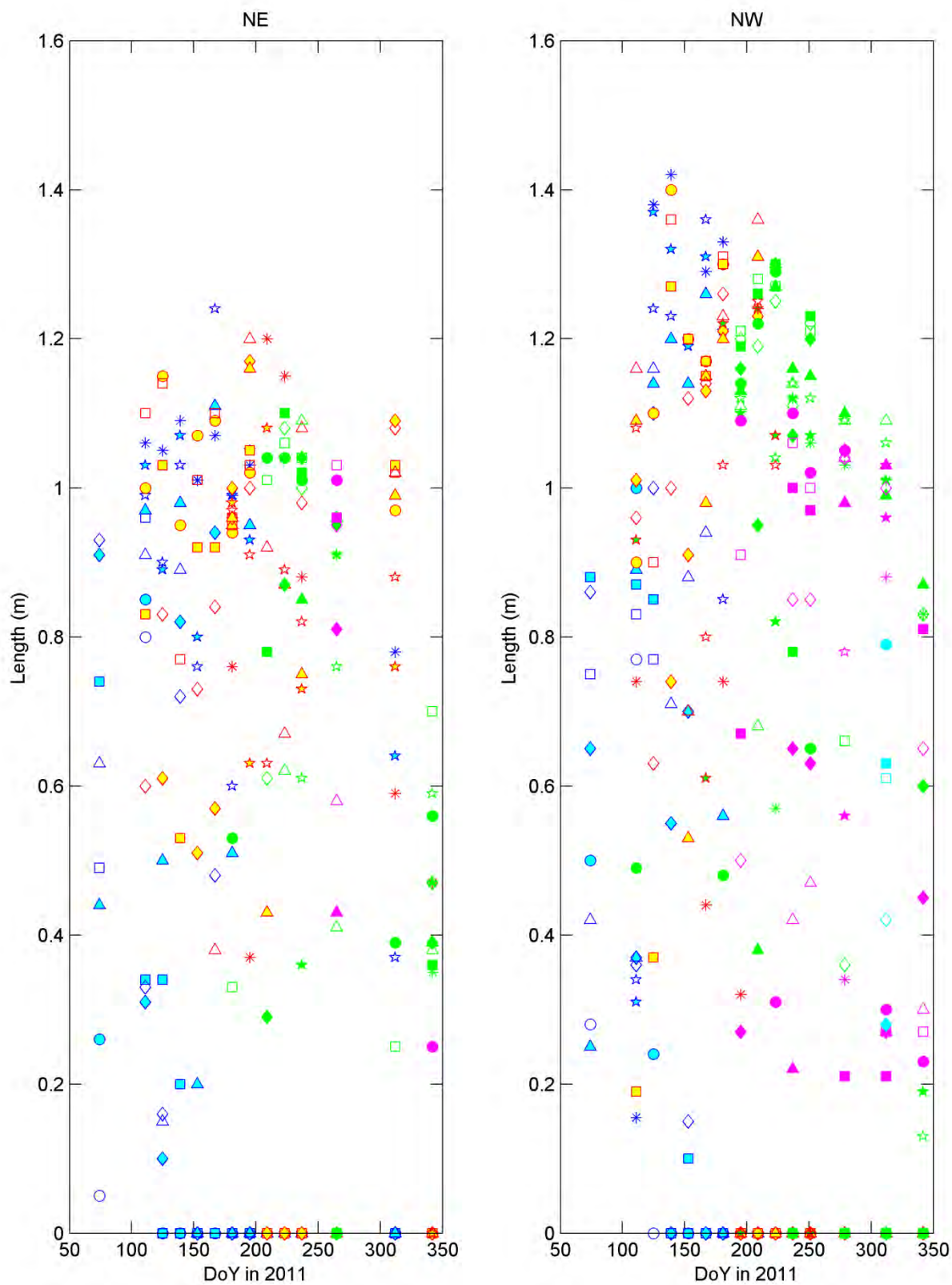


Figure A-33(a). Leaf length

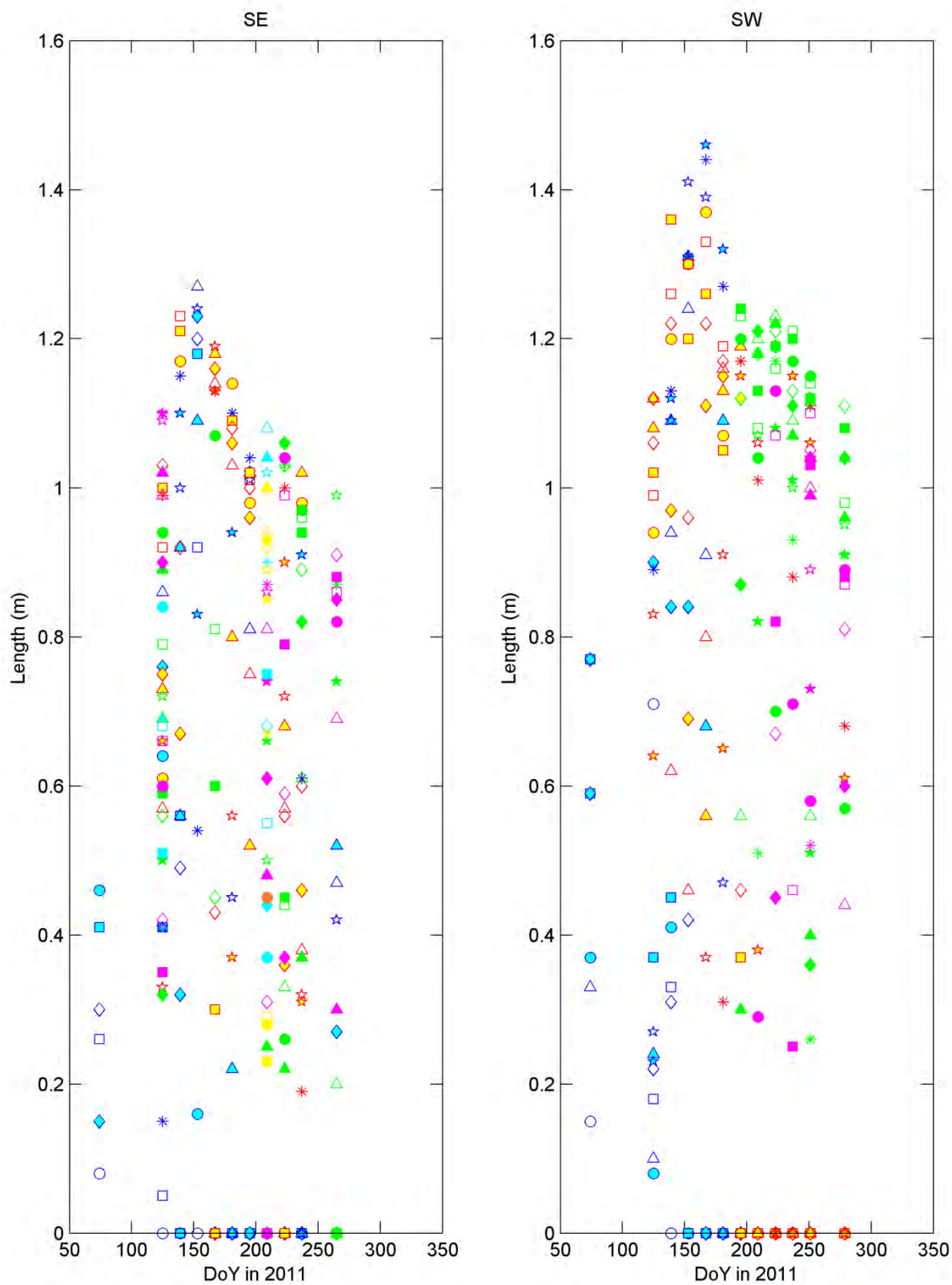


Figure A-33(b). Leaf length

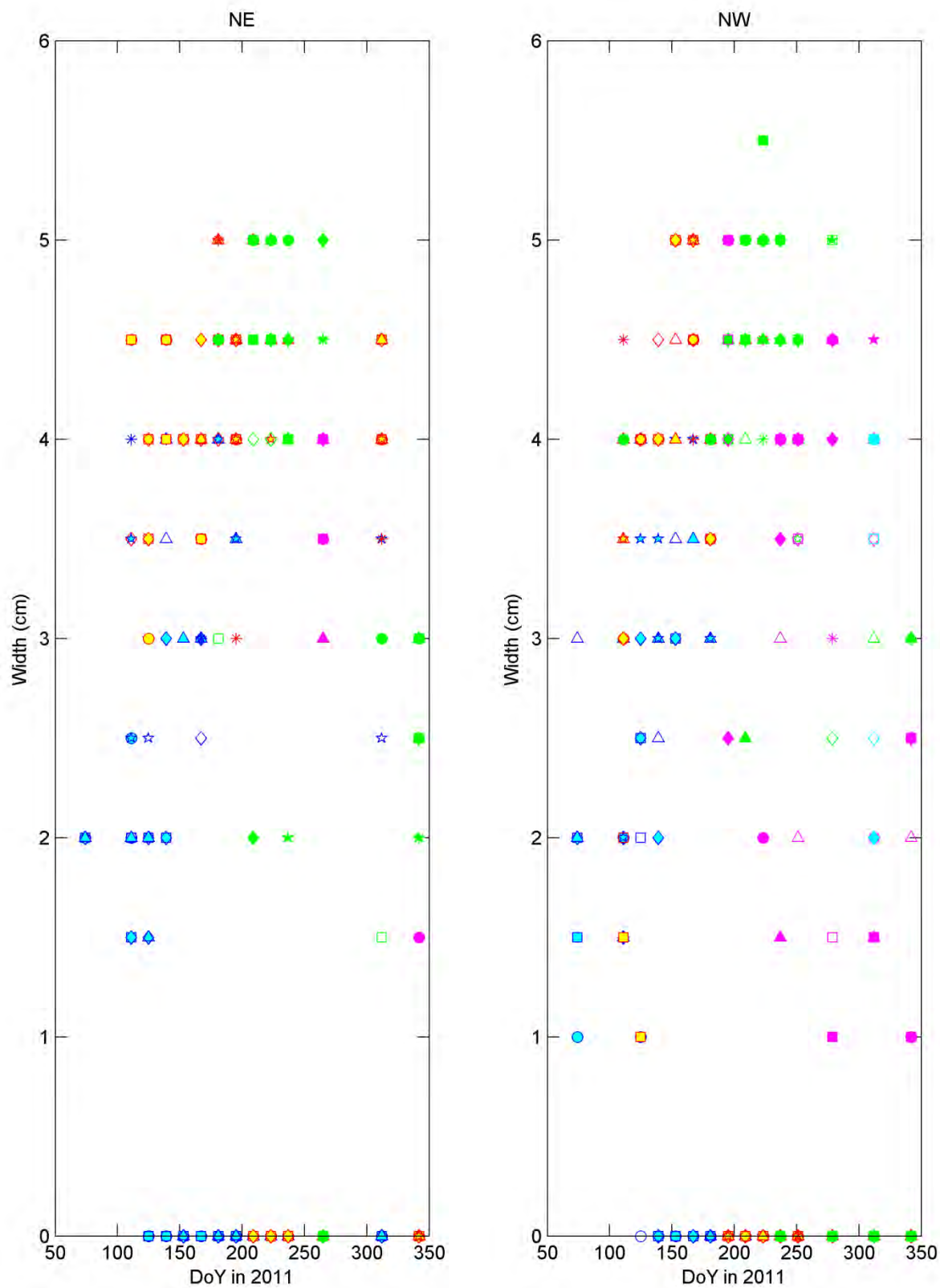


Figure A-34(a). Leaf width

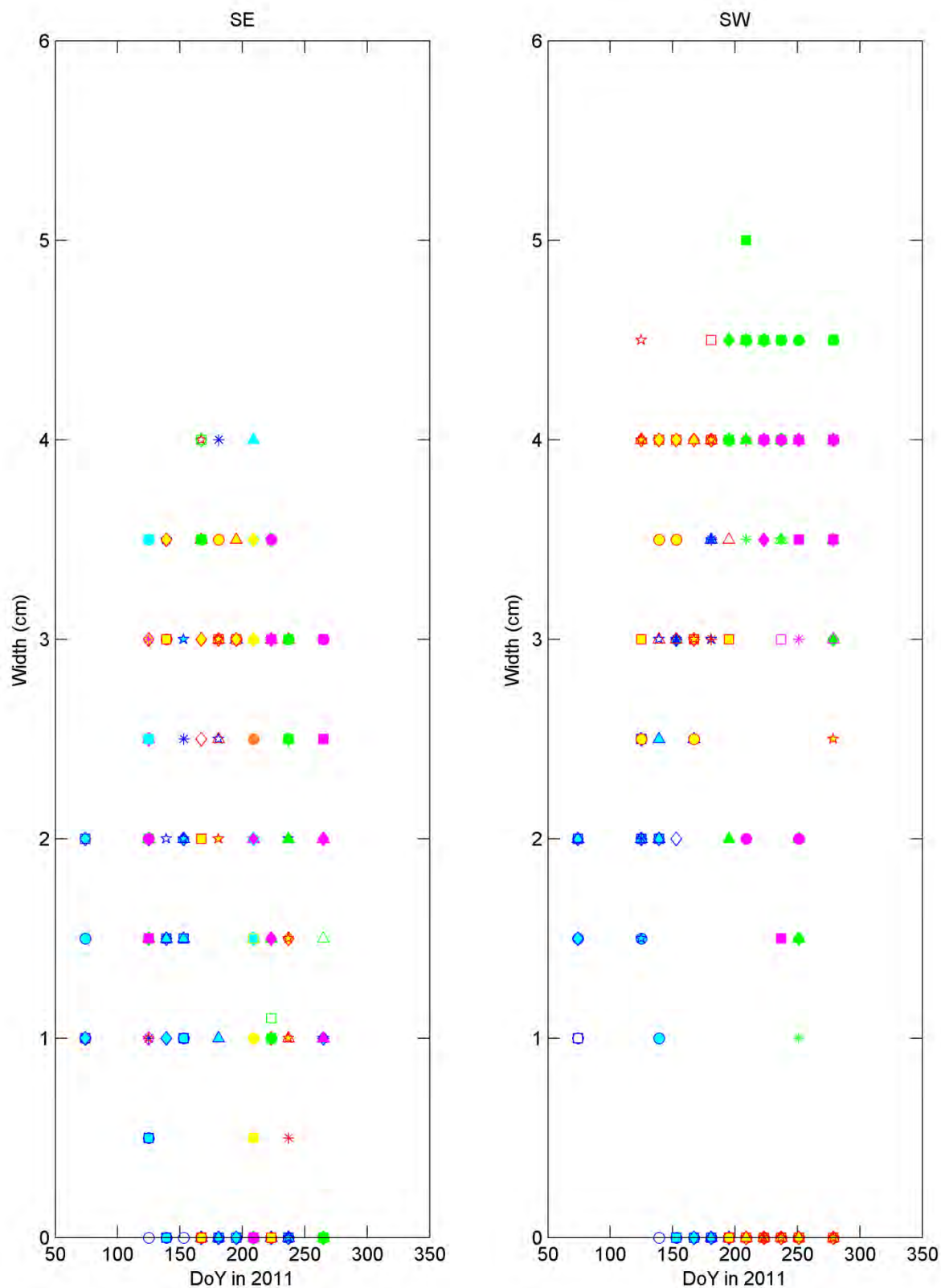


Figure A-34(b). Leaf width

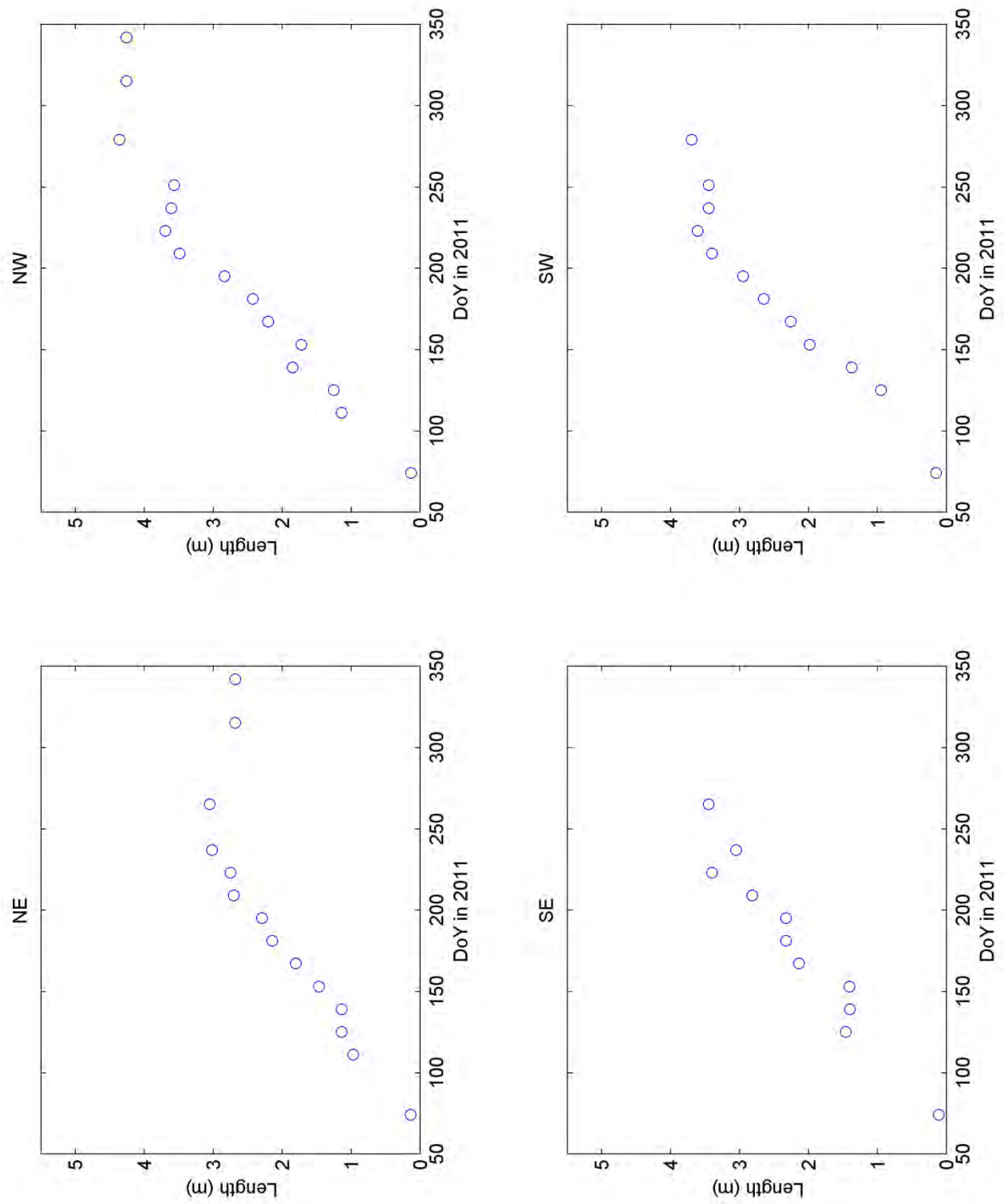


Figure A-35. Stem length

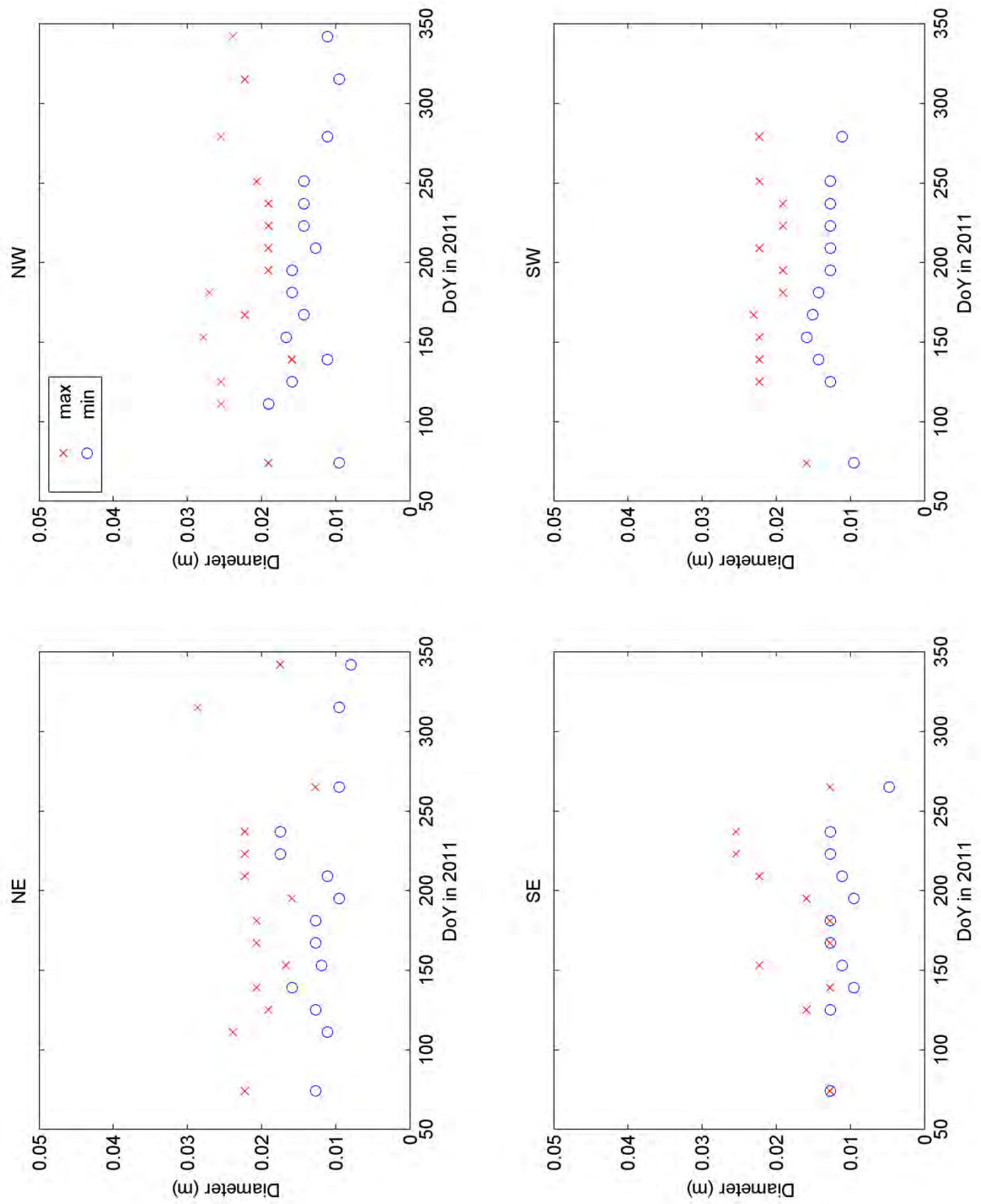


Figure A-36. Stem diameter

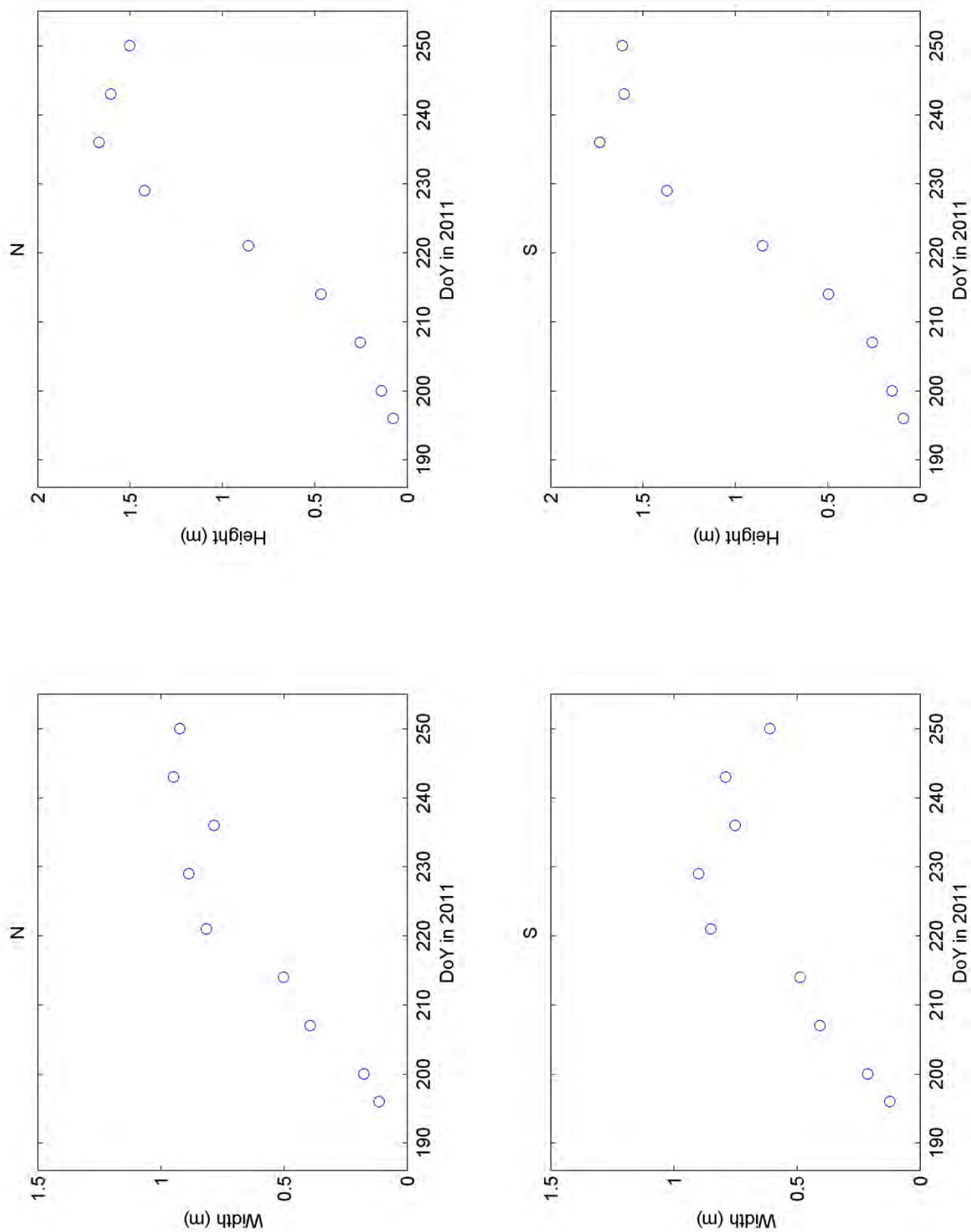


Figure A-37. Average crop height and width (corn)

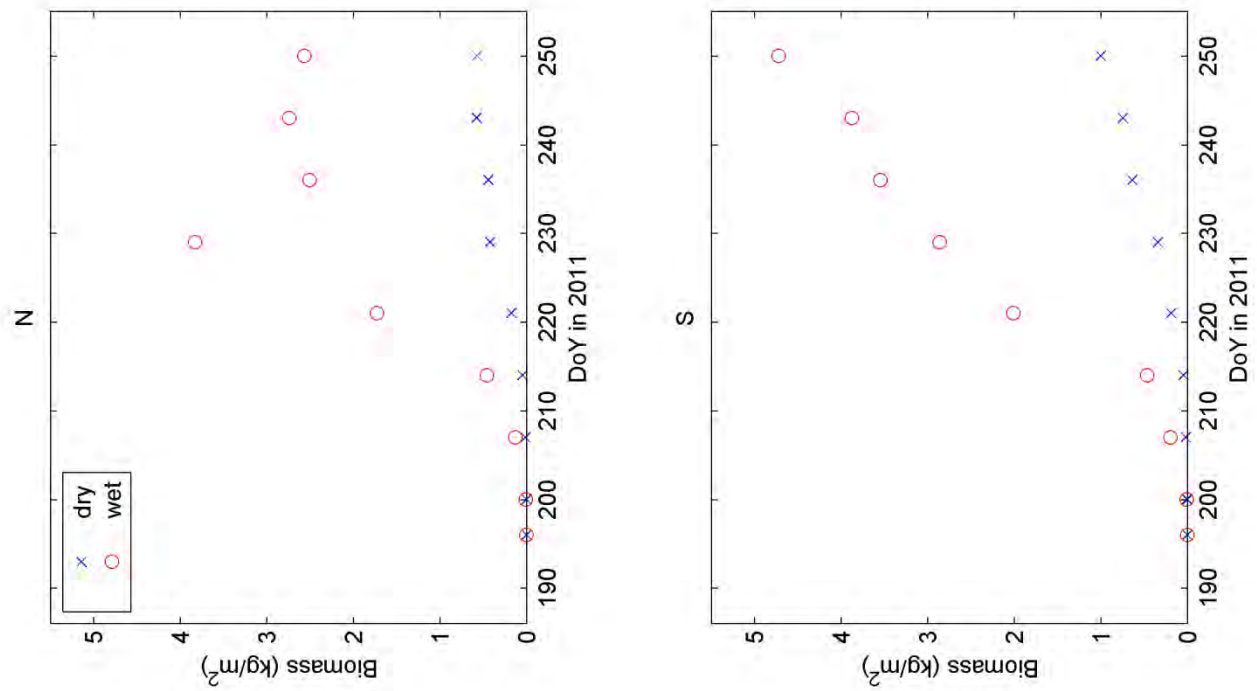


Figure A-38. Wet and dry canopy biomass

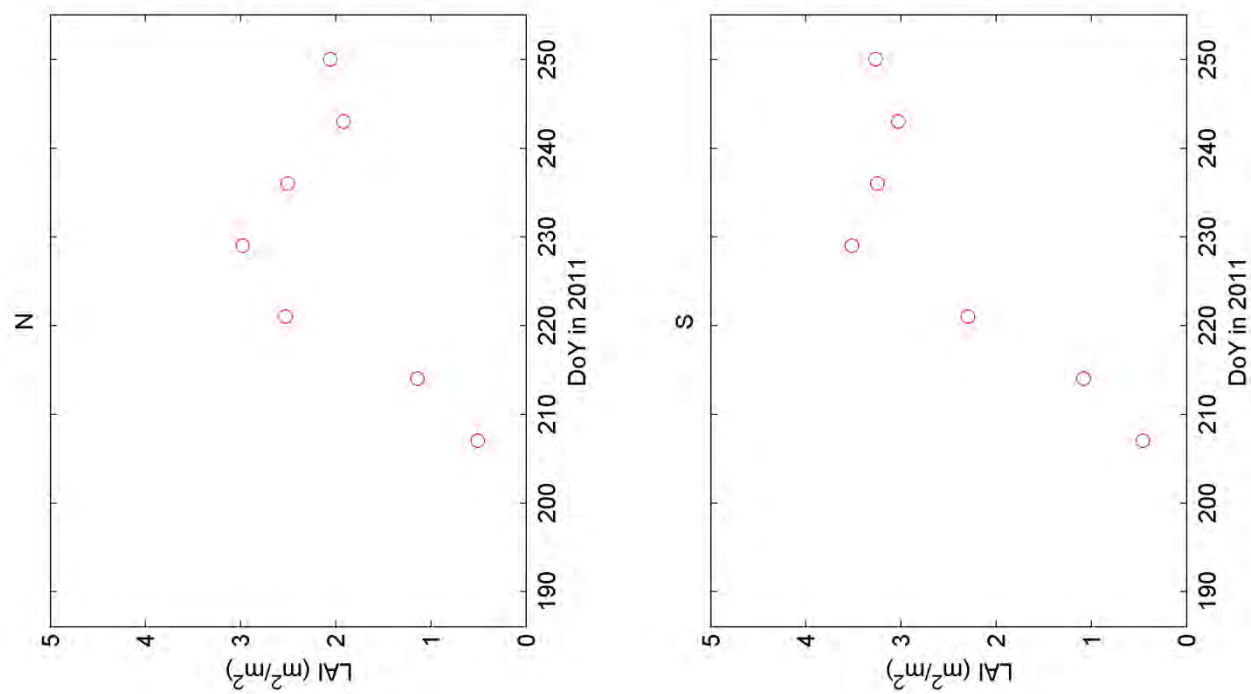


Figure A-39. Canopy LAI

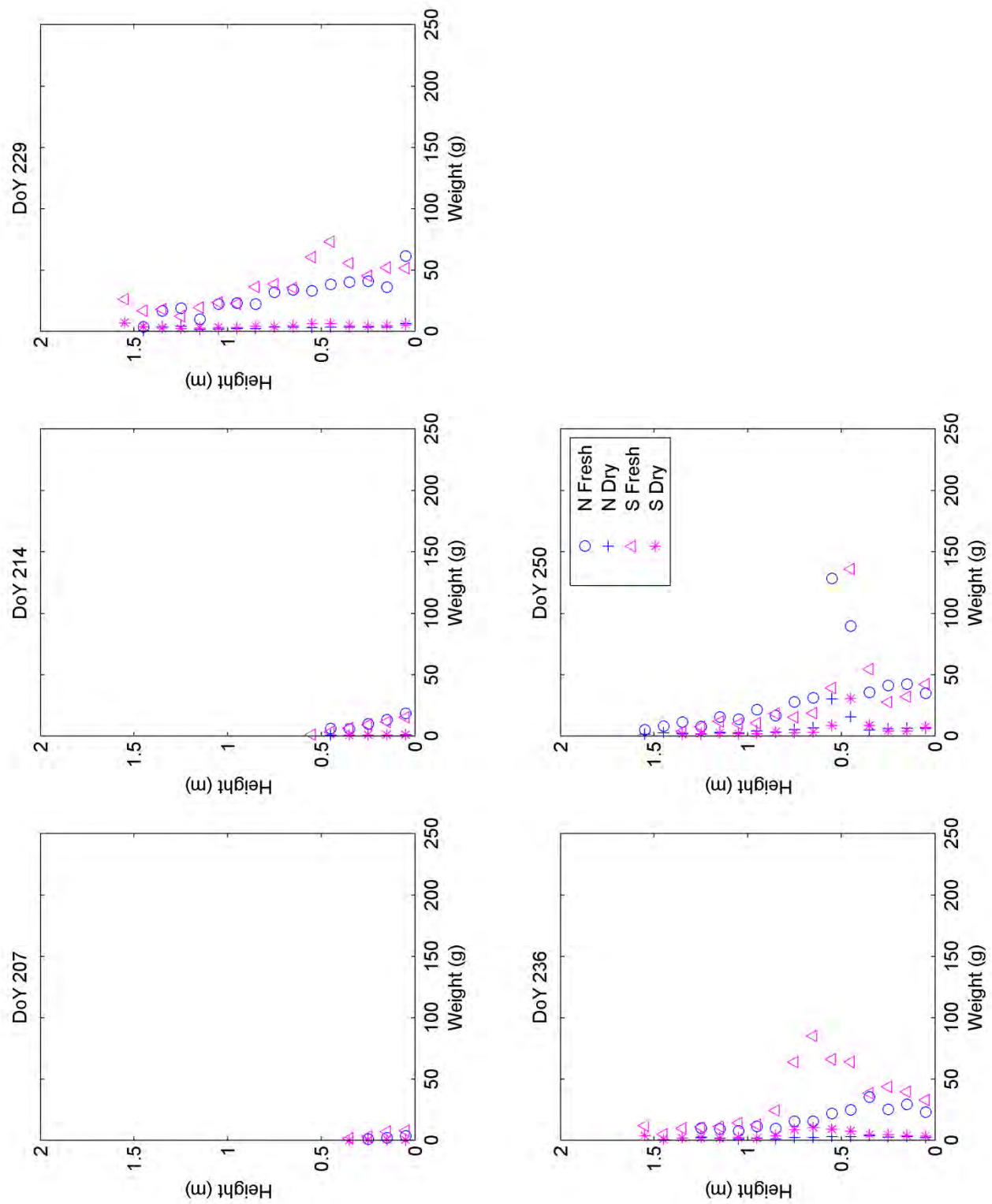


Figure A-40. Vertical distribution of wet and dry biomass

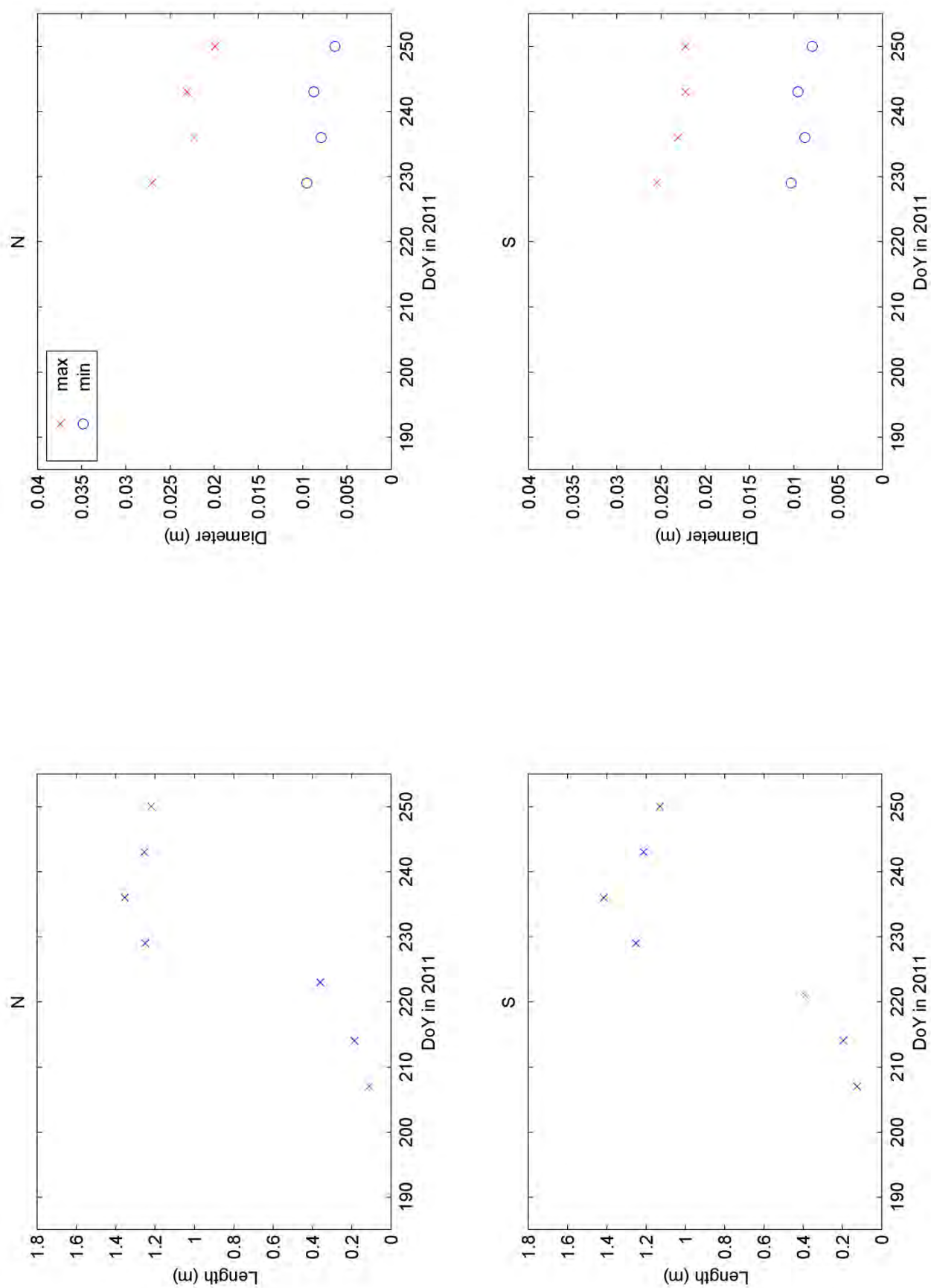


Figure A-41. Stem length and diameter

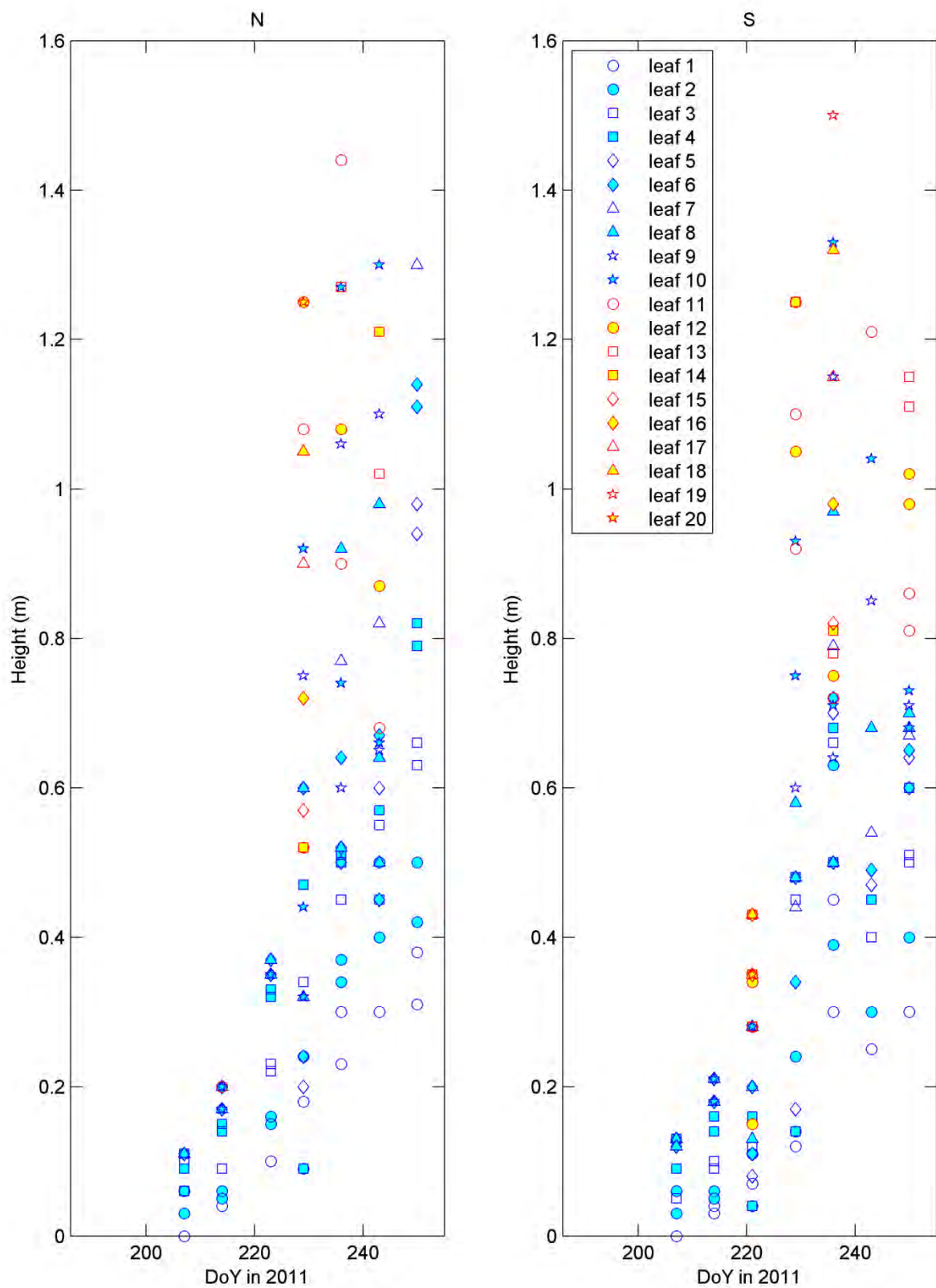


Figure A-42. Leaf height

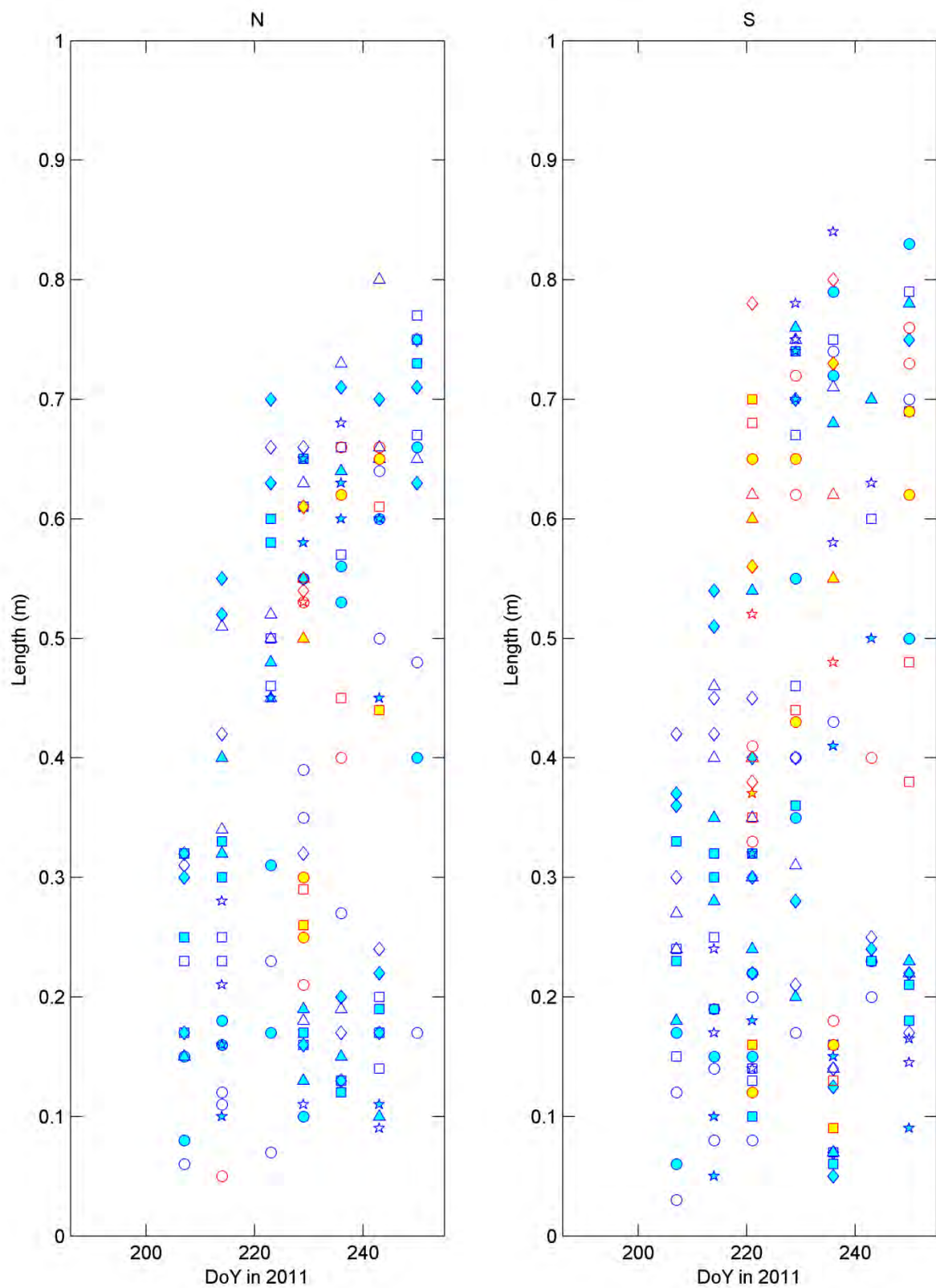


Figure A-43. Leaf length

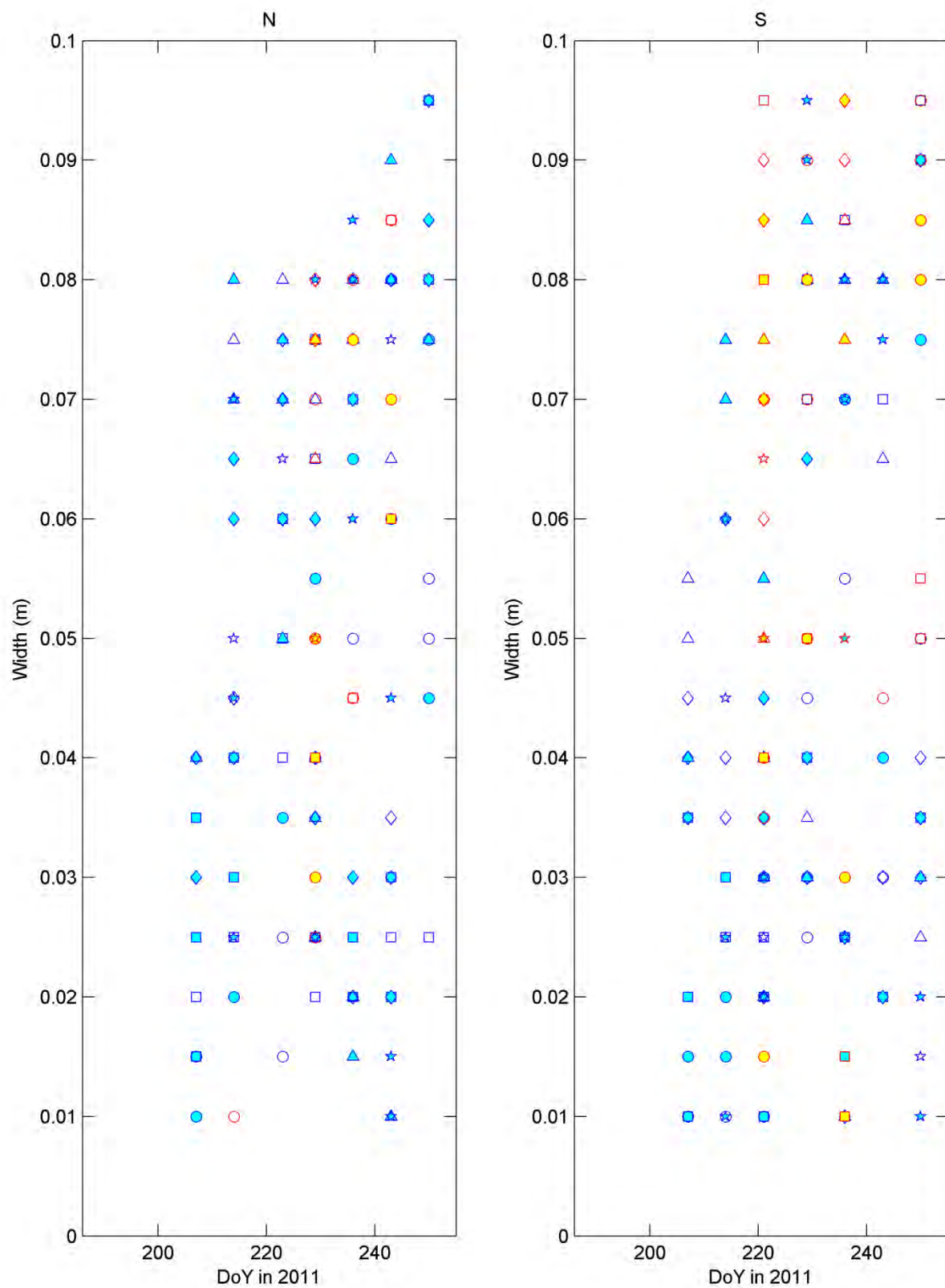


Figure A-44. Leaf width

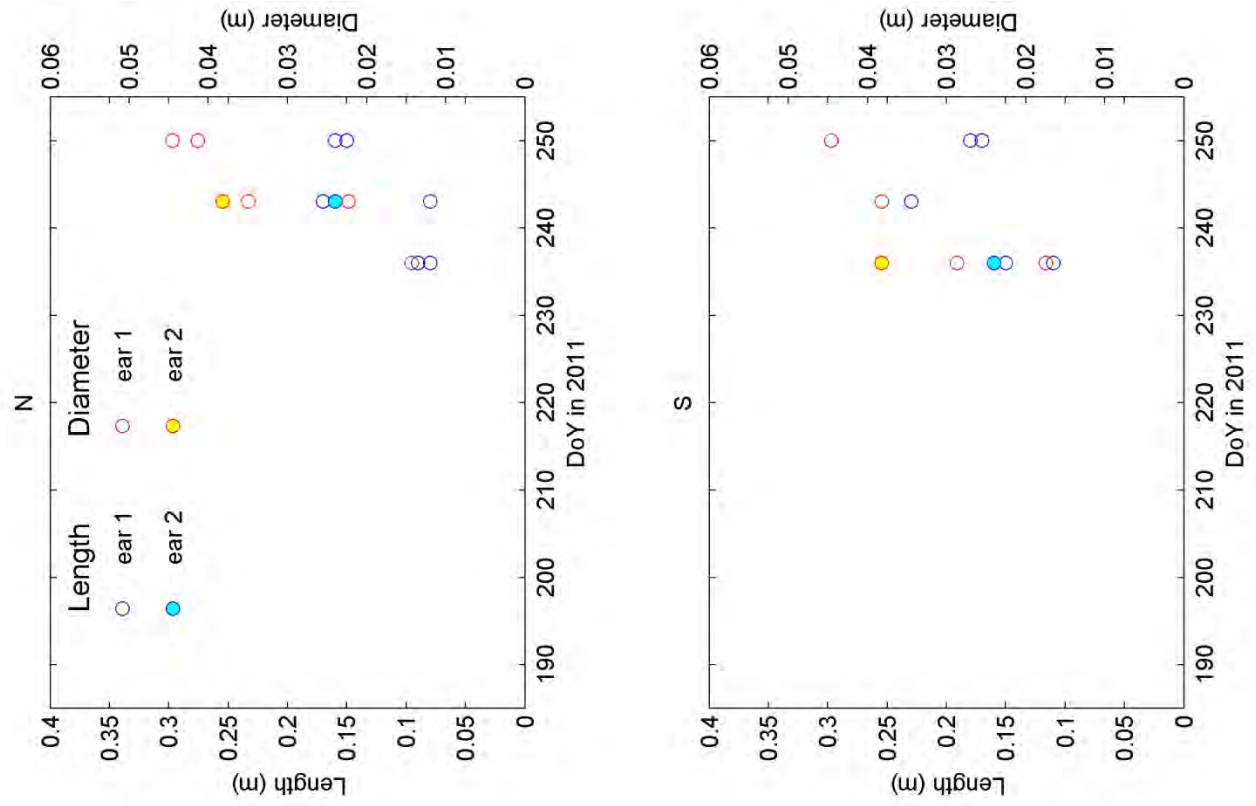
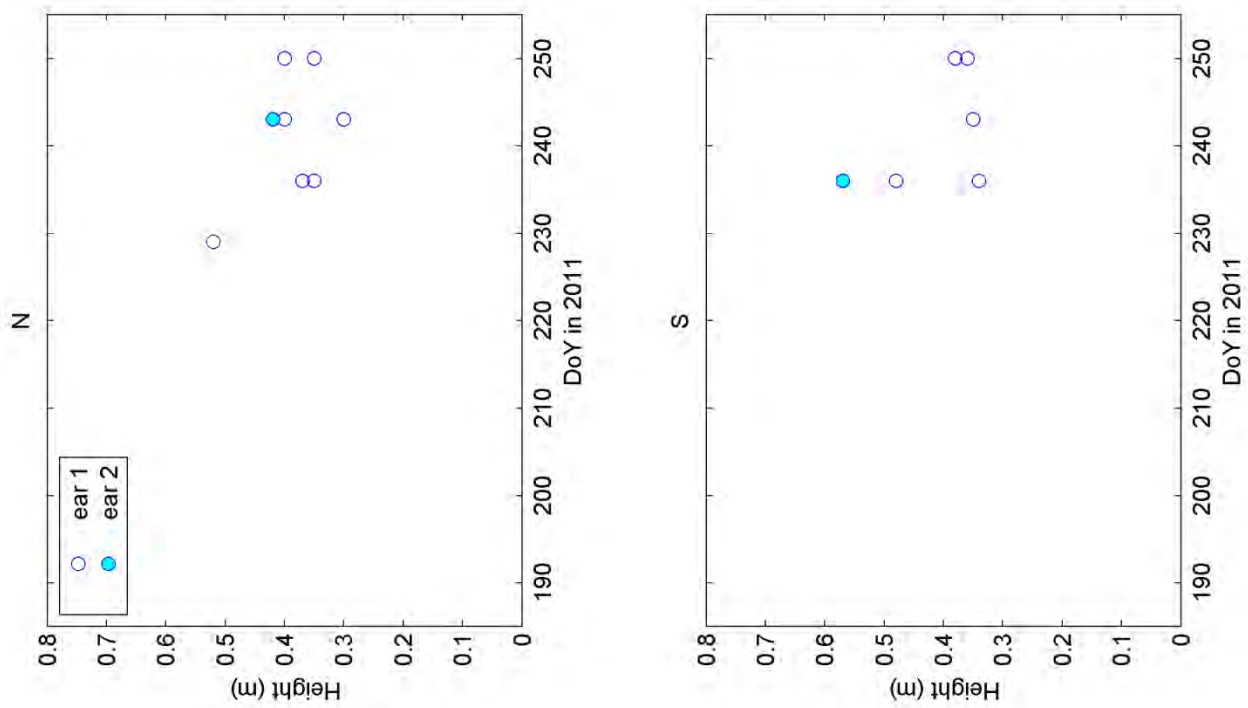


Figure A-45. Ear height, length, and diameter

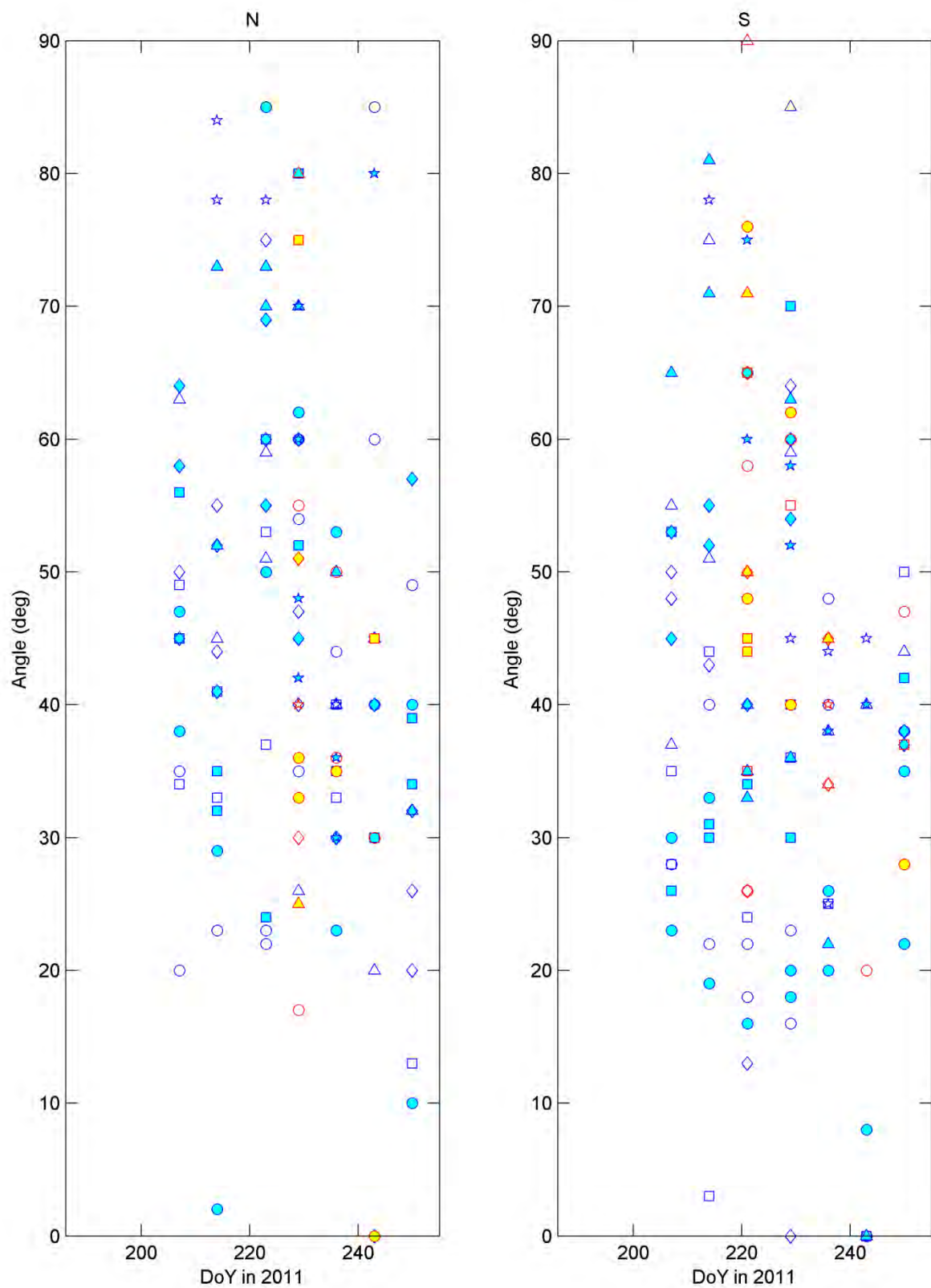


Figure A-46. Leaf angle (θ_1)

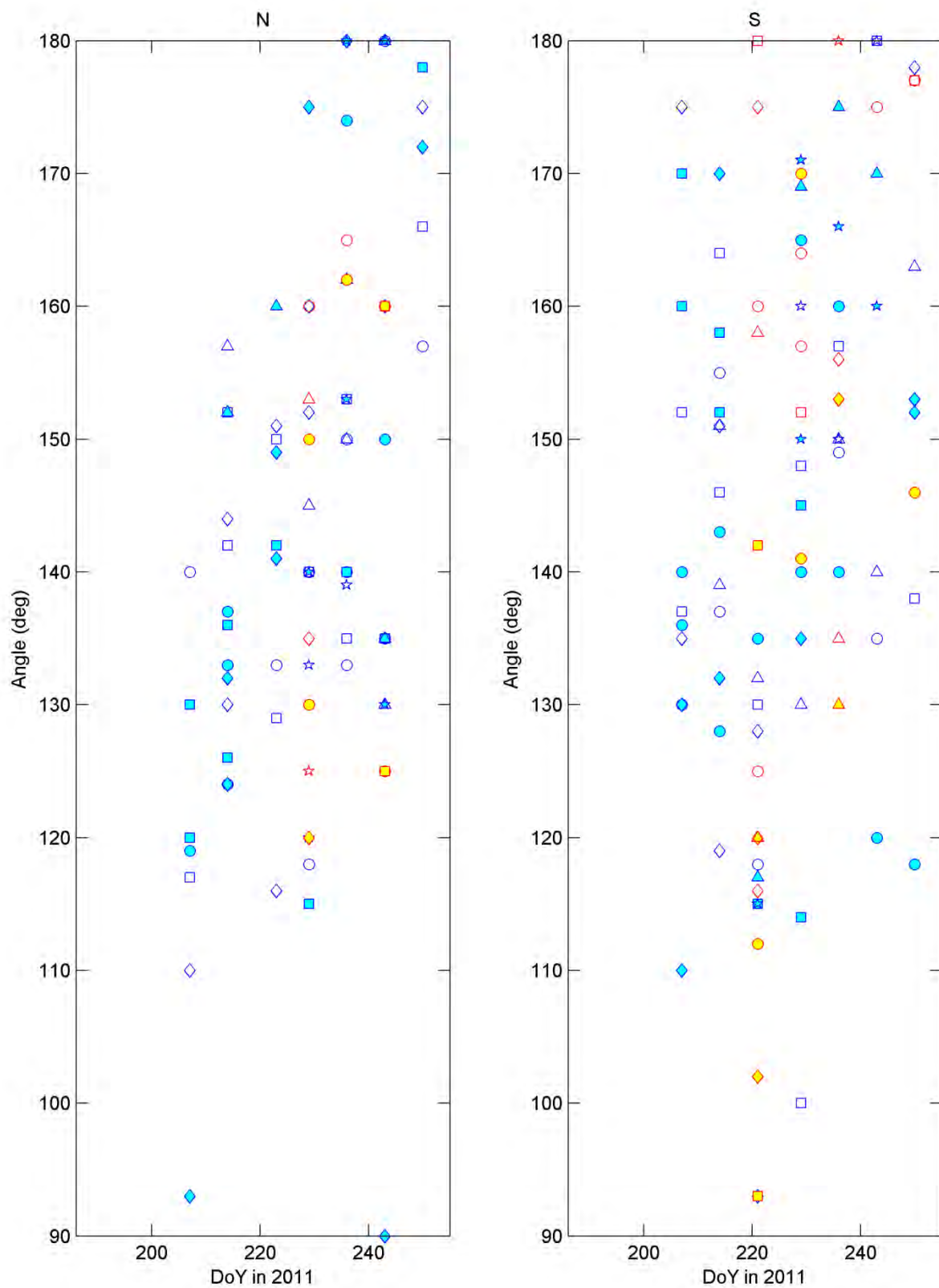


Figure A-47. Leaf angle (θ_2)

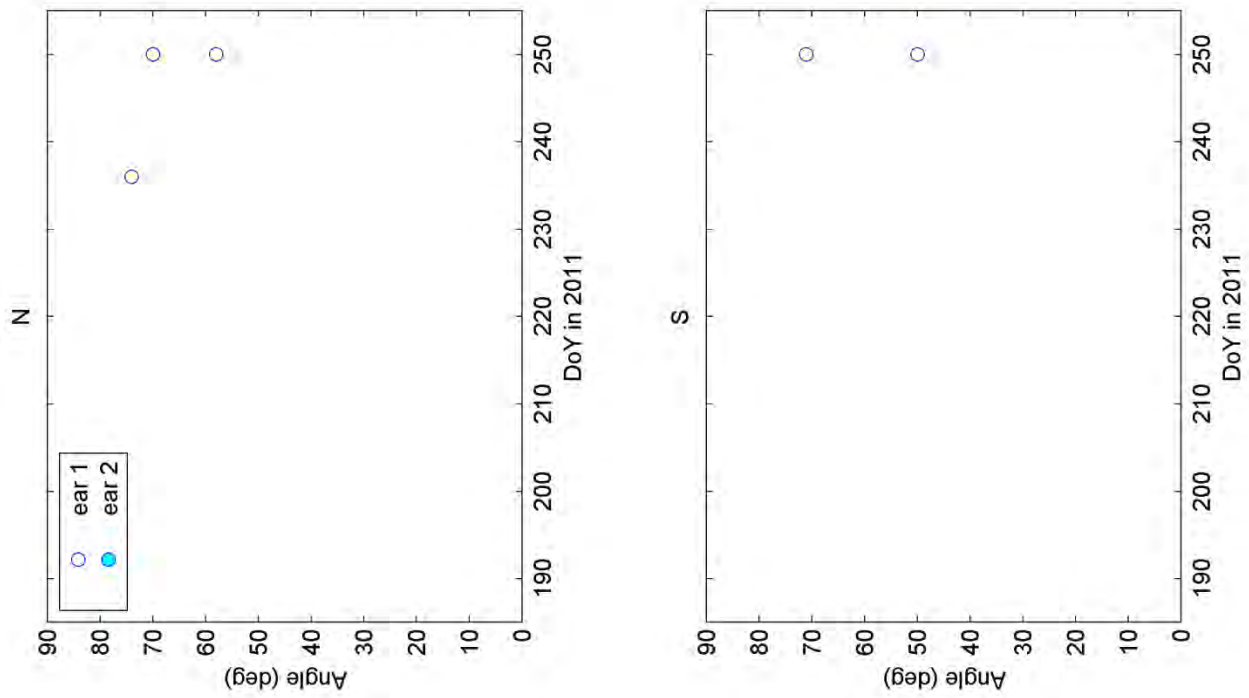


Figure A-48. Ear angle (θ_e)

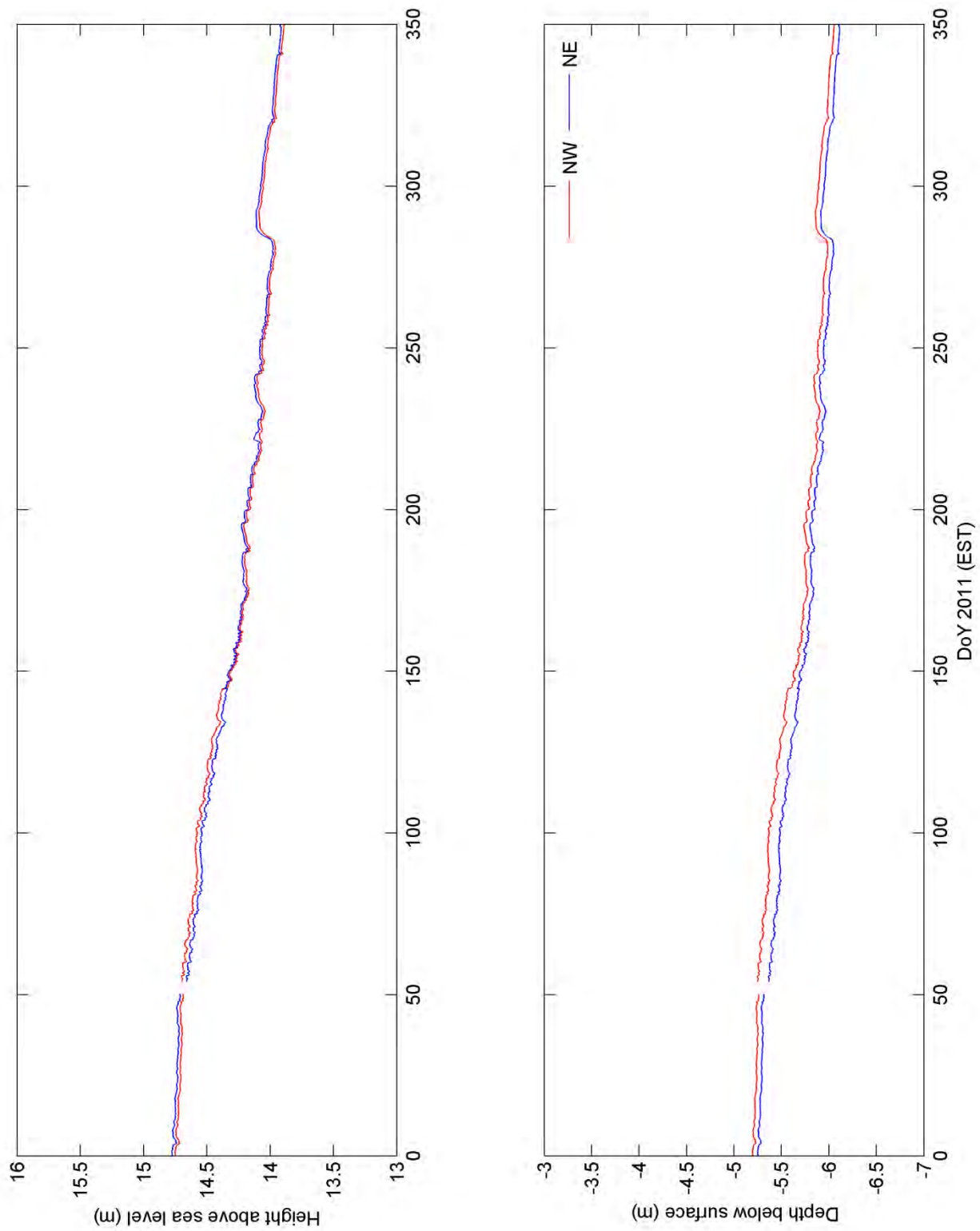


Figure A-49. Water table depth and elevation above sea level

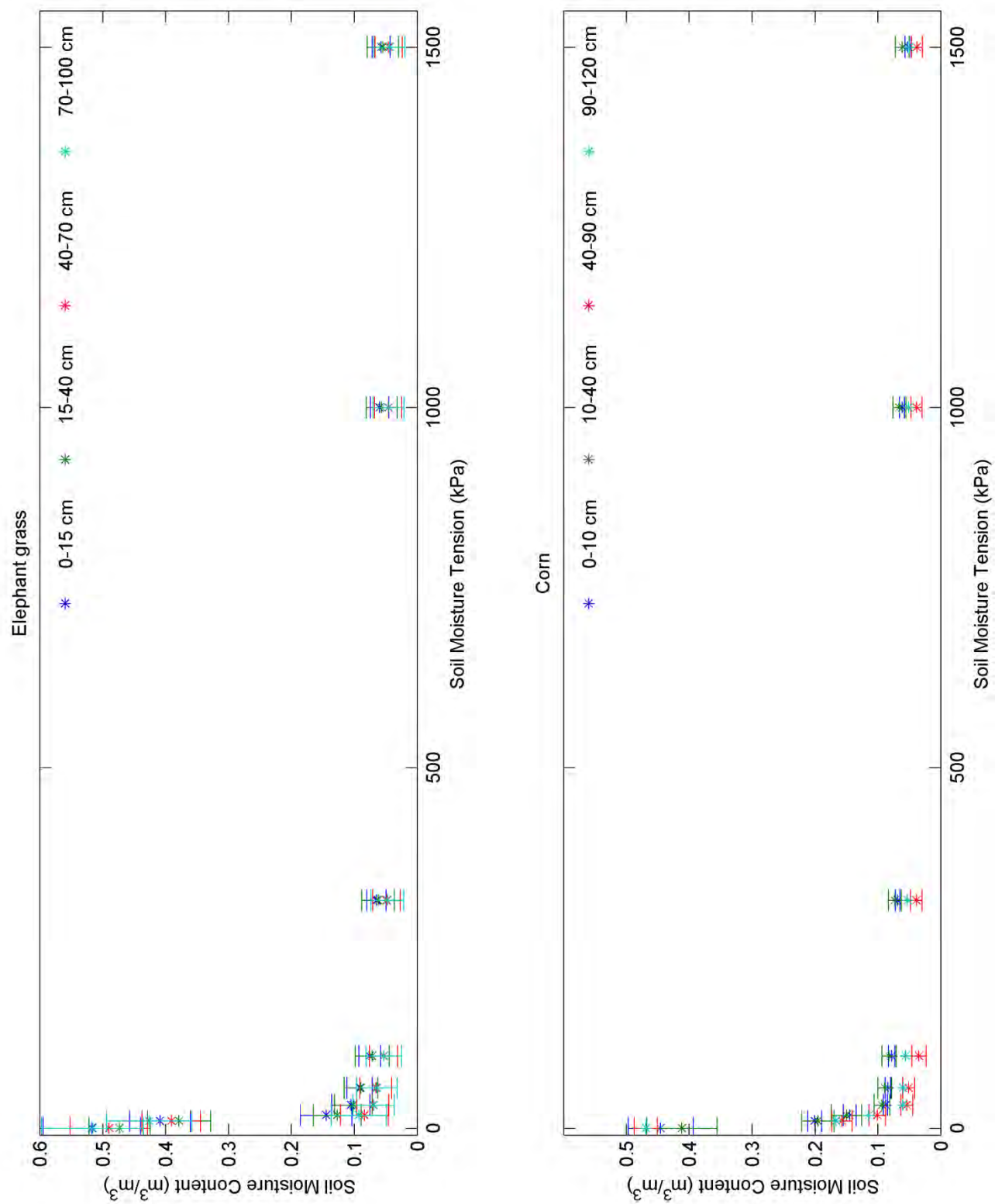


Figure A-50. Water retention curve

B. JULIAN DAY CALENDAR

Table B-1. Julian Day Calendar for non-leap years

	Jan	Feb	Mar	Apr	May	Jun	Jul	Aug	Sep	Oct	Nov	Dec
1	1	32	60	91	121	152	182	213	244	274	305	335
2	2	33	61	92	122	153	183	214	245	275	306	336
3	3	34	62	93	123	154	184	215	246	276	307	337
4	4	35	63	94	124	155	185	216	247	277	308	338
5	5	36	64	95	125	156	186	217	248	278	309	339
6	6	37	65	96	126	157	187	218	249	279	310	340
7	7	38	66	97	127	158	188	219	250	280	311	341
8	8	39	67	98	128	159	189	220	251	281	312	342
9	9	40	68	99	129	160	190	221	252	282	313	343
10	10	41	69	100	130	161	191	222	253	283	314	344
11	11	42	70	101	131	162	192	223	254	284	315	345
12	12	43	71	102	132	163	193	224	255	285	316	346
13	13	44	72	103	133	164	194	225	256	286	317	347
14	14	45	73	104	134	165	195	226	257	287	318	348
15	15	46	74	105	135	166	196	227	258	288	319	349
16	16	47	75	106	136	167	197	228	259	289	320	350
17	17	48	76	107	137	168	198	229	260	290	321	351
18	18	49	77	108	138	169	199	230	261	291	322	352
19	19	50	78	109	139	170	200	231	262	292	323	353
20	20	51	79	110	140	171	201	232	263	293	324	354
21	21	52	80	111	141	172	202	233	264	294	325	355
22	22	53	81	112	142	173	203	234	265	295	326	356
23	23	54	82	113	143	174	204	235	266	296	327	357
24	24	55	83	114	144	175	205	236	267	297	328	358
25	25	56	84	115	145	176	206	237	268	298	329	359
26	26	57	85	116	146	177	207	238	269	299	330	360
27	27	58	86	117	147	178	208	239	270	300	331	361
28	28	59	87	118	148	179	209	240	271	301	332	362
29	29		88	119	149	180	210	241	272	302	333	363
30	30		89	120	150	181	211	242	273	303	334	364
31	31		90		151		212	243		304		365